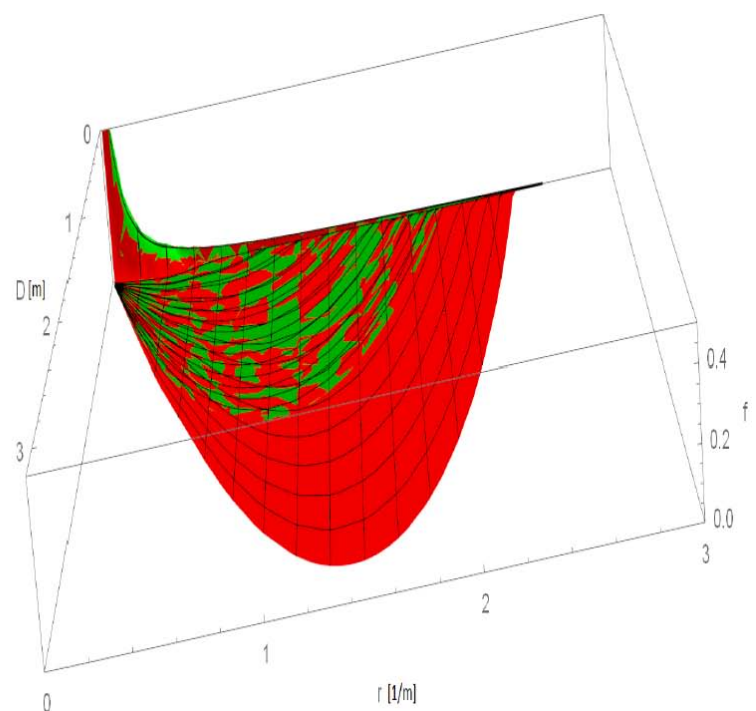
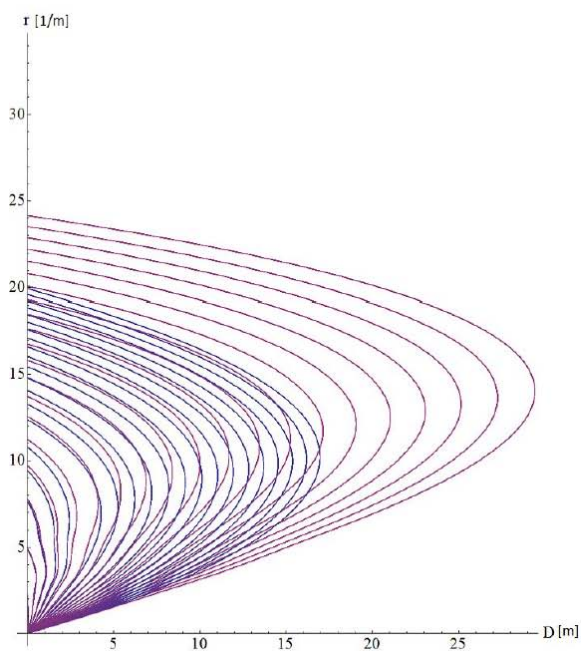


Numerical modeling of dynamic recrystallization in polycrystals

Hai Van Nguyen



RUHR-UNIVERSITÄT BOCHUM
Institut für Mechanik

**Numerical modeling of dynamic recrystallization in
polycrystals**

Mitteilungen aus dem Institut für Mechanik Nr. 177

Herausgeber (Publisher):

Institut für Mechanik

— Schriftenreihe —

Ruhr-Universität Bochum

D-44780 Bochum

ISBN 3-935892-55-1

This material is presented to ensure timely dissemination of scholarly and technical work. Copyright and all rights therein are retained by the copyright holders. All persons copying this information are expected to adhere to the terms and constraints invoked by the author's copyright. These works or parts of it may not be used to repost reprint/republish or for creating new collective works for resale or redistribution to servers or lists without the explicit permission of the copyright holder.

Dieses Werk ist urheberrechtlich geschützt. Die dadurch begründeten Rechte, insbesondere die der Übersetzung, des Nachdrucks, des Vortrags, der Entnahme von Abbildungen und Tabellen, der Funksendung, der Mikroverfilmung oder der Vervielfältigung auf anderen Wegen und der Speicherung in Datenverarbeitungsanlagen, bleiben, auch bei nur auszugsweiser Verwertung, vorbehalten. Eine Vervielfältigung dieses Werkes oder von Teilen dieses Werkes ist zulässig. Sie ist grundsätzlich vergütungspflichtig. Zuwiderhandlungen unterliegen den Strafbestimmungen des Urheberrechtsgesetzes.

©2018 Hai Van Nguyen, Institut für Mechanik, Ruhr-Universität Bochum

Printed in Germany

Einreichung der Dissertation (thesis submission): 16. January 2018

Tag der mündlichen Prüfung (thesis defense): 16. April 2018

Erster Referent (first referee):

Prof. Dr. rer. nat Klaus Hackl

Zweiter Referent (second referee):

Prof. Dr. Jörg Renner

Vorsitzender (committee chair):

Prof. Dr. Andreas H. Schumann

for Bao Binh and Quoc An

Acknowledgements

From 2014 to 2017, thanks to the funding of German Academic Exchange Service (Deutscher Akademischer Austauschdienst-DAAD), I had a chance to work as a PHD student at the Institute Mechanics of Materials in Ruhr University, Bochum. During that time, I would like to express my sincere gratitude to people who have helped me and have supported me to finish my thesis.

First, all my sincere and best regards are for Prof. K. Hackl who I would thank the most for many reasons. He is the one who has encouraged me to be back to the field of research and then back to Bochum. He is always a tremendous teacher and a kind supervisor. I have received his guidance not only in material modeling but also in microstructure using the minimum of the dissipation potential. I highly appreciate his patience since this topic was really strange and seemed to be challenge for me. His ideas and his approaches have a huge contribution to this thesis. Without him, this thesis obviously would be not created.

Moreover, I would like to thank Dr.-Ing. Bach Tuyet Trinh. She has encouraged me during this time. She has given me her reliable advice. She also made me more creative and more motivated in my work.

Finally, let me give a big thank to all those who have followed me during the entire duration to complete this thesis. I am thankful for my family and my friends for always supporting me and for giving the spirit encouragement. Especially, it will definitely be impossible if i don't thank my husband and my sons. Furthermore, I would like to thank all of my colleagues at the Institute of Mechanics and in particular at the Lehrstuhl für Allgemeine Mechanik. Their pleasant atmosphere and research conditions have predominantly been their merit. Let me express my gratitude also to a number of student assistants who gave me an enormous support in doing some of the cumbersome computational tasks of this research.

Summary

The scope of this thesis is the development of probabilistic models of dynamic recrystallization in polycrystalline materials. The goal is to predict the distribution of grain size and dislocation density as a function of the thermo-mechanical history of the material as well as the behavior of entire macroscopic bodies.

In the first part of the thesis, a probability distribution function is introduced in order to characterize the state of individual grains. The mean values of all relevant state variables are defined based on this function. By specifying free energy and dissipation within the polycrystalline aggregate we are able to derive an evolution equation for the probability density function via a thermodynamic extremum principle. Moreover, for distribution functions which are constant in time, describing a state of dynamic equilibrium, we obtain a partial differential equation in parameter space which can be solved using a marching algorithm. The results for the macroscopic stresses obtained this way are then compared to those from phenomenological models. As next step, a nucleation theory is introduced into the model for completion. Three different versions of that one are investigated.

The main objective of the second part of the thesis is to describe the behavior of macroscopic specimens. For this purpose, a two-scale scheme is developed involving a finite element scheme at the macroscale and the model based on the probability distribution function at the microscale implemented at the Gauss point level. For verification, the model is compared with an existing implementation in Abaqus as well.

Kurzfassung

Im Rahmen dieser Arbeit wurde ein probabilistisches Modell der dynamischen Rekristallisation von polykristallinen Materialien entwickelt. Ziel war, die Verteilung von Korngröße und Versetzungsdichte in Abhängigkeit von der thermomechanischen Behandlung des Materials sowie das Verhalten von makroskopischen Bauteilen vorherzusagen.

Im ersten Teil der Arbeit wird eine Wahrscheinlichkeitsverteilungsfunktion eingeführt, um den Zustand individueller Körner zu charakterisieren. Die Mittelwerte aller relevanten Zustandsvariablen können über diese Funktion definiert werden. Durch Spezifikation von freier Energie und Dissipation des polykristallinen Gefüges, konnte eine Evolutionsgleichung für die Wahrscheinlichkeitsverteilungsfunktion mittels eines thermodynamischen Extremalprinzips hergeleitet werden. Darüber hinaus erhalten wir für zeitlich konstante Verteilungsfunktionen, welche ein Fließgleichgewicht beschreiben, eine partielle Differentialgleichung im Parameterraum, welche durch einen Marching-Algorithmus gelöst wurde. Die auf diese Weise erhaltenen Ergebnisse für die makroskopischen Spannungen wurden dann mit jenen verglichen, die sich aus phänomenologischen Modellen ergaben. Als nächster Schritt wurde dann eine Nukleationstheorie zum Modell hinzugefügt, um es zu vervollständigen. Drei unterschiedliche Versionen dieser Theorie wurden studiert.

Ziel des zweiten Teils der Arbeit war dann die Modellierung makroskopischer Bauteile. Zu diesem Zweck wurde ein zweiskaliger Algorithmus entwickelt, welcher auf einem Finite Elemente Zugang auf der Makroskala basierte, sowie auf dem Modell unter Verwendung der Wahrscheinlichkeitsverteilungsfunktion auf der Mikroskala. Letzteres wurde auf der Gausspunktebene eingebunden. Zur Verifikation wurde das Zweiskalenmodell wiederum mit einem in Abaqus implementierten phänomenologischen Modell verglichen.

Contents

1	Introduction	1
1.1	Motivation	1
1.2	Methodology and organization of the thesis	2
2	Mathematical and mechanical fundamentals	5
2.1	Vector and tensor analysis	5
2.1.1	Vector and tensor definition	5
2.1.2	Vector and tensor calculus	8
2.2	Continuum mechanics	11
2.2.1	Displacement and strain	11
2.2.2	Force and stress	13
2.2.3	Conservation of mass	15
2.2.4	Constitutive equations	15
2.3	Polycrystalline materials	20
2.3.1	Crystals	20
2.3.2	Polycrystals	22
2.3.3	Defects	22
2.3.4	Grain boundaries	23
2.4	Recrystallization	26
2.4.1	Static recrystallization	26
2.4.2	Dynamic recrystallization	27
2.4.3	Nucleation mechanisms	28
2.4.4	Grain growth	29
2.4.5	Creep	29
2.4.6	Relaxation	34
2.5	General variational approach	34
3	Mathematical model	37
3.1	Variational approach for dynamic recrystallization	37
3.2	Microscale	43
3.2.1	The original model for the distribution function $f(D, \rho)$	43
3.2.2	The standard model for the distribution function $\bar{f}(D, r)$	45
3.2.3	The modified model for the distribution function $\hat{f}(s, r)$	46
3.2.4	The extended model with the distribution function $f(p, D, r)$	47
3.3	Macroscale	51
3.4	Nucleation	52
3.4.1	A global nucleation theory	52
3.4.2	The production based nucleation theory	54
3.4.3	The geometry based nucleation theory	56
4	Numerical implementation	59
4.1	Numerical scheme	59

4.1.1	Simpson's rule	59
4.1.2	Newton-Raphson scheme	60
4.2	Finite element method	60
4.2.1	FEM background	60
4.2.2	FEM for non-linear materials	63
4.3	Marching algorithm	66
4.3.1	Marching algorithm for the distribution function $\bar{f}(D, r)$	67
4.3.2	Marching algorithm for the distribution function $\tilde{f}(s, r)$	69
4.3.3	Marching algorithm for $\tilde{f}(s, r)$ and h	72
4.3.4	Fix-point algorithm	74
4.4	Macroscopic simulation	74
5	Numerical results	79
5.1	Methods	79
5.2	Numerical results in the microscale	81
5.2.1	Results for the distribution function, $\bar{f}(D, r)$	81
5.2.2	Results for the distribution function, $\tilde{f}(s, r)$	82
5.2.3	Results for the distribution function, $f(p, D, r)$	89
5.3	Relaxation test and creep test	89
5.4	Numerical results in the macroscale	93
5.4.1	The first model results	93
5.4.2	The second model results	96
5.4.3	The third model results	102
6	Conclusions and Outlook	109
	References	121

Nomenclature

The next list describes several symbols that will be later used within this thesis:

Latin notations

D_0	Nucleation parameter
\mathbb{C}	Elastic tensor
\mathbb{D}	Stiffness matrix, tangent matrix
\mathbf{b}	Burger's vector
e_i	Cartesian unit vectors
N	Shape function
\mathbf{n}	Unit normal vector
\mathbf{t}	Traction force
\mathbf{u}	Displacement field
$\mathbf{V}, \dot{\mathbf{X}}$	External variable's time derivative
$\mathbf{v}, \dot{\mathbf{x}}$	Internal variable's time derivative
\mathbf{X}	External variables
\mathbf{x}	Internal variables
\mathbf{x}, \mathbf{X}	Coordinates in the deformed and in the reference configuration
\mathbf{z}	Combination of internal variables and external variables
\mathcal{L}	Lagrange functional
A	Area of the needle point
A_d	Flow law multiplier for diffusion creep
A_p	Flow law multiplier for dislocation creep
a_p	Dislocation density evolution
D	Grain size
E	Young's modulus
g_0	Nucleation parameter

k_p	Material parameter related to the generation of dislocations
m	Material parameter
m	Number of discretized points in the horizontal direction
M_{\perp}	Diffusion mobility
M_{nuc}	Nucleation mobility
n	Number of discretized points in the vertical direction
p	Average dislocation density
r	Rescaled dislocation velocity
$t, \Delta t$	Time and time increment
v_{dis}	Dislocation velocity
x_1, x_2, x_3	Cartesian coordinates

Greek notations

Δ	Dissipation potential
δ	Width of grain boundary
Δ_{d}	Diffusion-related dissipation
Δ_{p}	Dissipation related to plastic deformation
Δ_{ρ}	Dissipation associated with a change in dislocation density
Δ_{D}	Dissipation associated with grain coarsening
δ_{ij}	Kronecker delta
$\dot{\rho}_{\dot{\epsilon}_e}$	Change in dislocation density caused by deformation
$\dot{\rho}_{\text{T}}$	Change in dislocation density for thermal process by deformation
$\dot{\epsilon}_{\text{d}}$	Time derivative of diffusion strain tensor
$\dot{\epsilon}_{\text{e}}$	Time derivative of elastic strain tensor
$\dot{\epsilon}_{\text{i}}$	Time derivative of inelastic strain tensor
$\dot{\epsilon}_{\text{p}}$	Time derivative of plastic strain tensor
ϵ_{d}	Effective strain of diffusion strain
ϵ_{p}	Effective strain of plastic strain
ϵ_{ijk}	Permutation symbol
γ	Specific grain boundary energy
γ_i	Kuhn-Tucker multiplier

$\hat{\Delta}_i$	Dissipation's assumption
$\hat{\mu}, \hat{\lambda}$	Elastic Lamé's moduli
λ	Lagrange multiplier
λ_i	Lagrange parameter
μ	Shear modulus
∇	Nabla operator
Ω	Body's volume
$\partial\Omega$	Body's surface
$\partial\Omega_t$	Body's boundary for given tractions
$\partial\Omega_u$	Body's boundary for given displacements
∂	(Partial) derivative
Ψ	Helmholtz free energy density
ψ_{dis}	Dislocation energy
ψ_e	Linear elastic energy
ψ_{gb}	Grain boundary energy
ρ	Dislocation density
$\boldsymbol{\sigma}$	Cauchy stress tensor
$\boldsymbol{\varepsilon}$	Linear strain tensor
$\boldsymbol{\varepsilon}_d$	Diffusion strain tensor
$\boldsymbol{\varepsilon}_e$	Elastic strain tensor
$\boldsymbol{\varepsilon}_i$	Inelastic strain tensor
$\boldsymbol{\varepsilon}_p$	Plastic strain tensor

List of Figures

2.1	Deformed and undeformed configuration.	12
2.2	Stress response.	14
2.3	Relationship between traction and stress.	14
2.4	Stress strain curve.	17
2.5	Rheological model for elasticity.	18
2.6	Rheological model for plasticity.	19
2.7	Rheological model for viscoelasticity.	19
2.8	Rheological model for viscoplasticity.	20
2.9	Rheological model for viscosity.	20
2.10	Metallic crystal structures.	21
2.11	Lattice parameters.	22
2.12	Different degrees of ordered structures.	22
2.13	Three types of defects.	23
2.14	Tilt boundary.	24
2.15	Twin boundary.	25
2.16	Recovery.	27
2.17	Dynamic recrystallization.	27
2.18	Grain size reduction by dynamic recrystallization (from Barnhoorn, 2003). Images reprinted by permission.	27
2.19	Dynamic recrystallization.	28
2.20	Creep strain vs. time.	30
2.21	Applied stress in creep test.	30
2.22	Strain v.s time in creep test.	30
2.23	Nabarro-Herring creep.	32
2.24	Coble creep.	33
2.25	Applied strain in relaxation test.	34
2.26	Stress v.s time in relaxation test.	34
3.1	Evolution of a nucleated grain.	43
3.2	Subset $d\Omega$ of the entire space, Ω	44
3.3	Evolution of a nucleated grain in $r - D$ domain.	46
3.4	Grain and its surrounding for the distribution function $f(p, D, r)$	47
3.5	Nucleation on triple lines.	48
3.6	Nucleation test.	53
3.7	Nucleation function depending on s	54
3.8	Arc curve.	55
3.9	Size of nucleated grain	56
4.1	Discretized body.	61
4.2	Uniformly meshed domain.	66
4.3	Uniformly meshed domain in $D \times r$	67
4.4	Uniformly meshed domain in $s \times r$	69

5.1	Typical analysis procedure in Abaqus.	80
5.2	“Life cycle” of grains.	82
5.3	Distribution function.	82
5.4	A part of the distribution function, $\gamma = 5.0 \times 10^{-3}$	82
5.5	Full distribution function, $\gamma = 5.0 \times 10^{-3}$	83
5.6	A part of the distribution function, $\gamma = 7.0 \times 10^{-0}$	83
5.7	Full distribution function, $\gamma = 7.0 \times 10^{-0}$	84
5.8	A part of the distribution function, $\mu = 6. \times 10^{+9}$	84
5.9	Full distribution function, $\mu = 6. \times 10^{+9}$	84
5.10	“Life cycle” of grains, $b = 5.34 \times 10^{-9}$	85
5.11	“Life cycle” of grains, $b = 5.34 \times 10^{-8}$	85
5.12	A part of the distribution function, $\ \dot{\epsilon}_p\ = 0.1407780 \times 10^{-1}$	86
5.13	Full distribution function, $\ \dot{\epsilon}_p\ = 0.1407780 \times 10^{-1}$	86
5.14	Full distribution function, $M_{\perp} = 2.2 \times 10^{-14}$	86
5.15	A part of the distribution function, $a_p = 1.03154 \times 10^{+6}$	87
5.16	Full distribution function, $a_p = 1.03154 \times 10^{+6}$	87
5.17	The “life cycle” of grains.	87
5.18	Full distribution function.	87
5.19	A part of the distribution function, $a_p = 1.03154 \times 10^{+6}$	88
5.20	“Life cycle” of grains, the distribution function, $k = 0.5$ and $k = 0.001$	88
5.21	“Life cycle” of grains, the distribution function, $\gamma = 0.0001$ and $\gamma = 0.00001$	90
5.22	“Life cycle” of grains, the distribution function, $D_0 = 0.0001$ and $D_0 = 0.000001$	90
5.23	Distribution function, $v = 1.13812 \times 10^{13}$	91
5.24	Distribution function, $\mu = 8. \times 10^{+8}$ and $\mu = 1. \times 10^{+9}$	91
5.25	Relaxation test; a) Geometry and boundary conditions; b) Applied deformation ; c) Applied strain, (from V. E.Isfahani, 2014). Images reprinted by permission.	93
5.26	Creep test; a) geometry and boundary conditions; b) Undeformed meshed body at $t_0 = 0s$, c) Deformed shape. Stress is constant in the spatial space, d) Applied pressure, (from V. E.Isfahani, 2014). Images reprinted by permission.	93
5.27	Total effective creep strain v.s plastic strain.	95
5.28	Evolution of mean rescaled dislocation density.	95
5.29	Evolution of mean grain size.	95
5.30	Evolution of λ	96
5.31	Diffusion strain rate v.s diffusion strain.	97
5.32	Evolution of Von Mises stress.	97
5.33	Flow law multiplier of dislocation creep.	97
5.34	Total effective creep strain in H-R model and in Abaqus.	97
5.35	Flow law multiplier of diffusion creep, $b = 5.34 \times 10^{-9}$	98
5.36	Evolution of creep strain rate, $b = 5.34 \times 10^{-9}$	98
5.37	Flow law multiplier of dislocation creep, $b = 5.34 \times 10^{-9}$	98
5.38	Evolution of diffusion creep rate, $b = 5.34 \times 10^{-9}$	98
5.39	Evolution of creep strain rate, $\mu = 3 \times 10^{+10}$	99
5.40	Evolution of diffusion creep rate, $\mu = 3 \times 10^{+10}$	99
5.41	Evolution of creep strain rate, $\mu = 3 \times 10^{+10}$	99
5.42	Evolution of diffusion creep rate, $\mu = 3 \times 10^{+10}$	99
5.43	Evolution of creep strain rate, $\mu = 3 \times 10^{+10}$	99
5.44	Evolution of Von Mises stress.	100

5.45	Plastic strain and total creep strain.	100
5.46	Evolution of diffusion strain.	100
5.47	Evolution of $\bar{\lambda}$	101
5.48	Plastic strain rate and plastic strain.	101
5.49	Total creep strain in Abaqus and in HR.	101
5.50	Flow multiplier of dislocation creep.	102
5.51	Evolution of plastic strain.	102
5.52	Evolution of mean rescaled dislocation density.	103
5.53	Evolution of mean grain size.	103
5.54	Evolution of Von Mises stress.	104
5.55	Evolution of plastic strain rate.	104
5.56	Diffusion strain rate v.s diffusion strain.	105
5.57	Plastic strain v.s total creep strain.	105
5.58	The flow multiplier for diffusion creep.	105
5.59	Total effective creep strain in H-R model and in Abaqus.	105
5.60	Plastic strain.	106
5.61	Total effective creep strain.	106
5.62	Diffusion strain rate v.s diffusion strain.	106
5.63	Flow law multiplier for dislocation creep.	106
5.64	Flow law multiplier for diffusion creep.	106
5.65	Probability distribution function.	107

List of Tables

3.1	Material parameters information	44
5.1	Material parameters for the model, $\bar{f}(D, r)$	81
5.2	Material parameters for the model, $f(p, D, r)$	89
5.3	Material parameters for the first model.	94
5.4	State-dependent variables for the first model.	94
5.5	Material parameters for the second model.	96
5.6	Material parameters for the third model	103

1 Introduction

1.1 Motivation

When homogeneous materials are under a load that exceeds the melting temperature, the microstructure of these material will be rearranged to build a new microstructure [Dmitrieva et al., 2009]. As a result, with the connection to the macroscopic, its behavior will be impacted. Moreover, Hall-Petch relationship indicates that grain size will strongly influence the yield stress. Consequently, the study of microstructure modification is very significant. One trendy method to see the mechanical properties and structure is material modelling. This method in continuum mechanics is to find a consistent set of evolution equations to exhibit the response of materials. One common model is called micromechanical models. When these models are derived successfully, in order to verify these models, a comparison by numerical results with an another believable result, for example, experiments should be carried out. Actually, a general material model is ability to predict material responses, especially, for complex materials.

Polycrystalline materials are the most widely used group of structural materials nowadays. At microscopic scale polycrystalline materials consist of many grains, which have different sizes and arrange in random crystallographic orientations, making the deformation in these materials complicated. Recrystallization occurs when the net of the grain boundaries in a polycrystalline material is rearranged. Dynamic recrystallization (DRX), which is associated with high temperature plastic deformation [Ding and Guo, 2001], happens during thermal and mechanical processes [Bernacki et al., 2009], and characterize mechanical properties of minerals and metallic materials. DRX can be observed in different materials such as minerals (olivine, sodium and potassium chlorides) [Poirier and Nicolas, 1975; Guillope and Poirier, 1979; Urai et al., 1986], metals (aluminium, ferritic steels, LiF, ferritic stainless) [Gourdet and Montheillet, 2003; Kim et al., 2001; Sitdikov and Kaibyshev, 2002], superalloys [Huber et al., 2008]. The recrystallization forms a new grain microstructures and indicated by the formation and migration of high angle grain boundaries driven by the stored energy of deformation [Doherty et al., 1997]. Therefore, investigating of DRX plays an important role to control microstructure evolution and mechanical properties of materials.

Modeling DRX can be based on phenomenological and semi-empirical models [Sandström and Lagneborg, 1975; Roberts and Ahlblom, 1978; Luton and Sellars, 1969] and reviewed details [Ding and Guo, 2001]. To simulate microstructure evolution during DRX, several studies base on the Monte Carlo model [Rollett et al., 1992; Peczak and Luton, 1993b,a, 1994; Peczak, 1995] and the cellular automaton method coupling fundamental metallurgical principles [Qian and Guo, 2004; Chen et al., 2009]. Very limited works attempt to relate macroscopic and microscopic behaviour, for example, Lui et al. [Liu et al., 2008]. They introduced a model of flow stress as the function of the peak stress and the strain and considered recrystallized volume fraction as the function of strain. Recently, K. Hackl and J. Renner [Hackl and Renner, 2013] proposed a variational approach for DRX to analyse microstructure evolution during a high temperature deformation. Their model is based on

an introduction of a distribution function to characterize the state of individual grains by grain size and dislocation density and can predict mechanical behaviours on macroscopic and microscopic scale. Different physical mechanisms such as dislocation mechanisms and diffusive mass transport are coupled to investigate DRX. Evolutions of grain size and dislocation density as well as flow laws for dislocation and diffusion creep were derived by the constrained minimization [Hackl and Fischer, 2008]. Continuing their work we will explore algorithms and numerical aspects to solve DRX problem at the microscopic scale. Then, mechanical behaviours of materials in microscopic scale will be linked to the macroscopic scale by two-scale modeling in Abaqus. Our model can apply for metallurgy and, especially, minerals in geology. We expect that numerical examples with the realistic parameters are shown to perform the theoretical formulation [Hackl and Renner, 2013]. Our aim is to construct a variational approach to study dynamic recrystallization of polycrystals at high temperatures. Basing on the mechanism of nucleation, the theory of nucleation is proposal in this work as well. This theory is essential as the initial guess for the distribution function on the numerical implementation. In order to deal with this problem numerically, a two-scale modelling (including a micro scale and a macro scale) is introduced. Marching algorithm is established to solve the microscale problem. The evolution of the microstructure on the material's rheology is captured via this result of the evolution of the distribution function. From the microscale problem, the required average quantities are calculated for the macroscale problem. Mechanical behaviours of materials in microscopic scale will be linked to macroscopic scale by two-scale modeling.

1.2 Methodology and organization of the thesis

In continuum mechanics, the purpose to model materials, the equations which show the reaction of materials during a test will be found. The entire framework to describe the behavior of a certain material will be called material modeling. Based on different principles, there are many directions to build a model. There are two kinds of models in material modeling, phenomenological models and micromechanical models. By fitting a set of parameters, engineers try to exhibit the material behavior via phenomenological models. Micromechanical models are obtained from understanding the real processes under loading. With the micromechanical models, these models will be validated by comparing the simulation results with experiments.

A brief introduction of mathematical fundamentals will be explained in Section 2. Then with these notations of mathematical knowledge, discussing related continuum mechanics is essential since we develop a model basing on it. The next topic of Section 2 will be about polycrystalline materials, dynamic recrystallization and some phenomena concerning dynamic recrystallization and polycrystalline materials.

Section 3 is dedicated to the mathematical model in detail. Since the model will be a multi-scale model then it will be convenient to discuss two smaller problems separately. Section 3.1 will deal with the variational approach which will be the root of the following mathematical model. In Section 3.2, some different version of the distribution function, which specifies each grain by grain size and dislocation density, will be presented. In this section, the new form of the distribution function will be discussed as well. Within this form, the distribution function characterizing a grain by a compound of three components: grain size, dislocation density and neighboring dislocation density. Next section in Chapter 3 will be the description of the problem at the macroscale. Moreover, the progress in generating the nucleation theory will be presented in Section 3.3.

The main duty of Section 4 is how to solve our mathematical model numerically. Section 4.1 will talk about the approximatedly numerical methods. These methods will be used in our numerical treatment. Section 4.2 will be spent on pointing out the marching algorithm. With this algorithm, the solution of the problem at the microscale will be found. How this algorithm is applied in each type version of the distribution function will be clarified in Section 4.2.1, Section 4.2.2 and Section 4.2.3. The last part of Section 4 is for the numerical implementation of the problem at the macroscale.

Section 5 will show the results after implementing our models numerically. The outcome of the microscale problem will be analyzed by comparing them with existing phenomenological ones. This is the main content of Section 5.2. After linking two problems in two scales will be compared with existing models in Abaqus. We will combine different kinds of distribution function and various nucleation theory. Section 5.4.1 discusses about the result of the first model where the first theory of nucleation and the distribution function $f(s, r)$ are applied. Section 5.4.2 and section 5.4.3 talk about the outcome of the second model and the third model, respectively. While within the second model, the distribution function is a function of s and r and the second nucleation theory is used, the third model is the combination of the standard distribution function and the third term concerning the nucleation process.

2 Mathematical and mechanical fundamentals

This part is devoted to some basic knowledge of mathematics and mechanics. The fundamentals will help to develop the mathematical model for dynamic recrystallization in polycrystals. Before introducing the fundamentals of mechanics concerning this thesis, the short review of basic mathematical concepts is considered. For more details relating to vector and tensor terms, readers can refer to [Holzapfel, 2000; E. A. de Souza Neto and Owen, 2008; R. B. Hetnarski, 2010; Chou and Pagano, 1992; Chadwick, 1999].

2.1 Vector and tensor analysis

2.1.1 Vector and tensor definition

This part introduces shortly mathematical fundamentals concerning vectors and tensors. It is just sufficient for the following parts. The definitions of scalars, vectors, and tensors will be discussed. This definition will be restricted to an open region Ω of a n -dimensional Euclidean space \mathbb{R}^n . Not only their definitions but also their operations are shown here.

Scalars

A function f is called a scalar field on Ω , for each x , we have a corresponding value of a scalar $f(x)$. A scalar is understood as a tensor of zero order. Small letters will denote scalars, for example, the scalar a is written as a .

Vectors

A set of scalars in a one dimensional array is a vector. A vector is a tensor of the first order. It has its length and direction in a geometric interpretation. Some physical quantities, e.g. position, velocity, acceleration, force are vectors. Bold letters are used to denote a vector field. For example, if $n = 3$, a vector \mathbf{x} is defined as

$$\mathbf{x} = \begin{pmatrix} x_1 \\ x_2 \\ x_3 \end{pmatrix} \text{ or } \mathbf{x} = (x_1, x_2, x_3)^T. \quad (2.1)$$

In general, a vector is a collection of n elements, we have

$$\mathbf{x} = \begin{pmatrix} x_1 \\ x_2 \\ \vdots \\ x_n \end{pmatrix} \text{ or } \mathbf{x} = (x_1, x_2, \dots, x_n)^T. \quad (2.2)$$

The magnitude or the length of vector \mathbf{x} , denoted by $\|\mathbf{x}\|$, is calculated as

$$\|\mathbf{x}\| = \sqrt{x_1^2 + x_2^2 + \dots + x_n^2}. \quad (2.3)$$

Definitions including multiplication, addition, and orthogonality are defined in the vector spaces. First multiplication by a scalar quantity λ is equal to

$$\lambda \mathbf{x} = \lambda \begin{pmatrix} x_1 \\ x_2 \\ \vdots \\ x_n \end{pmatrix} = \begin{pmatrix} \lambda x_1 \\ \lambda x_2 \\ \vdots \\ \lambda x_n \end{pmatrix}. \quad (2.4)$$

The summation of 2 vectors \mathbf{x} and \mathbf{y} on Ω , which we denote $\mathbf{x} + \mathbf{y}$, is a scalar calculated by

$$\mathbf{x} + \mathbf{y} = \begin{pmatrix} x_1 \\ x_2 \\ \vdots \\ x_n \end{pmatrix} + \begin{pmatrix} y_1 \\ y_2 \\ \vdots \\ y_n \end{pmatrix} = \begin{pmatrix} x_1 + y_1 \\ x_2 + y_2 \\ \vdots \\ x_n + y_n \end{pmatrix}. \quad (2.5)$$

We don't discuss all properties of commutative in this thesis. Only the below property is required that

$$\mathbf{x} + \mathbf{y} = \mathbf{y} + \mathbf{x}. \quad (2.6)$$

Furthermore, a dot product (or an inner product) of vector \mathbf{x} and vector \mathbf{y} , denoted by $\mathbf{x} \cdot \mathbf{y}$, assigns to this pair of vectors in Ω a scalar as follows

$$\mathbf{x} \cdot \mathbf{y} = x_1 y_1 + x_2 y_2 + \cdots + x_n y_n. \quad (2.7)$$

One property of the dot product is

$$\mathbf{x} \cdot \mathbf{y} = \|\mathbf{x}\| \|\mathbf{y}\| \cos \phi, \quad (2.8)$$

here ϕ is the angle enclosed by the two vectors.

Orthogonality

If the inner product of vector \mathbf{x} and vector \mathbf{y} is zero, they are called orthogonal. In the mathematical expression, we have

$$\mathbf{x} \perp \mathbf{y} = 0 \Leftrightarrow \mathbf{x} \cdot \mathbf{y} = 0. \quad (2.9)$$

Orthonormality

Two vectors \mathbf{x} and \mathbf{y} in Ω are called orthogonal if the two following conditions are fulfilled,

$$\begin{cases} \mathbf{x} \cdot \mathbf{y} = 0, \\ \|\mathbf{x}\| = \|\mathbf{y}\| = 1. \end{cases} \quad (2.10)$$

Tensors

In accordance to [R. B. Hetnarski, 2010], a linear transformation \mathbf{T} from a vector \mathbf{x} into a vector \mathbf{y} is a second-order tensor in a vector space $V \subset \mathbb{R}^n$ as below

$$\mathbf{y} = \mathbf{T} \mathbf{x}, \quad (2.11)$$

where $\mathbf{y} = (y_1, y_2, \dots, y_n)^T$, $\mathbf{x} = (x_1, x_2, \dots, x_n)^T$ and

$$\mathbf{T} = \begin{pmatrix} T_{11} & T_{12} & \cdots & T_{1n} \\ T_{21} & T_{22} & \cdots & T_{2n} \\ \vdots & \vdots & \vdots & \vdots \\ T_{n1} & T_{n2} & \cdots & T_{nn} \end{pmatrix}. \quad (2.12)$$

Some physical quantities in continuum mechanics are second-order tensors, such as the stress tensor, the strain tensor, and the conductivity tensor. This scheme can be extended to the definition of a tensor of arbitrary order. Based on the definition of the second order tensor, the third order tensor is similarly defined as a linear mapping transforming each vector into a second order tensor. Then a fourth order tensor is a linear mapping which converts a vector into a third order tensor. A tensor of the fourth order, for instance, can be represented as a matrix having matrices themselves as components. One familiar tensor of the fourth order is the elasticity tensor. The fourth order tensors is indicated by double stroke symbols, for example \mathbb{C} .

Mechanical and physical phenomena take place in the physical space \mathbb{R}^3 . Then let us limit our review here to the physical space \mathbb{R}^3 . In some literature, one useful way to represent a tensor is to use index-notation. Index-notation is a powerful tool to express tensors and their actions as well. To illustrate how this tool works, the orthogonal triad e.g. $\{\mathbf{e}_1, \mathbf{e}_2, \mathbf{e}_3\}$, the Cartesian basis, is introduced in a three-dimensional space. The unit basis $\{\mathbf{e}_1, \mathbf{e}_2, \mathbf{e}_3\}$ is indicated by

$$\mathbf{e}_1 = \begin{pmatrix} 1 \\ 0 \\ 0 \end{pmatrix}, \quad \mathbf{e}_2 = \begin{pmatrix} 0 \\ 1 \\ 0 \end{pmatrix}, \quad \text{and} \quad \mathbf{e}_3 = \begin{pmatrix} 0 \\ 0 \\ 1 \end{pmatrix}. \quad (2.13)$$

Thus, an arbitrary vector \mathbf{v} in \mathbb{R}^3 is expressed uniquely in terms of the components v_i in the given basis as

$$\mathbf{v} = v_1 \mathbf{e}_1 + v_2 \mathbf{e}_2 + v_3 \mathbf{e}_3 = \sum_{i=1}^3 v_i \mathbf{e}_i. \quad (2.14)$$

By using the summation convention of Einstein, we have

$$\mathbf{v} = \sum_{i=1}^3 v_i \mathbf{e}_i = v_i \mathbf{e}_i. \quad (2.15)$$

A second-order tensor can be expressed in terms of its components A_{ij} and the basis vectors \mathbf{e}_i as

$$\mathbf{A} = \sum_{i,j} A_{ij} \mathbf{e}_i \otimes \mathbf{e}_j = A_{ij} \mathbf{e}_i \mathbf{e}_j, \quad (2.16)$$

where \otimes is a dyadic product. The trace of a tensor \mathbf{A} is defined as $\text{tr}(\mathbf{A}) = \sum_i A_{ii}$. In the similar way, a fourth-order tensor is also written as

$$\mathbb{C} = \sum_{i,j,k,l} \mathbb{C}_{ijkl} \mathbf{e}_i \otimes \mathbf{e}_j \otimes \mathbf{e}_k \otimes \mathbf{e}_l = \mathbb{C}_{ijkl} \mathbf{e}_i \mathbf{e}_j \mathbf{e}_k \mathbf{e}_l, \quad (2.17)$$

where $i, j, k, l = (1, 2, 3)$.

2.1.2 Vector and tensor calculus

Transpose, symmetric and skew tensors

The transpose tensor of a tensor field $\mathbf{T} = T_{ij}\mathbf{e}_i\mathbf{e}_j$, denoted by \mathbf{T}^T , is a tensor, its components are determined by T_{ji} . We have

$$\mathbf{T}^T = T_{ji}\mathbf{e}_i\mathbf{e}_j. \quad (2.18)$$

Tensor, \mathbf{T} fulfills the following rule

$$\mathbf{T}\mathbf{u} \cdot \mathbf{v} = \mathbf{u} \cdot \mathbf{T}^T\mathbf{v}, \quad (2.19)$$

where \mathbf{u} and \mathbf{v} are vectors belonging to $\Omega \subset \mathbb{R}^3$.

The tensor \mathbf{T} is called a symmetric tensor when $\mathbf{T} = \mathbf{T}^T$. When the condition $T_{ij} = -T_{ji}$ is satisfied, the tensor \mathbf{T} is called as a skew tensor.

Products

A second-order tensor \mathbf{T} multiplied by a scalar α gives a second-order tensor, whose components are computed by multiplying every single component of the tensor \mathbf{T} with the scalar

$$\alpha\mathbf{T} = \begin{pmatrix} \alpha T_{11} & \alpha T_{12} & \cdots & \alpha T_{1n} \\ \alpha T_{21} & \alpha T_{22} & \cdots & \alpha T_{2n} \\ & \vdots & \vdots & \vdots \\ \alpha T_{n1} & \alpha T_{n2} & \cdots & \alpha T_{nn} \end{pmatrix}. \quad (2.20)$$

The dyadic product

The dyadic product between two vectors \mathbf{x} and \mathbf{y} is defined as

$$\mathbf{x} \otimes \mathbf{y} = \begin{bmatrix} x_1 \\ x_2 \\ x_3 \end{bmatrix} \otimes \begin{bmatrix} y_1 \\ y_2 \\ y_3 \end{bmatrix} = \begin{bmatrix} x_1y_1 & x_1y_2 & x_1y_3 \\ x_2y_1 & x_2y_2 & x_2y_3 \\ x_3y_1 & x_3y_2 & x_3y_3 \end{bmatrix}.$$

Gradient Operators

In \mathbb{R}^3 , the Nabla operator is defined as

$$\nabla = \frac{\partial}{\partial x_1}\mathbf{e}_1 + \frac{\partial}{\partial x_2}\mathbf{e}_2 + \frac{\partial}{\partial x_3}\mathbf{e}_3 = \frac{\partial}{\partial x_i}\mathbf{e}_i, \quad (2.21)$$

In general, the Nabla operator is $\nabla = (\partial/\partial x_1, \partial/\partial x_2, \dots, \partial/\partial x_n)^T$. Then gradient operator of a scalar function f is denoted as ∇f or $\text{grad}f$. Applying the gradient definition to a scalar field $f = f(x_1, x_2, \dots, x_n)$ reads

$$\nabla f = \frac{\partial f}{\partial x_1}\mathbf{e}_1 + \frac{\partial f}{\partial x_2}\mathbf{e}_2 + \cdots + \frac{\partial f}{\partial x_n}\mathbf{e}_n. \quad (2.22)$$

With a vector field \mathbf{F} , $\mathbf{F} = F_i \mathbf{e}_i$, and $F_i = F_i(x_1, \dots, x_n)$, where $i = 1, \dots, n$, its gradient is a second-order tensor as

$$\nabla \mathbf{F} = \begin{bmatrix} \frac{\partial F_1}{\partial x_1} & \frac{\partial F_1}{\partial x_2} & \dots & \frac{\partial F_1}{\partial x_n} \\ \frac{\partial F_2}{\partial x_1} & \frac{\partial F_2}{\partial x_2} & \dots & \frac{\partial F_2}{\partial x_n} \\ \vdots & \vdots & \dots & \vdots \\ \frac{\partial F_m}{\partial x_1} & \frac{\partial F_m}{\partial x_2} & \dots & \frac{\partial F_m}{\partial x_n} \end{bmatrix}.$$

In index-notation, the gradient of a vector \mathbf{F} has the following ansatz

$$\nabla \mathbf{F} = F_{i,j} \mathbf{e}_i \mathbf{e}_j, \quad (2.23)$$

where $F_{i,j}$ is the derivative of the components F_i with respect to x_j , i.e. $F_{i,j} = \partial F_i / \partial x_j$. The gradient of a tensor \mathbf{T} is defined as

$$\nabla \mathbf{T} = T_{i,j,k} \mathbf{e}_i \mathbf{e}_j \mathbf{e}_k, \quad (2.24)$$

where $T_{i,j,k}$ is the derivative of the components T_{ij} with respect to x_k .

Divergence Operators

The divergence of a vector field \mathbf{F} , denoted as $\nabla \cdot \mathbf{F}$ or $\text{div} \mathbf{F}$ is calculated as

$$\nabla \cdot \mathbf{F} = \text{div} \mathbf{F} = \frac{\partial F_1}{\partial x_1} + \frac{\partial F_2}{\partial x_2} + \dots + \frac{\partial F_n}{\partial x_n}. \quad (2.25)$$

This operator is rewritten as

$$\nabla \cdot \mathbf{F} = \text{div} \mathbf{F} = F_{i,i} = \frac{\partial F_i}{\partial x_i}. \quad (2.26)$$

In general, the divergence of an arbitrary tensor \mathbf{T} , $\nabla \cdot \mathbf{T}$, is defined as a dot product of a Nabla operator and the tensor by

$$\nabla \cdot \mathbf{T} = \text{div} \mathbf{T} = T_{i,j} \mathbf{e}_i. \quad (2.27)$$

Special Tensors

Here some special tensors are introduced. Let us assume to work in the n -dimensional space \mathbb{R}^n . The basis is composed of n orthogonal vectors, $\mathbf{e}_i = \{\mathbf{e}_1, \dots, \mathbf{e}_n\}$. This set also fulfills the condition

$$\mathbf{e}_i \cdot \mathbf{e}_j = \delta_{ij}, \quad (2.28)$$

where

$$\delta_{ij} = \begin{cases} 1 & \text{if } i = j \\ 0 & \text{if } i \neq j \end{cases}$$

δ_{ij} is the Kronecker delta. The unit second-order tensor has its components given by the Kronecker delta δ_{ij} .

Lagrange Method

The Lagrange multipliers method is a strong tool which helps us to solve a problem to maximize or minimize objective function with constraints. This method is based on considering critical points. Some examples are now discussed to clarify and understand this method. For example, in \mathbb{R}^n , we need to maximize (or minimize) a function $F(\mathbf{x})$ subject to the equality constraints $g_i(\mathbf{x}) = 0$, where $\mathbf{x} = \{x_1, x_2, \dots, x_n\}^T$. Here the number of constraints is m . Then the problem is written as

$$F(\mathbf{x}) \rightarrow \min_{\mathbf{x}}, \quad (2.29)$$

$$\text{s.t. } g_i(\mathbf{x}) = 0. \quad (2.30)$$

The following steps should be done to obtain the solution after establishing the problem,

1. Construct the Lagrange function \mathcal{L} ,
2. Calculate the gradient of the Lagrange function, $\nabla \mathcal{L}$,
3. Solve the equations $\nabla \mathcal{L} = \mathbf{0}$ to get the stationary points.

The Lagrange function is defined as follows

$$\mathcal{L}(\mathbf{x}, \boldsymbol{\lambda}) = F(\mathbf{x}) + \sum_1^m \lambda_i g_i(\mathbf{x}), \quad (2.31)$$

where λ_i are called Lagrange multipliers. The points satisfying the condition $\nabla \mathcal{L} = 0$ are called critical points.

The Karush Kuhn Tucker (KKT) conditions (the Kuhn Tucker conditions)

In the Lagrange method, only equality constraints are considered, Karush Kuhn Tucker (KKT) conditions are used to deal with inequality constraints. Let us consider the following problem which minimizes a function $F(\mathbf{x})$ subject to $g_i(\mathbf{x}) \leq 0$ and $h_j(\mathbf{x}) = 0$, the number of constraints of g and h are m and l , respectively. The problem is built as

$$F(\mathbf{x}) \rightarrow \min_{\mathbf{x}}, \quad (2.32)$$

$$\text{s.t. } g_i(\mathbf{x}) \leq 0, \quad (2.33)$$

$$h_j(\mathbf{x}) = 0. \quad (2.34)$$

The Lagrange function has the following form

$$\mathcal{L}(\mathbf{x}, \boldsymbol{\lambda}, \boldsymbol{\mu}) = F(\mathbf{x}) + \sum_1^l \lambda_j h_j + \sum_1^m \mu_i g_i, \quad (2.35)$$

where the Kuhn Tucker conditions are given as

$$\mu_i \geq 0 \quad \text{for all } i = 1, \dots, m, \quad (2.36)$$

$$\mu_i g_i = 0 \quad \text{for all } i = 1, \dots, m. \quad (2.37)$$

The chain rule

Let us consider a functional F depending on a function f . The function f itself is controlled by $x \in \Omega$ in the vector space $V \subset \mathbb{R}$.

$$\frac{dF}{dx} = \frac{dF}{df} \frac{df}{dx}. \quad (2.38)$$

In general, in \mathbb{R}^n with $\mathbf{x} = (x_1, x_2, \dots, x_n)^T$, we have

$$\frac{dF}{dx} = \frac{dF}{df} \frac{\partial f}{\partial x_1} + \frac{dF}{df} \frac{\partial f}{\partial x_2} + \dots + \frac{dF}{df} \frac{\partial f}{\partial x_n}. \quad (2.39)$$

The divergence theorem

This theory is known as Gauss's theorem. Let us consider a closed region \mathcal{B} with its surface or its boundary $\partial\mathcal{B}$. A scalar field λ , a vector field \mathbf{v} , and a tensor field \mathbf{T} are considered in this region. The divergence theorem shows the relationship between the volume integral over \mathcal{B} , $\int_{\mathcal{B}} dV$, and the surface integral on the boundary $\partial\mathcal{B}$, $\int_{\partial\mathcal{B}} dA$, divergence theorem are given by

$$\int_{\mathcal{B}} \nabla \lambda dV = \int_{\partial\mathcal{B}} \lambda \mathbf{n} dA, \quad (2.40)$$

$$\int_{\mathcal{B}} \nabla \cdot \mathbf{v} dV = \int_{\partial\mathcal{B}} \mathbf{v} \mathbf{n} dA, \quad \text{and} \quad (2.41)$$

$$\int_{\mathcal{B}} \nabla \cdot \mathbf{T} dV = \int_{\partial\mathcal{B}} \mathbf{T} \mathbf{n} dA, \quad (2.42)$$

where \mathbf{n} is the outward unit normal vector of the boundary $\partial\mathcal{B}$.

2.2 Continuum mechanics

In modelling materials, continuum mechanics mainly considers continuous masses. When materials are under certain loads, physical behaviors of materials can be observed. Continuum mechanics will help engineers to understand these behaviors by mathematical models. Moreover, to predict the material responses is a huge interest in the field of engineering. As we already knew, continuum mechanics deals with the dynamics of materials. Therefore, first let us introduce the displacement of an object as a continuum. Then the definition of strain tensor and stress tensor as well as their relationship are given. The next important part in continuum mechanics are the mass conservation and the constitutive law. More detailed information can be found in [Chadwick, 1999; Chou and Pagano, 1992].

2.2.1 Displacement and strain

In order to understand the mechanical behavior of materials, we need to build a mathematical model from the physical phenomenon. Basing on the classical continuum theory [Chadwick, 1999], a material body is considered as a continuum body. This body is an ensemble points, distributed continuously in space. Let us consider a body Ω_0 in \mathbb{R}^3 and its surface $\partial\Omega_0$. We will discuss about its particles. The motion of this body is also characterized by the motion of particles. In order to discuss the motion of every material point, we define a Cartesian coordinate system, constructed by a basis $\{\mathbf{e}_1, \mathbf{e}_2, \mathbf{e}_3\}$ and the fixed origin 0 . Therefore,

the position of a point P, given by \mathbf{x} in space, in the undeformed (original) configuration is expressed in terms of the components of the basis as

$$\mathbf{x} = x_1 \mathbf{e}_1 + x_2 \mathbf{e}_2 + x_3 \mathbf{e}_3. \quad (2.43)$$

Under the external actions, e.g. forces, heating, the body is deformed. The deformed body is denoted as Ω . In the deformed (current) configuration, the position of the material point Q is determined by the vector $\bar{\mathbf{x}}$ as

$$\bar{\mathbf{x}} = \bar{x}_1 \mathbf{e}_1 + \bar{x}_2 \mathbf{e}_2 + \bar{x}_3 \mathbf{e}_3. \quad (2.44)$$

The difference between the vector \mathbf{x} and $\bar{\mathbf{x}}$ is

$$u_i = \bar{x}_i - x_i, \quad i = 1, 2, 3. \quad (2.45)$$

Collection of all u_i will be defined as \mathbf{u} . This vector is called the displacement vector. As can be seen in Figure 2.13, a mapping illustrates the deformation mapping, $\phi : \Omega_0(\mathbb{R}^3) \rightarrow \Omega(\mathbb{R}^3)$. This mapping transfers \mathbf{x} to $\phi(\mathbf{x})$. In another expression, $\bar{\mathbf{x}} = \phi(\mathbf{x})$. Then the displacement is rewritten in terms of ϕ and \mathbf{x} as

$$\mathbf{u} = \bar{\mathbf{x}} - \mathbf{x} = \phi(\mathbf{x}) - \mathbf{x}. \quad (2.46)$$

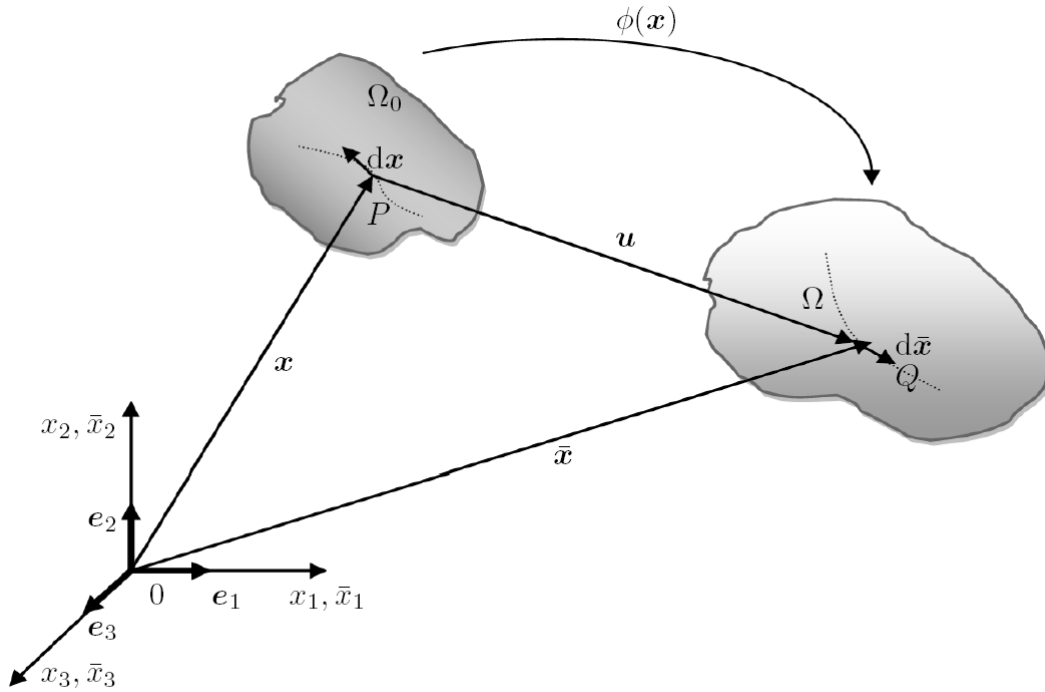


Figure 2.1: Deformed and undeformed configuration.

An infinitesimal line segment $d\mathbf{x}$ is transferred into $d\bar{\mathbf{x}}$ by

$$d\mathbf{x} = \frac{\partial \bar{\mathbf{x}}}{\partial \mathbf{x}} \cdot d\bar{\mathbf{x}} = \mathbf{F} \cdot d\bar{\mathbf{x}}, \quad (2.47)$$

where \mathbf{F} is called the deformation gradient tensor and $\mathbf{F} = \nabla \phi$. The symmetric small strains is defined as

$$\boldsymbol{\varepsilon} := \frac{1}{2}(\nabla \mathbf{u} + \mathbf{u} \nabla) = \frac{1}{2}(\nabla \mathbf{u} + (\nabla \mathbf{u})^T). \quad (2.48)$$

2.2.2 Force and stress

This part is devoted to discussing the forces which cause bodies to deform. Let us consider an arbitrary body Ω with the surface $\partial\Omega$. This surface is divided into two parts as

$$\partial\Omega = \partial\Omega_u \cup \partial\Omega_t,$$

where $\partial\Omega_u$ and $\partial\Omega_t$ are the surfaces on which surface forces and prescribed displacements are applied, respectively. These surfaces will be discussed later. In general, external forces, which will make this body to move, consist of two specific types, body forces and surface forces. The body forces are denoted by \mathbf{q} , $\mathbf{q}(\mathbf{x}) = q_i(\mathbf{x})\mathbf{e}_i$, $\mathbf{x} \in \Omega$.

These forces (e.g. gravitational forces, electromagnetic forces) are continuously distributed in the whole body Ω . Surface forces are denoted by \mathbf{p} , these forces are applied on $\partial\Omega_t$,

$$\mathbf{p}(\mathbf{x}, \mathbf{n}) = p_i(\mathbf{x}, \mathbf{n})\mathbf{e}_i, \quad \mathbf{x} \in \partial\Omega_t. \quad (2.49)$$

When the body is moved, reactions in the body will be created. These reactions are called internal forces. Now let us cut a body, an infinitesimal cube around the material point, we see an internal stress tensor or vector \mathbf{t} . As depicted in Figure 2.3, this force acts on an infinitesimal area element dA . With the geometry in the form of a cube, there are six normal vectors corresponding to six cut areas. Thus we also have six traction vectors \mathbf{t}_i . By collecting all terms \mathbf{t}_i , a second-order tensor $\boldsymbol{\sigma}$ is obtained. Then the Cauchy stress tensor $\boldsymbol{\sigma}$ is defined as

$$\boldsymbol{\sigma} \cdot \mathbf{n} = \mathbf{t}, \quad (2.50)$$

where $\mathbf{n} = (\mathbf{n}_1, \mathbf{n}_2, \mathbf{n}_3, -\mathbf{n}_1, -\mathbf{n}_2, -\mathbf{n}_3)^\top$, here \mathbf{n}_i is the unit normal vector to the plan i which is created by two basic vectors \mathbf{e}_j and \mathbf{e}_k subject to the condition $i \neq j \neq k$. Based on Cauchy theorem which postulates of a traction vector \mathbf{t} on an arbitrary cross section of a material body. The traction vector is defined as the ratio of the force Δf acting on the section and the cross-sectional area dA , when the area approaches zero. Thus the traction vector is

$$\mathbf{t} := \lim_{dA \rightarrow 0} \frac{\Delta f}{dA}. \quad (2.51)$$

In the index notation, traction vector's component is

$$\mathbf{t}^j = t_i^j \cdot \mathbf{e}_i, \quad (2.52)$$

where \mathbf{t}^j is the traction vector for the plane j . Thus, the index form of the stress tensor is given

$$\boldsymbol{\sigma} = \begin{pmatrix} \sigma_{11} & \sigma_{12} & \sigma_{13} \\ \sigma_{21} & \sigma_{22} & \sigma_{23} \\ \sigma_{31} & \sigma_{32} & \sigma_{33} \end{pmatrix}. \quad (2.53)$$

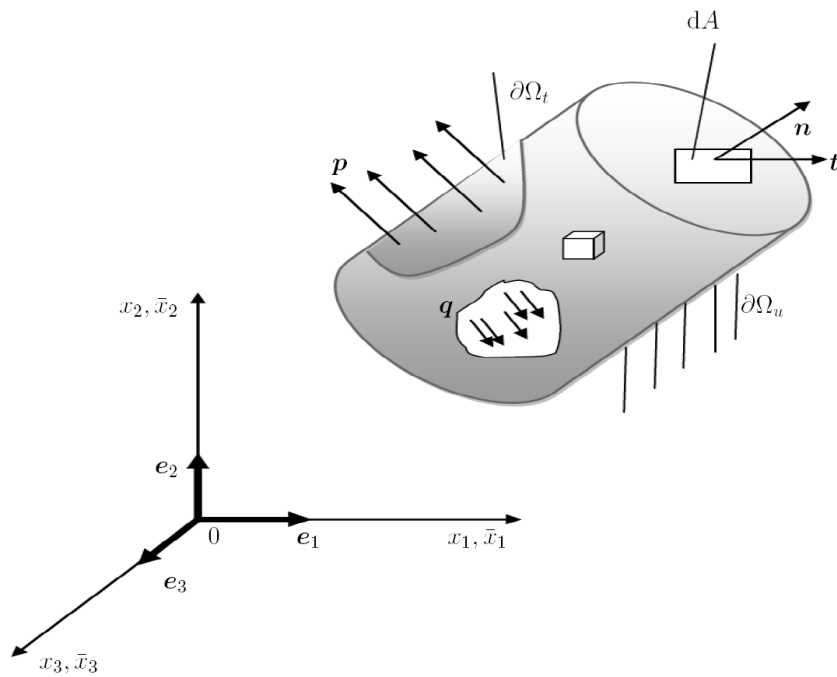


Figure 2.2: Stress response.

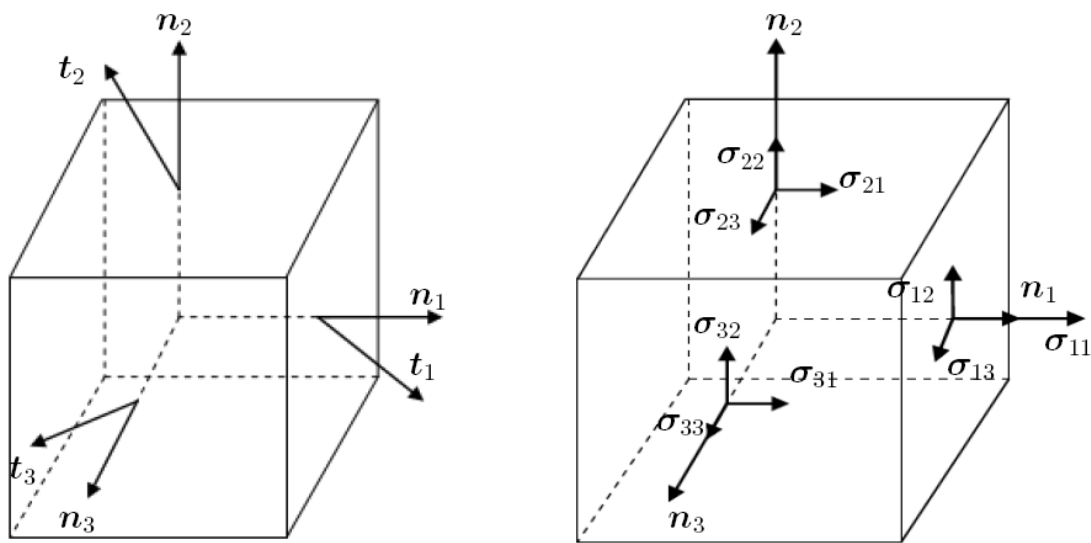


Figure 2.3: Relationship between traction and stress.

2.2.3 Conservation of mass

In the undeformed configuration, the mass of a body $\Omega_0 \subset \mathbb{R}^3$ is denoted as m . The conservation of mass postulates that mass can neither be created nor destroyed. Mass is a constant during deformation in the absence of sinks and source for mass. As mathematical expression, this law has the following form

$$m = \int_{\Omega_0} \rho(\mathbf{x}, t) dv = \text{const}, \quad (2.54)$$

where $\rho(\mathbf{x}, t)$ is the mass density in the original configuration and \mathbf{x} is an arbitrary point of the body Ω_0 . This law yields that the rate of the mass (the evolution of the mass) is zero as

$$\dot{m} = 0. \quad (2.55)$$

This rule also indicates that

$$\int_{\Omega_0} \rho(\mathbf{x}, t) dv = \int_{\Omega} \bar{\rho}(\bar{\mathbf{x}}, t) d\bar{v}, \quad (2.56)$$

with $\bar{\rho}(\bar{\mathbf{x}}, t)$ representing the mass density of the deformed body in the current configuration. The relationship between dv and $d\bar{v}$ is given as

$$d\bar{v} = dvJ, \quad (2.57)$$

here J is calculated by $J = \text{del} \mathbf{F}$. Equation (2.56) is rewritten as

$$\int_{\Omega} (\bar{\rho}(\bar{\mathbf{x}}, t) - \rho(\mathbf{x}, t)J^{-1}) d\bar{v} = 0 \quad \forall \mathbf{x}, \quad (2.58)$$

therefore,

$$\bar{\rho} = \rho J^{-1}. \quad (2.59)$$

Because the mass density in the original configuration is a function of the space, independent of time, this law is expressed as follows

$$\dot{\bar{\rho}} + \bar{\rho} \text{div} \dot{\bar{\mathbf{x}}} = 0. \quad (2.60)$$

This equation will be used in our model in the next part.

2.2.4 Constitutive equations

The link or the relationship between the strain tensor and the stress tensor is called a constitutive law which is expressed by a mathematical equation. It is also the aim of a mathematical model to describe the physical behavior of the material body. In this part, first of all, the general definitions concerning the constitutive equations will be discussed, then some simple examples of rheological models for elasticity, plasticity, and viscoplasticity will be introduced.

By observing a tensile experiment, the change in stress-strain relationship will be investigated step by step. Let us consider a simple uniaxial test for steel, a stress-strain relationship is depicted in Figure 2.4. As can be seen in Figure 2.4, this test is load-controlled. It can be illustrated in this Figure 2.4, from point O to point A, this is an elastic part and is a linear

curve. When we increase the load in this part, the stress-strain curve behaves linearly with the proportional factor E (Young's modulus). In this part, if a material body is unloaded, the body will return to point O or the strain is vanished. This part is also called the reversible part. In another expression, the initial state can be recovered by unloading. After the point A , if the load is continuously loaded, the linear relationship doesn't exist anymore. The plastic flow starts to occur. Then, we call A the yield point and the stress at point A is called the yield stress σ_y . After point A , the material is continued to exhibit the plastic flow before fracture. Before the fracture part, if the load is unloaded at point B , the stress-strain curve will be the line BC . This line is parallel to the line OA . In contrast to point O , the strain of point C is different from zero. Here let us remind again that in our work, only infinitesimal strains or small strains are considered. We still have the irreversible plastic strain ϵ_p . It means that the plastic deformation is considered as the permanent deformation. As can be seen in Figure 2.4, the total strain has two components, including elastic strain and plastic strain by

$$\boldsymbol{\epsilon} = \boldsymbol{\epsilon}_e + \boldsymbol{\epsilon}_p. \quad (2.61)$$

In the elastic theory, the constitutive equation for linear elasticity is characterized by Hooke's law as

$$\boldsymbol{\sigma} = \mathbb{C} : \boldsymbol{\epsilon}_e. \quad (2.62)$$

where \mathbb{C} is the elasticity tensor. The fourth-order elasticity tensor is given by

$$\mathbb{C} = \mathbb{C}_{ijkl} \mathbf{e}_i \otimes \mathbf{e}_j \otimes \mathbf{e}_k \otimes \mathbf{e}_l. \quad (2.63)$$

For isotropic materials, by using two independent material parameters, e.g. the Lamé' elastic moduli μ and λ , the elasticity tensor can be expressed as follows

$$\mathbb{C}_{ijkl} = \lambda \delta_{ij} \delta_{kl} + \mu (\delta_{ik} \delta_{jl} + \delta_{il} \delta_{jk}), \quad (2.64)$$

as a result, the constitutive law for linear elasticity reduces to

$$\boldsymbol{\sigma} = \lambda \text{tr}(\boldsymbol{\epsilon}) \mathbf{I} + 2\mu \boldsymbol{\epsilon}. \quad (2.65)$$

In index-notation, this law reads

$$\sigma_{ij} = \lambda \epsilon_{kk} \delta_{ij} + 2\mu \epsilon_{ij}. \quad (2.66)$$

Instead of using two parameters, the Lamé' constants μ and λ , we employ other parameters, for example, the Young's modulus E and the Poisson's ratio ν . Three terms, Young's modulus E , Poisson's ratio ν and the bulk modulus, K are related to others by

$$E = \nu \frac{3\lambda + 2\mu}{\lambda + \mu}, \quad \nu = \frac{\lambda}{2(\lambda + \mu)}, \quad K = \lambda + \frac{2}{3}\mu. \quad (2.67)$$

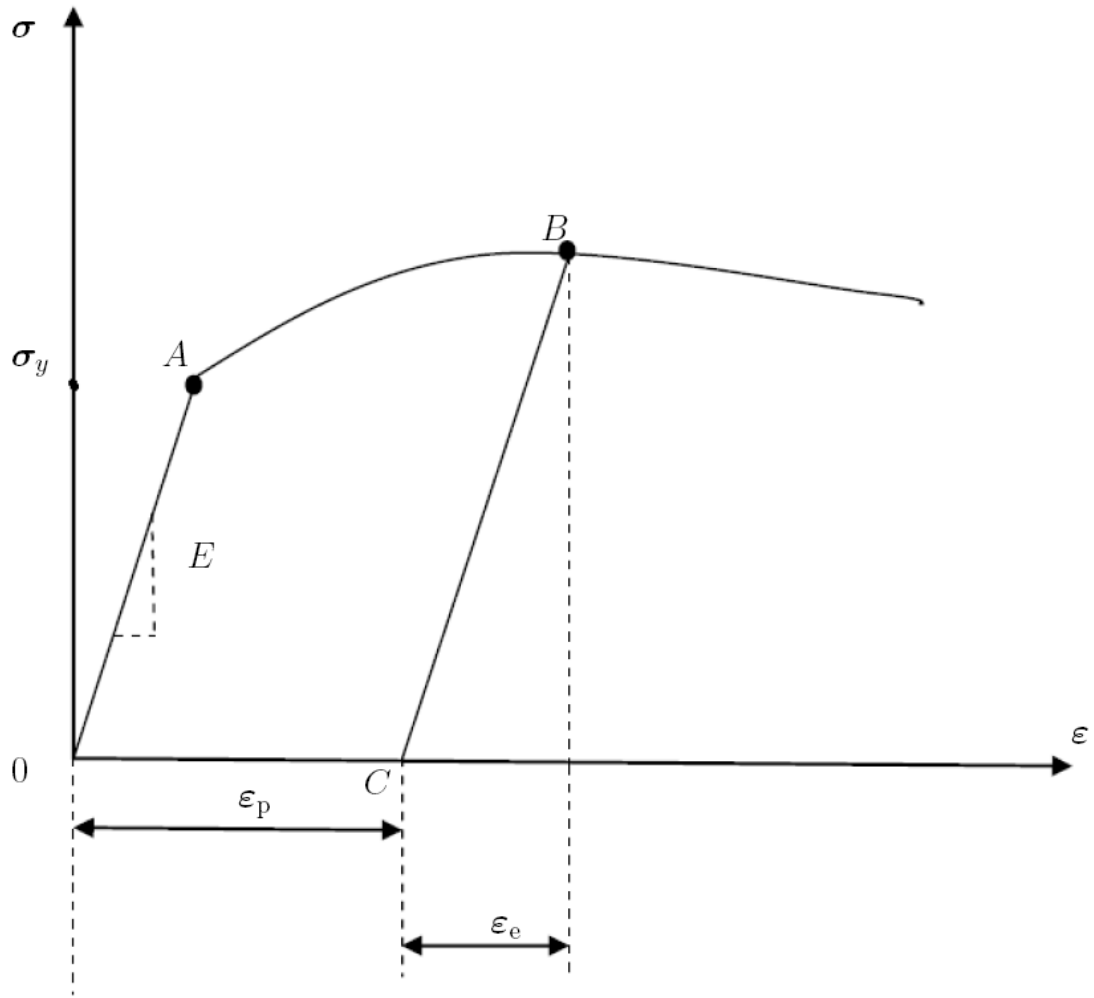


Figure 2.4: Stress strain curve.

In many engineering applications, it is easier to use these quantities (the stress tensor and the strain tensor) as vectors than as tensors. Let us introduce the Voigt notation for stresses and strains, then two terms are given by

$$\bar{\sigma} = (\sigma_{11}, \sigma_{22}, \sigma_{33}, \sigma_{12}, \sigma_{23}, \sigma_{31})^T, \quad (2.68)$$

$$\bar{\varepsilon}_e = (\varepsilon_{11}^e, \varepsilon_{22}^e, \varepsilon_{33}^e, \varepsilon_{12}^e, \varepsilon_{23}^e, \varepsilon_{31}^e)^T. \quad (2.69)$$

Then the constitutive equation for linear elasticity is expressed as

$$\bar{\sigma} = \mathbb{C} \cdot \bar{\varepsilon}_e, \quad (2.70)$$

the elasticity tensor has the following form

$$\mathbb{C} = \frac{E}{(1+\nu)(1-2\nu)} \begin{pmatrix} 1-\nu & \nu & \nu & 0 & 0 & 0 \\ \nu & 1-\nu & \nu & 0 & 0 & 0 \\ \nu & \nu & 1-\nu & 0 & 0 & 0 \\ 0 & 0 & 0 & \frac{1-2\nu}{\nu} & 0 & 0 \\ 0 & 0 & 0 & 0 & \frac{1-2\nu}{\nu} & 0 \\ 0 & 0 & 0 & 0 & 0 & \frac{1-2\nu}{\nu} \end{pmatrix} \quad (2.71)$$

Another direction to obtain a constitutive law indirectly from an elastic energy potential. The free energy for an elastic material is

$$\Psi(\boldsymbol{\varepsilon}) = \frac{1}{2} \boldsymbol{\varepsilon}_e^T : \mathbb{C} : \boldsymbol{\varepsilon}_e^T. \quad (2.72)$$

One possibility of the energy potential Ψ is the Helmholtz free energy, the stored elastic energy at a given point of the material body. This energy can be derived from experimental results, other phenomenological approaches. Since the restrict of this work is only for small deformation, then the derivative of the energy potential with respect to elastic strain $\boldsymbol{\varepsilon}_e$ is stress tensor as follows Moreover, the free energy Ψ for elastic materials can be derived in terms of $\boldsymbol{\varepsilon}$. The evaluation of the second derivative of the free energy at $\boldsymbol{\varepsilon} = \mathbf{0}$ is obviously a constant which is called elasticity tensor and denoted as

$$\mathbb{C} = \frac{\partial^2 \Psi}{\partial \boldsymbol{\varepsilon}^2} \Big|_{\boldsymbol{\varepsilon}=\mathbf{0}}. \quad (2.73)$$

Since stress $\boldsymbol{\sigma}$ and strain $\boldsymbol{\varepsilon}$ are both symmetric, respectively, the elastic constant \mathbb{C} is also a symmetry tensor as

$$\mathbb{C}_{ijkl} = \mathbb{C}_{ijlk} \quad \text{and} \quad \mathbb{C}_{ijkl} = \mathbb{C}_{jikl}. \quad (2.74)$$

Now the rheological models for some specific cases will be discussed.

Elasticity

The most simple case is elasticity (linear stress-strain dependence), the rheological model composes of a spring, as illustrated in Figure 2.5. When the spring is loaded with an increasing load, the strain increases as well. If the device is unloaded, the strain vanishes completely.



Figure 2.5: Rheological model for elasticity.

In this case, the total strain $\boldsymbol{\varepsilon}$ is equal to $\boldsymbol{\varepsilon}_e$. Then the constitutive law for the most simple case is computed as

$$\boldsymbol{\sigma} = \lambda \text{tr}(\boldsymbol{\varepsilon}) \mathbf{I} + 2\mu \boldsymbol{\varepsilon}. \quad (2.75)$$

In many texts, this case is called an ideal material behavior.

Plasticity



Figure 2.6: Rheological model for plasticity.

A system includes a friction device and a spring is the rheological model for elasto-plasticity, as can be seen in Figure 2.6. When the load is small and doesn't reach σ_y , strains only occur in the spring.

Viscoelasticity

When materials behave viscous as well as elastic characteristics under deformation, it will be called viscoelasticity. The viscous components can be modeled as dashpots. The stress and strain rate relationship can be given as

$$\sigma = \mu \frac{d\varepsilon}{dt} \quad (2.76)$$

where μ is the viscosity of the material. The Maxwell model is a rheological model for viscoelasticity. This model composes of a spring and a dashpot.



Figure 2.7: Rheological model for viscoelasticity.

Viscoplasticity

In continuum mechanics, a theory explaining the rate-dependent behavior of solid materials is considered as viscoplasticity. It means that the deformation of solids is dependent on the rate of the load which is applied on materials. As discussed above, the behavior of solids in viscoplasticity is also plastic deformation. The material experiences unrecoverable deformations when a load level is reached. Moreover, under the applied load, the viscoplastic material models has not only permanent deformations but also a creep flow as a function of time. Hookean spring elements are used to demonstrate the elastic response of viscoplastic materials in one-dimension. As same as in viscoelasticity, to illustrate the rate-dependence, a nonlinear dashpot element is utilized. By adding a sliding frictional element, plasticity can be taken into account as depicted in Figure 2.8.

While plasticity and elasticity are often used for solid materials, viscosity is deployed in fluids. Similar to plasticity, viscosity is hold in materials whose behaviors are time dependent. As can be seen in Figure 2.9, an example of the rheological model for viscosity can be a compose of a damper. As same as in the rheological model for plasticity, the damper will need the coefficient corresponding to the viscosity.

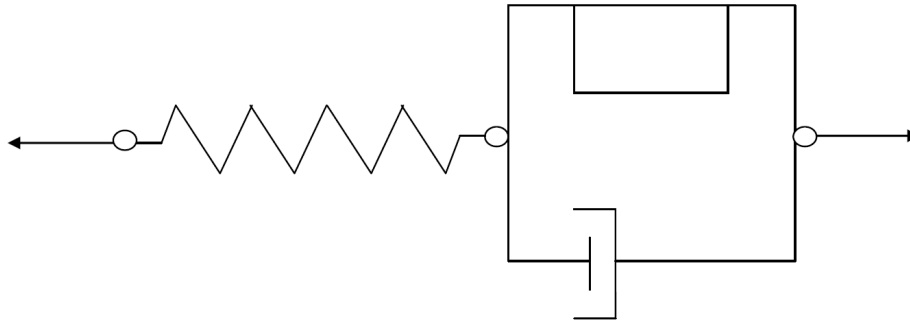


Figure 2.8: Rheological model for viscoplasticity.

Viscosity

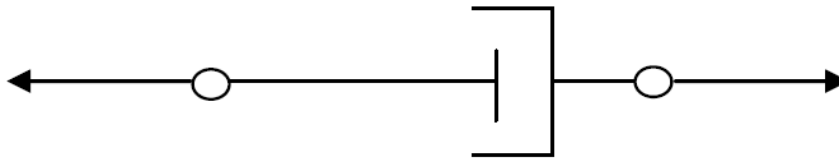


Figure 2.9: Rheological model for viscosity.

2.3 Polycrystalline materials

The previous parts were concerned primarily with the mathematical fundamentals and mechanical fundamentals. The present discussion is devoted to the structure of materials. Specifically, in the solid state, metals are formed by an assemble of atoms. As a result, first how atoms are arranged in materials will be discussed. Within this framework, concepts of crystallinity and noncrystallinity are introduced. Single crystals, polycrystalline materials, and noncrystalline materials are considered. Moreover, grain boundaries and defects are components of polycrystals are presented. The final section of this chapter briefly describes the phenomena for which we will build the mathematical models for polycrystalline materials. This is dynamic recrystallization. In order to get better understanding about this phenomena, some additive concepts are discussed as well. These concepts are recrystallization, static recrystallization and creep.

2.3.1 Crystals

The arrangement of atoms forms metals. Now let us define a crystalline solid or a crystal. In the microscopic structure, a crystal composes of constituents (such as atoms, molecules, or ions) which are arranged in a periodic way or structure way. These constituents will be situated in a repeating pattern. This repeating group creates a unit cell, the smallest structure block. The unit cell also defines the crystal structure by virtue of its geometry

and the atom positions within. Crystalline materials have different properties since they have different the unit cells, or the crystal structures. Based on the organization of atoms, the metallic crystal structure will be classified into three most common groups. They are the face-centered cubic crystal structure (FCC), the body-centered cubic crystal structure (BCC) and hexagonal close-packed crystal structure (HCP). The below figures will illustrate these different types of crystal structures. As can be seen in Figure 2.10, in an (FCC) crystal structure, the atoms are located at each of the corners as well as the centers of all the cube faces while in a (BCC) structure, atoms are located at all eight corners and a single atom at the cube center. Besides the unit cell with a cubic symmetry, a hexagonal is also used as a unit cell. In Figure 2.10, an (HCP) unit cell is shown. Each face on the top and at the bottom has six atoms. Another plane that provides three additional atoms to the unit cell is situated between the top and bottom planes. The atoms in this midplane have the nearest neighbors atoms in both of the two adjacent planes. The equivalent of six atoms is contained in each unit cell; one-sixth of each of the 12 top and bottom face corner atoms, one-half of each of the 2 center face atoms, and all 3 midplane interior atoms. Six lattice parameters: the three edge lengths a_1 , a_2 , and a_3 , and the three angles between three edges α , β , and γ will provide the geometry of the unit cell geometry completely. These parameters can be illustrated in Figure 2.12. These are considered as the lattice parameters of a crystal structure. As a result, it exists 14 types of called lattices. The detailed information of this lattices, the readers can refer to [Callister, 2007]. A crystallite is a small or even microscopic crystal which forms. Crystallites are also referred to as grains. In Figure 2.12, amorphous materials, such as glass and many polymers, are non-crystalline and do not display any structures as their constituents are not arranged in an ordered manner. The process of crystal formation via mechanisms of crystal growth is called crystallization or solidification. Each crystal has its crystallographic orientation.

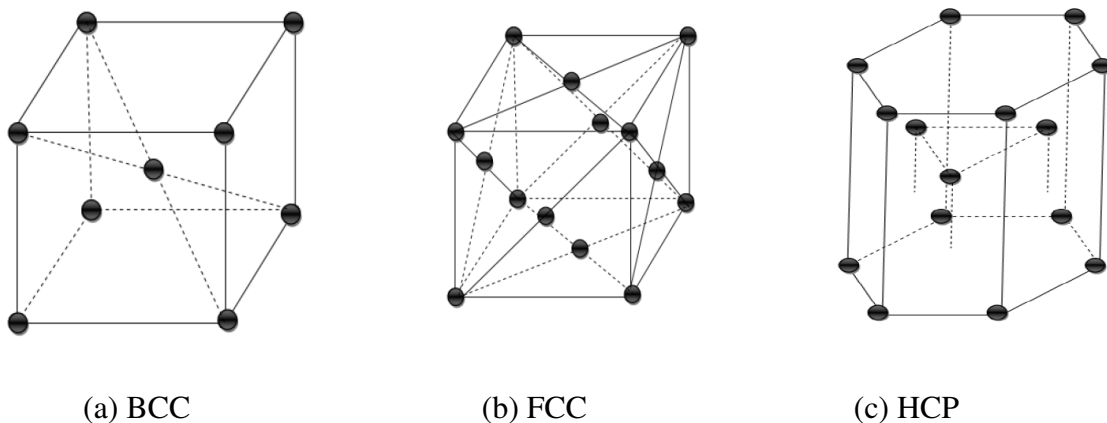


Figure 2.10: Metallic crystal structures.

2.3.2 Polycrystals

Polycrystalline materials are comprised of many small crystals or grains with different orientations joined at interfaces called grain boundaries. The term crystallography is used to discuss or research about crystals and crystal formation. Crystals have random crystallographic orientations, as indicated by the square grids which are represented by "balls". Microstructures have both geometric and crystallographic characteristics which influence their properties.

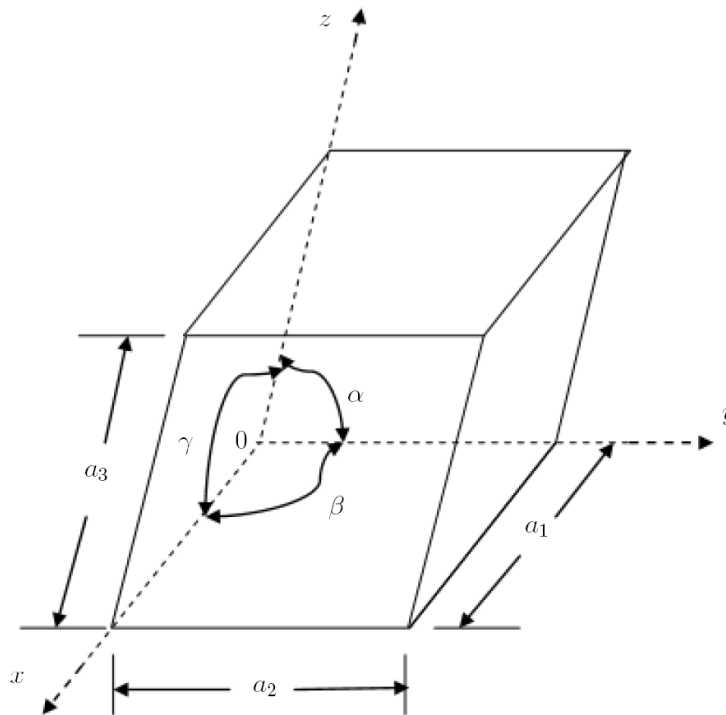
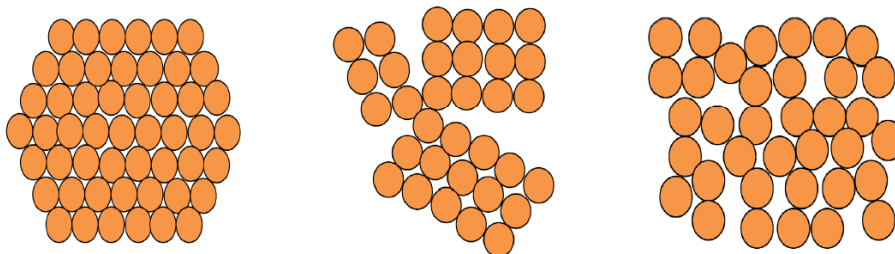


Figure 2.11: Lattice parameters.



(a) Crystalline

(b) Polycrystalline

(c) Amorphous

Figure 2.12: Different degrees of ordered structures.

2.3.3 Defects

In the reality, it is impossible to have perfect crystalline materials. Actually, materials always contain a huge number of defects. Experiments also show this problem. The purpose of this

part is to investigate defects. As we maybe know, defects will make a difference to the relationship between stress rate and strain rate as well as deformation mechanisms. Due to this affect, now let us classify the defects. Three groups of defects exist. They are point defects, line defects, and two-dimensional defects. Then the details and examples of these defects will be discussed.

- (*) Point defects: the simplest point defects are vacancies. This defect is because of a missing atom. Vacancies exist in all crystalline solids. Deformation by transport of vacancies, ions or atoms in the crystal structure is known as diffusion creep.
- (**) Line defects: lines along which the arrangement of atoms at the whole row in a solid is abnormal. As a result, the irregularity in spacing is most severe along a line called the line of dislocation. An example of line defects is a dislocation. This defect can weaken or strengthen solids. The phenomena when the dislocations are propagated via the crystal structure is known as dislocation glide and dislocation creep.
- (***) Two-dimensional defects: or surface defects, these defects occur at the boundary between two grains, or small crystals, within a polycrystal. Therefore, grain boundaries are two-dimensional defects. At certain conditions, grain centers exhibit relative motion. This deformation mechanism is known as grain boundary sliding. Other types of boundaries, along which the transport can occur, are phase boundaries, pores and particularly for calcite twin boundaries.

All three types of defects will affect microstructural characteristics, such as dynamic recrystallization which will be discussed in the following parts as well. Some of these defects are illustrated in Figure 2.13.

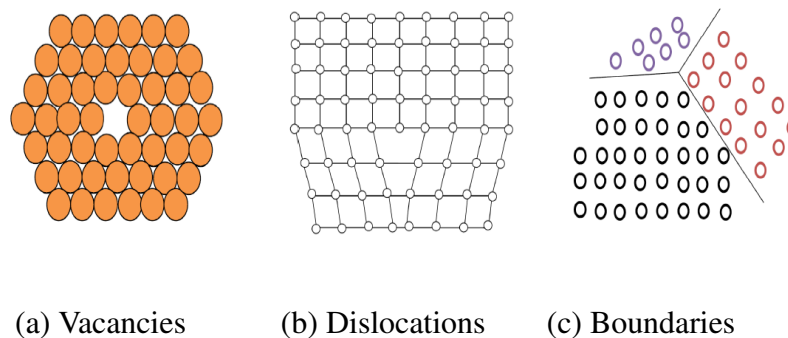


Figure 2.13: Three types of defects.

2.3.4 Grain boundaries

As discussed in the previous parts, an assemble of many grains or many crystals is polycrystalline material. Therefore, the interaction among grains plays an important role in understanding the microstructure. Thus, now the study of grain boundaries is conducted in this part. First, the definition of grain boundaries is presented. A grain boundary is an interfacial defect. Two grains or crystals with two different crystallographic orientations are separated by the interface which is called the grain boundary [Callister, 2007]. Moreover, if the grain size is smaller and finer, more grain boundaries are constructed. Grain boundaries also prevent the motion of dislocations in a material, so reducing crystallite size is a com-

mon way to improve mechanical strength. This can be seen from the Hall-Petch equation, a general relationship between mechanical properties and grain size is given by

$$\sigma_y = \sigma_0 + kd^{-1/2}, \quad (2.77)$$

where σ_y , k , and d are the yield strength, proportionality factor and grain size, respectively. σ_0 is material dependent intrinsic strength [Hirth, 1972].

Single crystal, only one grain, there is no grain boundaries. Deformation in metals stems mainly from dislocation motion and grain boundaries. However, grain boundaries stop dislocations from moving. Hence, the presence of more grain boundaries (finer grain size) will increase the resistance to deformation and enhance the strength. They are also important to many mechanisms of creep. Within the boundary region, each grain has its own crystallographic orientation, then there is some atomic mismatch in a transition from the crystalline orientation of one grain to that of an adjacent one. As a result, between two neighboring grains, there will be different degrees of crystallographic misalignment. Based on how large these degrees are, the grain boundaries will be sorted into two smaller groups: high angle grain boundaries (HAGBs) and low angle grain boundaries (LAGBs). LAGBs are used for boundaries with a mis-orientation smaller than around 15 degrees, in contrast to LAGBs, HAGBs are counterparts with the mis-orientation between the two grains larger than around 11 degrees. However, there are 'special boundaries' at particular orientations whose interfacial energies are notably lower than those of general HAGBs.

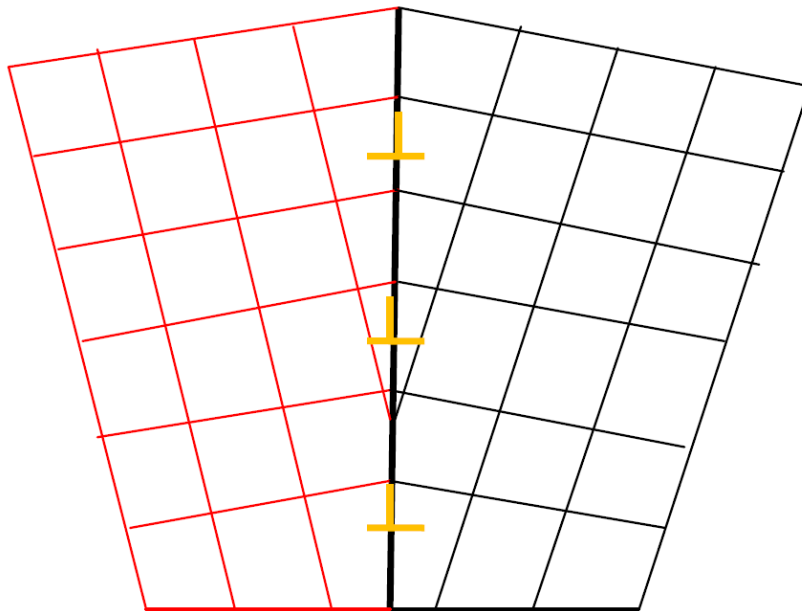


Figure 2.14: Tilt boundary.

They are special boundaries such as a tilt boundary and a twist boundary which are part of the low angle grain boundaries. As illustrated in Figure 2.14, the tilt boundary is depicted. This is the simplest boundary. Employing external force makes a single grain bent. This phenomenon will form the tilt boundary. The energy associated with the elastic bending of the lattice can be reduced by inserting a dislocation. This is essentially a half-plane of atoms acting like a wedge, which creates a permanent misorientation between the two sides. As the grain is bent further, more and more dislocations must be introduced to accommodate the deformation resulting in a growing wall of dislocations a low-angle boundary. The grain can now be divided into two sub-grains with different orientation. However, two grains are still related together crystallography. An alternative is a twist boundary where the misorientation occurs around an axis, perpendicular to the boundary plane. Two groups of screw dislocation incorporating each other creates the twist boundary. These concepts of tilt and twist boundaries represent somewhat idealized cases. In reality, to create the best fit between the adjacent grains, the majority of boundaries are formed by the mixture of various type of boundaries. An another special boundary is twin boundary as in Figure 2.15. If the dislocations in the boundary remain isolated and distinct, the boundary can be considered to be low-angle. If deformation continues, there is an increase in density of dislocations, then the space between neighboring dislocations is decreased. Eventually, the cores of the dislocations will begin to overlap and the ordered nature of the boundary will begin to break down. At this point, the boundary can be considered to be high-angle and the original grain to have separated into two entirely separate grains. In comparison to LAGBs, high-angle boundaries are considerably more disordered, with large areas of poor fit and a comparatively open structure. Indeed, they were originally thought to be some form of an amorphous or even liquid layer between the grains. Recovery can be defined as all annealing processes occurring in deformed materials that occur without the migration of a high angle grain boundary. Grain coarsening can, in turn, be defined as processes involving the migration of grain boundaries when the driving force for migration is solely the reduction of the grain boundary area itself [Callister, 2007].

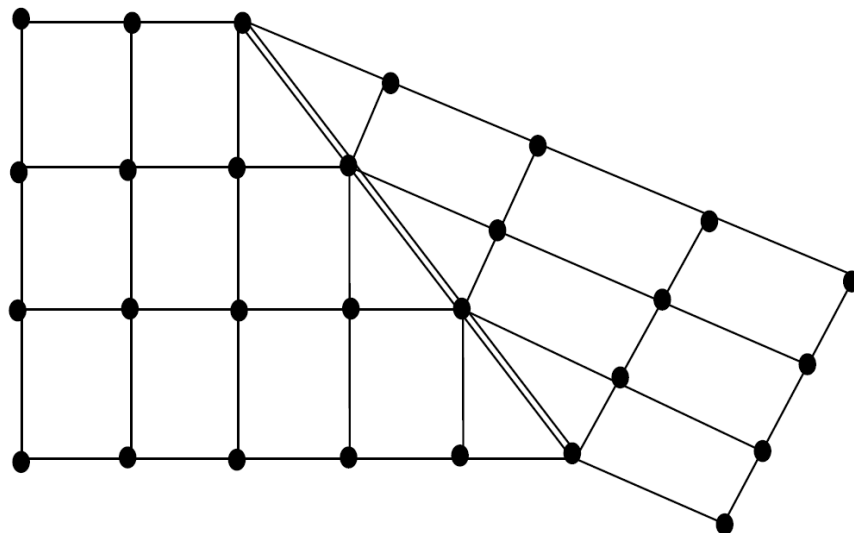


Figure 2.15: Twin boundary.

2.4 Recrystallization

In material science, the aim of the engineers is to find the properties of metallic materials. However, some properties are dependent largely on the structure of grain of microstructure in materials. Based on the grain microstructure, it is possible to predict the material properties by controlling and getting benefits of designed microstructures. Thus, it is vital to control advantage aspects of the grain microstructure in practical applications. Properties influenced by the grain structure contain strength, ductility, and resistance to creep deformation which are important quantities. Let us mention again that grain boundaries are one of the most important aspects of the grain microstructure. The reduction of the grain size yields an increasing amount of grain boundaries in the microstructure. The internally stored energy in the material will be increased by plastic deformation which is mostly because of the dislocation creation and dislocation rearrangement. Grain boundaries prevent the motion of dislocation motion and the accumulation of dislocation at the grain boundaries. This problem also affects the macroscopic deformation hardening of the material. Reducing the weight of products as well as controlling, these jobs can be done by customizing material properties reasonably. One of the main processes to develop or adjust the structure of grains at the micro is recrystallization. Firstly let us define recrystallization. Recrystallization is a process which rearranges grain boundaries in polycrystalline aggregates [Hackl and Renner, 2013]. In recrystallization, in order to reduce the stored energy in the material, a new grain can be grown up by consuming the surrounding cold-worked microstructure. The temperature as well as the rate of deformation will impact on the progress of recrystallization [material]. Static recrystallization and dynamic recrystallization are two different kinds of recrystallization. As mentioned before, recrystallization stems from effect of high temperature and plastic deformation. Therefore, static recrystallization is defined as a process which can be taken place by only high temperature without any deformation. At high temperature, it is a good condition for grain boundaries to migrate; this will reduce the internal energy. On the contrary, when the recrystallization happens together with an inelastic deformation, it is called dynamic or syntectonic recrystallization [Hackl and Renner, 2013].

2.4.1 Static recrystallization

Modifying the microstructure without deformation is known as static recrystallization. Now let us discuss more static recrystallization. Static recrystallization consists mainly of two processes: grain boundary migration (GBM) and grain boundary area reduction (GBAR). The minimum value of internal energy of the system obtained by the migration process of grain boundaries is called as grain boundary migration. It is handled by defect density gradients. Grain boundary migration refers to the movement of the boundary separating two grains. The second term is controlled by the boundary energy. Static (GBM) recrystallization occurs in a similar way as (GBM) during deformation. It produces irregular grain boundaries and some grains will be consumed whereas others will grow. During (GBAR) the surface area of grain boundaries is reduced. This also reduces the internal free energy. According to the theory, (GBAR) can happen during deformation, however, in the reality, it is more dominant after deformation terminated. Static recrystallization induced by heating of a previously deformed rock is known as annealing. It involves both (GBM) and (GBAR) reduction [Barnhoorn, 2003]. For more information regarding this term, readers can have a look [Humphreys and Hatherly, 2004].

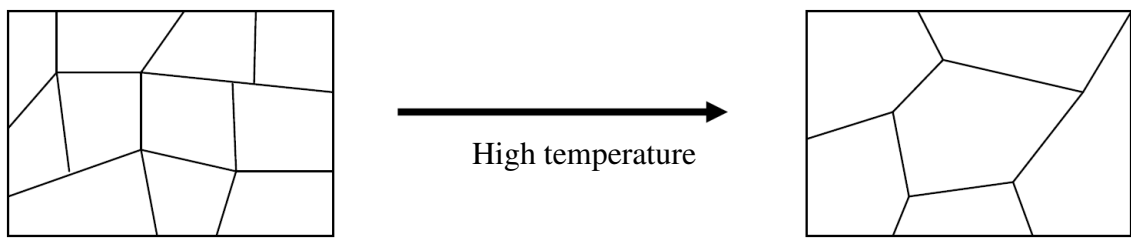


Figure 2.16: Recovery.

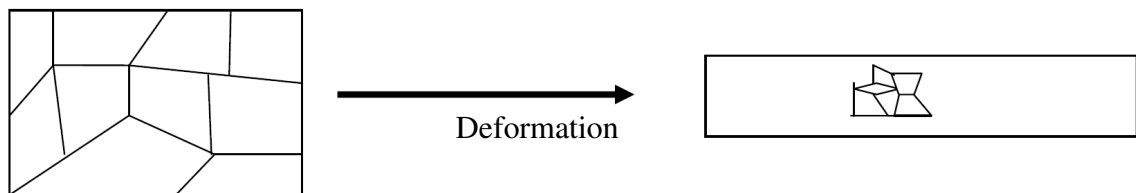


Figure 2.17: Dynamic recrystallization.

2.4.2 Dynamic recrystallization

At low to intermediate temperature, grain size is strongly effected by the kinetics of inelastic deformation. The organization of partial individual are dependent on stationary grain boundaries. Consequently, when sinks, sources, or obstacles are employed, boundaries make dislocation move. After that, gradients in dislocation density may trigger off grain boundary migration. Then the nucleation process of new grains takes place at the area of very high dislocation density, which leads to recovery.

In [Barnhoorn, 2003], dislocation creep is the dominant mechanism making the number of dislocation in materials raise. This progressive makes dislocations tangle. It prevents grains form moving and deforming and the internal energy increases as well. As mentioned before, boundary is the place where two grains contact with each other. The part of grains belongs to boundary is called subgrain boundaries. Each subgrain boundary has small misorientation. During deformation, the dislocations are increased, this leads to an increase of dislocations entering subgrain boundaries. This makes misorientation larger. When the misorientation reaches between 10-15 degree, a new grain boundary is formed. The process of the for-

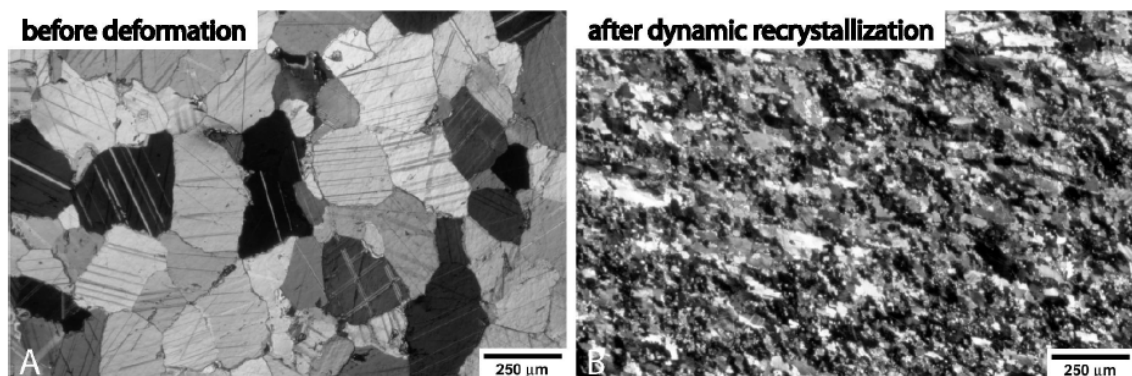


Figure 2.18: Grain size reduction by dynamic recrystallization (from Barnhoorn, 2003). Images reprinted by permission.

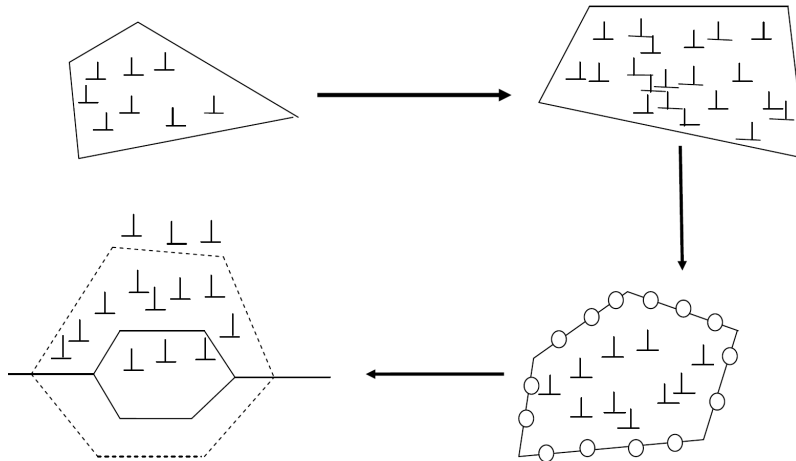


Figure 2.19: Dynamic recrystallization.

mation of these new grains from the old grains is called subgrain rotation recrystallization (SR). SR recrystallization is active when sufficient climb of dislocations occurs so that they can enter the subgrain boundary.

Another process reducing the number of dislocations in a crystal is the migration of grain boundaries. When differences in dislocation densities exist between neighbouring grains, there is a difference in internal energy. The system tries to reach a minimum internal energy by reorganizing free dislocations in the high-energy grain into lower energy configurations within the grain boundary. The result is that the boundary moves from the low energy grain (low dislocation density) towards the high energy grain (high dislocation density). In this way, the grain boundary migrates slightly at the expense of the highest dislocation density grain. In accordance with [Humphreys and Hatherly, 2004], dynamic recrystallization is defined as a combine grain boundary migration and subgrain rotation recrystallization (SR). Two mechanisms can happen simultaneously or one can dominate than the other. GBM may also take over from (SR) when a large number of subgrains are formed during deformation. In [Hackl and Renner, 2013], two significant mechanisms of dynamic recrystallization are nucleation and grain growth. We call the grains with small dislocation density are the young grains, and those with large dislocation density are old grains. Young grains have small energy while old grains have large energy. The details of two mechanisms will be discussed later. Now let brief introduce three steps of dynamic recrystallization. The first step is an increase of dislocations from few dislocations to many dislocations by plastic deformation. The increase of dislocations forces more dislocations move to the grain boundary. At the grain boundary, a new grain is nucleated by accumulating the dislocation with high energy. Nucleation process is the second step. Lastly, the new grains are formed and then grow up. These steps can be shown in Figure 2.19.

2.4.3 Nucleation mechanisms

Plastic deformation increases dislocation density. At a certain time, the number of dislocations can not be larger. At that time, the nucleation process is the next step to from a new grain by accumulating high energy dislocations and as a result, the material will have a new structure by self-organization. Nucleation is typically defined to be the process that calculates the time until a new phase or a new microstructure which is established. Nucleation is dependent mainly on the impurities of the system. This is the criteria to distinguish

different kinds of nucleation. Nucleation process is categorized into two groups: heterogeneous nucleation and homogeneous nucleation. The distinction between them is made according to the site at which nucleating events occur. If new grains of the new phase nucleate uniformly throughout the parent grains, the nucleation is defined as the homogeneous nucleation. When new grains are formed at structural inhomogeneities, for example, grain boundaries, dislocations, and container surfaces, the nucleation process is considered as the heterogeneous one.

2.4.4 Grain growth

Grain growth is the increase in size of grains (crystallites) in a material at high temperature. This further reduces the internal energy as well as the total area of the grain boundary. At high temperatures, the opposite is true since the open, disordered nature of grain boundaries means that vacancies can diffuse more rapidly down boundaries leading to more rapid Coble creep. It will be an advantage to have a good knowledge of grain growth to control the microstructures and then properties of materials in macroscale during deformation. According to [Humphreys and Hatherly, 2004], grain growth can be categorized into two types: normal grain growth and abnormal grain growth. The first item is defined when the microstructure coarsens uniformly. This is a continuous process. Contrary to the normal grain growth, abnormal grain growth is a discontinuous process, only some grains in the microstructure increase in length and consume smaller grains. After an initial transient period of growth, the microstructure reaches a quasi-stationary state in which the grain size distribution has an invariant form when expressed in terms of the grain size scaled by its mean value, and only the scale varies with some power of time. Such self-similarity is found for several growth processes such as particle coarsening or bubble growth (Mullins 1986), making this a challenging problem for modelers, who are often attracted more by the mathematical intricacies than the intrinsic importance of grain growth. During abnormal grain growth, which is a discontinuous process, a few grains in the microstructure grow and consume the matrix of smaller grains and a bimodal grain size distribution develops. However, eventually, these large grains impinge and normal grain growth may then resume. picture With a steel bar is applied by a small strain at high temperatures, then modelling materials by using the linear elasticity theory is no longer accurate. Then the introduction of time-dependent effects (creep/relaxation) may be reasonably considered to have a better result.

2.4.5 Creep

Creep is the plastic deformation, time-dependent deformation under a certain applied load. This deformation often occurs at high temperature. This is the reason why discussing creep is also important and relevant to this dissertation. The curve of classical creep showing the dependence of the creep on time is illustrated in Figure ???. This curve is for a tensile test of a steel bar. The test is controlled by the applied stress. There creep stages are displayed. They are primary creep, secondary creep, and tertiary creep. Now let us present creep stages. The primary creep firstly begins at a high strain rate and then reduces the rate with an increasing time. The strain rate then reaches a minimum and almost considers to be constant. This is because of work hardening. On the contrary, the secondary creep has a relatively uniform rate. In some literature, it is called a steady-state creep. In the end, this is tertiary creep which is accelerated with the creep rate and stops at the same time the material breaks. Fracture always occurs at the tertiary stage.

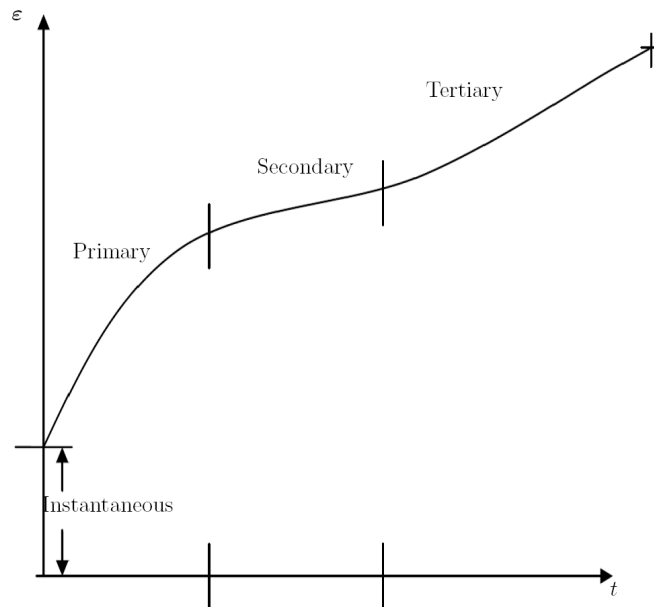


Figure 2.20: Creep strain vs. time.

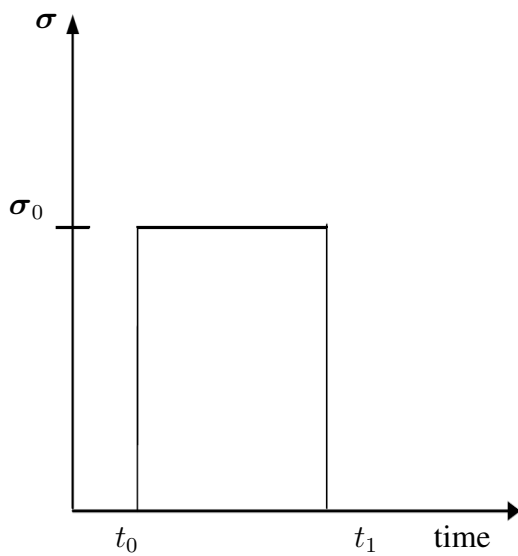


Figure 2.21: Applied stress in creep test.

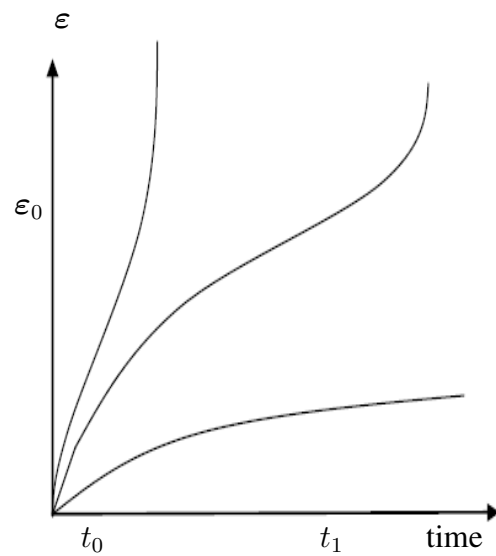


Figure 2.22: Strain v.s time in creep test.

Creep mechanisms

There are some creep mechanisms as follows

1. Diffusion creep: for instance, Nabarro-Herring creep.
2. Dislocation creep: this mechanism is managed by the motion of dislocations, it depends more on the applied stress.

The details of each mechanisms are discussed later.

Diffusion creep

The movement of defects through the lattice of a crystal in polycrystalline materials is caused by applying a large load. This movement will lead the migration of crystalline defects at the crystal faces along the direction of compression. This migration is called diffusion creep or the diffusion of vacancies through their crystal lattice. This also yields a net mass transfer of particles, for instance, atoms, ions or molecules, that shortens the crystal in the direction of maximum compression. This kind of creep leads plastic deformation. The diffusion creep is more dependent on temperature than on other deformation mechanisms. As a result, at high temperature, this phenomenon usually occurs. Let us mention two kinds of diffusion mechanisms. They are substitutional diffusion (or vacancy diffusion) and interstitial diffusion [Callister, 2007]. The previous one occurs at the place where atoms can move from one atomic site to another. Once the lattice has any vacancy, the substitutional diffusion will occur. The interstitial diffusion is the process when this is a movement of atoms through the atomic sites of the lattice. Another way to categorize the diffusion creeps, by using how the vacancies are diffused through a crystal. Due to the existence of grain boundaries in polycrystals, particles may move through the grains and also along the boundaries. If vacancies move through the crystal (in the material sciences often called a grain), this is called Herring-Nabarro Creep. Vacancies can move along the grain boundaries, a mechanism called Coble creep.

- Nabarro-Herring creep: Diffusion through Grain Volume

Transport of atoms through the crystal structure by intracrystalline diffusion is called Nabarro-Herring creep. Material is transported from high stress to low stresses by solid-state diffusion through the crystal. Nabarro-Herring creep rate equations typically have grain size exponents m of 2:

$$\dot{\epsilon} = \frac{ADGB}{kT} \frac{\delta}{b} \left(\frac{b}{d}\right)^3 \frac{\sigma}{G}, \quad (2.78)$$

where A , D , G , B , K , T , b , G are parameter material, d is grain size and σ is stress tensor.

- Coble creep: accommodation of strain by diffusion of atoms along the grain boundaries is called Coble creep, as illustrated in Figure ???. When the mean grain size is reduced, diffusion increase due to increases in internal interfaces. Transport of material by diffusion from high stress sites to low stress sites occurs not only inside of the crystals as in Nabarro-Herring creep, but can also occur along the grain boundaries of

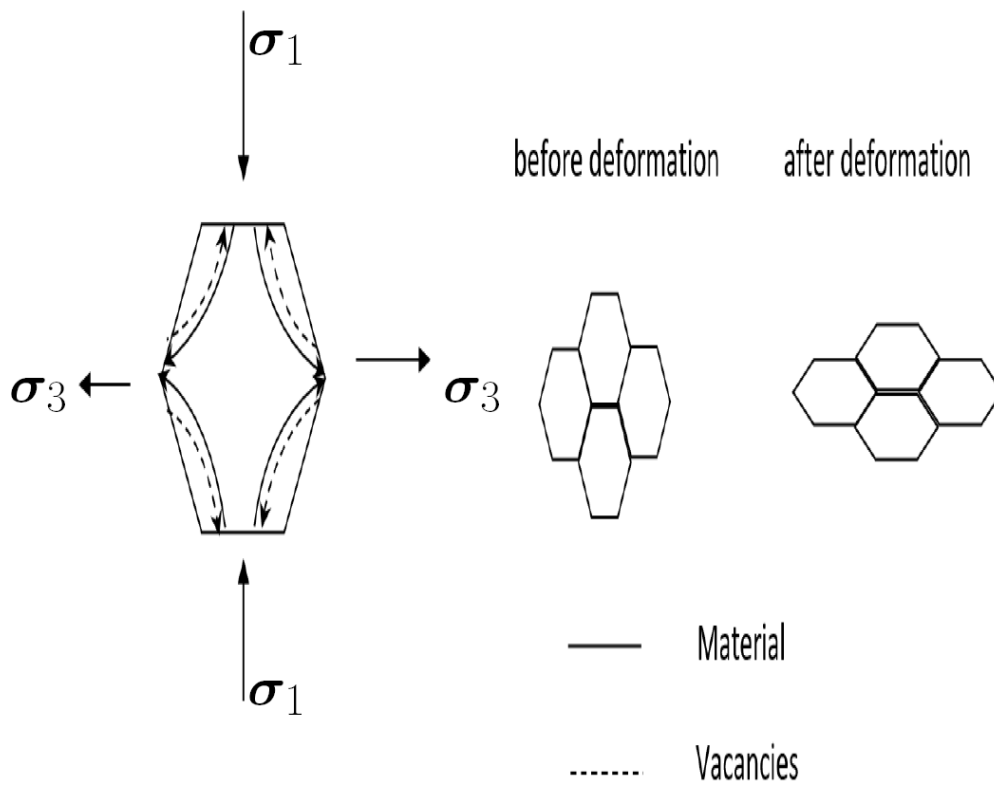


Figure 2.23: Nabarro-Herring creep.

grains. Coble creep can be described by a slightly different constitutive rate equation from that of Nabarro-Herring creep. Thus, Coble creep is expected to be more dominant with smaller grain sizes. As the stress increases and the temperature decreases, the rate of solid state diffusion along grain boundaries becomes more intense than in the bulk of the grains and hence it becomes the determinant of the creep strain. The following relationship for the creep rate was first obtained by Coble

$$\dot{\epsilon} = \frac{ADGB}{kT} \left(\frac{b}{d}\right)^2 \frac{\sigma}{G}, \quad (2.79)$$

where A , D , G , B , K , T , δ , b , G are parameter material, d is grain size and σ is stress tensor. To illustrate the creep, the typical creep rate equation is introduced.

Dislocation creep

From the name, dislocation creep, we can guess that this mechanism relates to dislocations. However, the more information how this mechanism depends on dislocation will be reviewed here. Firstly, dislocation creep is naturally a deformation mechanism in polycrystalline materials. Moreover, it connects with the movement of dislocations the crystal lattice of the material. Thus, dislocation creep is defined as the migration of dislocations within the lattice generating dissipation, which results in more stability of the microstructure. Dislocations migrate with a specific velocity which was estimated by Orowan:

$$\|\dot{\epsilon}_p\| = \chi_p b \rho v_{dis}, \quad (2.80)$$

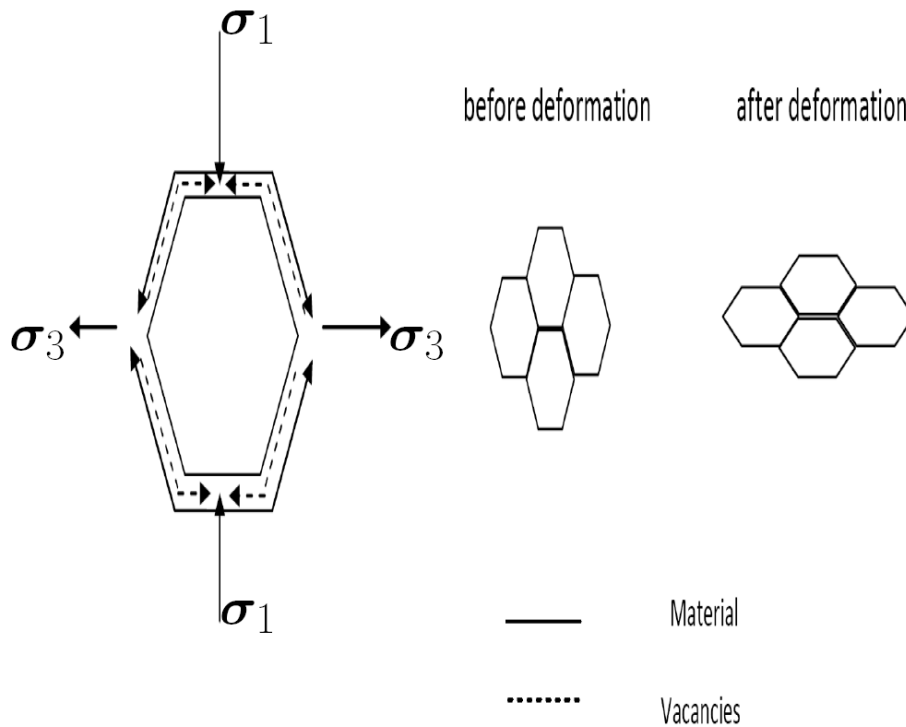


Figure 2.24: Coble creep.

here ε_p , χ_p and b are the plastic strain, a proportionality constant concerning the fraction of mobile dislocations, and the Burgers vector, respectively. Let us denote ρ one of the internal variables, called the dislocation density. Moreover, v_{dis} is the dislocation velocity which is determined by internal variables. As same as in diffusion creep, this creep leads plastic deformation as well. However, while diffusion creep is highly sensitive to the high temperature, the dislocation creep is hugely affected by the differential stress on the material. This mechanism will be the dominant mechanism when materials are deformed at relatively low temperatures. At high temperatures, material experiences mostly migration of dislocations instead of an increase in dislocation density [Hackl and Renner, 2013]. Some specific mechanisms belong to dislocation creep are introduced shortly as below. They are dislocation climb and dislocation glide.

- Dislocation climb

Because of the microstructure of polycrystalline materials, dislocations move out of the barriers easily to climb to another glide plane to avoid other dislocations. This phenomena is called dislocation climb. This phenomena is caused by self-spreading in the lattice at high temperature.

- Dislocation glide

When dislocations move, if the slip plane does not go up or down, the process is called dislocation glide. Dislocation glide is driven by the shear stress, which should be higher than a critical value so that dislocations can move.

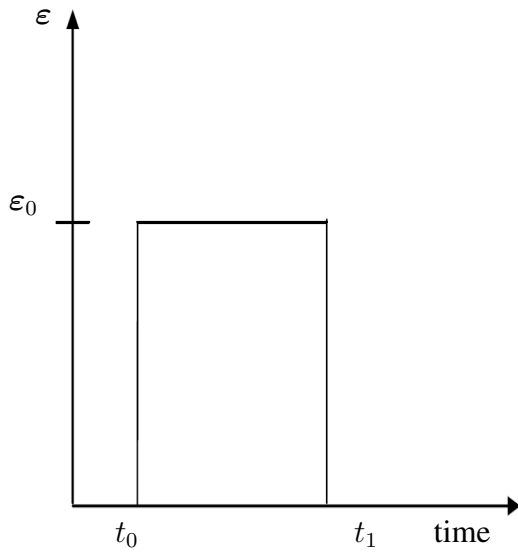


Figure 2.25: Applied strain in relaxation test.

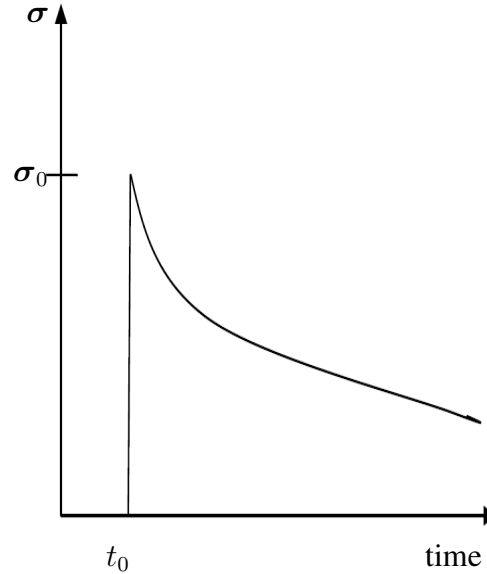


Figure 2.26: Stress v.s time in relaxation test.

2.4.6 Relaxation

Relaxation is the stress response due to a strain constant over a long range of time. In viscoplastic materials, relaxation tests demonstrate the stress relaxation in uniaxial loading at a constant strain. In fact, these tests characterize the viscosity and can be used to determine the relation which exists between the stress and the rate of viscoplastic strain. Therefore, the relaxation curve can be used to determine the rate of viscoplastic strain and hence the viscosity of the dashpot in a one-dimensional viscoplastic material model. The residual value that is reached when the stress has plateaued at the end of a relaxation test corresponds to the upper limit of elasticity. For some materials such as rock salt, such an upper limit of elasticity occurs at a very small value of stress and relaxation tests can be continued for more than a year without any observable plateau in the stress.

2.5 General variational approach

The success of a constitutive model describing the behaviour of a particular material depends critically on the choice of an appropriate set of internal variables. No plausible model will be general enough to describe the response of a material for all processes. If strain becomes larger, however, linear elasticity may no longer capture the observed response satisfactorily. In this case, a plasticity theory may be more appropriate. The main key of the constitutive model is the specific constitutive equation which characterizes the relationship between stress and strain. In reality, this equation will be more complicated than in the theory of elasticity where Hooke's law is employed. This complication is due to the large deformation and the range of materials in which the change in physical properties will affect the macroscopic material behavior. The purpose of this research is to simulate the dynamic recrystallization in polycrystalline materials, a general discussion of mechanical modelling of inelastic materials will be presented in this part. Since the importance of internal variables, first of all, let us introduce the set of internal variables as

$$\mathbf{x} = \{\mathbf{x}_k\}, \quad (2.81)$$

where $k = 1, \dots, n$, n is the number of internal variables. The external variables of the system are denoted as

$$\mathbf{X} = \{\mathbf{X}_k\}. \quad (2.82)$$

Internal variables and external variables might be scalars, vectors, and tensors. In our case, external variable is ε , the total strain. The combination of internal variables and external variables is addressed by

$$\mathbf{z} = \mathbf{z}(\mathbf{X}, \mathbf{x}). \quad (2.83)$$

Taking the derivative of internal variables and external variables with respect to time provides information of the evolution of variables by

$$\mathbf{V} = \dot{\mathbf{X}}, \quad \mathbf{v} = \dot{\mathbf{x}}. \quad (2.84)$$

Then the next step is define the specific Helmholtz free energy $\psi(\mathbf{z})$. The derivative of this energy will yield

$$\dot{\psi} = \frac{\partial \psi}{\partial \mathbf{X}} \cdot \frac{\partial \mathbf{X}}{\partial t} + \frac{\partial \psi}{\partial \mathbf{x}} \cdot \frac{\partial \mathbf{x}}{\partial t}. \quad (2.85)$$

This equation is rewritten by using \mathbf{V} , and dissipation function Δ

$$\dot{\psi} = \frac{\partial \psi}{\partial \mathbf{X}} \cdot \mathbf{V} - \Delta, \quad (2.86)$$

where the specific dissipation Δ has the following ansatz

$$\Delta = \sum_{i=1}^n \left(-\frac{\partial \psi}{\partial \mathbf{x}_i} \right) \cdot \mathbf{v}_i = \sum_{i=1}^n \Delta_i(\mathbf{z}, \mathbf{v}_i). \quad (2.87)$$

From this equation, the dissipation of the system is split into different dissipation process corresponding to each internal variable. Moreover, assumptions concerning the constraints of different kinds of dissipation are given by

$$\Delta_i(\mathbf{z}, \mathbf{v}_i) = \hat{\Delta}_i(\mathbf{z}, \mathbf{v}_i).$$

Using the variational principle, the optimization problem is now formulated as

$$\dot{\psi} \rightarrow \min_{\mathbf{v}_i}, \quad (2.88)$$

$$\text{s.t. } \Delta_i = \hat{\Delta}_i. \quad (2.89)$$

Employing the principle of maximum dissipation (PMD) for the problem (2.88) [Hackl and Fischer, 2008], Lagrange function with Lagrange multipliers λ_i , $i = 1, \dots, n$ is built as

$$\mathcal{L} = \dot{\psi} + \sum_{i=1}^n \lambda_i (\Delta_i - \hat{\Delta}_i), \quad (2.90)$$

using the stationarity conditions, $\partial \mathcal{L} / \partial \mathbf{v}_i = 0$ yields

$$\hat{\Delta}_i = \frac{\lambda_i}{1 - \lambda_i} \frac{\partial \hat{\Delta}}{\partial \mathbf{v}_i} \cdot \mathbf{v}_i. \quad (2.91)$$

Lastly, the implicit evolution equations for \mathbf{v}_i in terms of the observable variables \mathbf{z} is

$$\mathbf{v}_i = f(\mathbf{X}, \mathbf{v}). \quad (2.92)$$

We then have the general constitutive law

$$\begin{cases} \psi = \psi(\mathbf{X}, \mathbf{x}), \\ \boldsymbol{\sigma} = \frac{\partial \psi}{\partial \boldsymbol{\varepsilon}} = \boldsymbol{\sigma}(\mathbf{X}, \mathbf{x}), \\ \mathbf{v}_i = f(\mathbf{X}, \mathbf{v}). \end{cases} \quad (2.93)$$

The time is discretized into $[t_0, t_1, \dots, t_n]$. The general constitutive law will be performed implicitly. Let us consider a general interval $[t_k, t_{k+1}]$. The values of $\mathbf{x}_k, \mathbf{X}_k$ are given, the prescribed incremental external variables $\Delta \mathbf{X}$ for internal variables are given as well. The main requirement of modeling a physical phenomena is to build a mathematical model by introducing the constitutive equation for inelastic materials. As a result, that the incremental stress-strain function reads

$$\boldsymbol{\sigma}_{n+1} = \boldsymbol{\sigma}(\mathbf{X}_{n+1}, \mathbf{x}_{n+1}). \quad (2.94)$$

Consequently, consistent tangent modulus for numerical integration algorithms is derived as

$$\mathbb{D} = \frac{\partial \boldsymbol{\sigma}}{\partial \boldsymbol{\varepsilon}_{n+1}}. \quad (2.95)$$

For more information relating the numerical treatment for plasticity, readers can refer to [E. A. de Souza Neto and Owen, 2008].

3 Mathematical model

The aim of this part is to derive a mathematical model for dynamic recrystallization of polycrystalline materials. From the variational framework for deriving microstructure evolution during inelastic high-temperature deformation, a summary of Hackl-Renner (H-R) model proposed in [Hackl and Renner, 2013] is first described. From this framework, we establish the problem at the microscale with the volume constraint. In dynamic recrystallization, nucleation is the initial process to create a new microstructure. Thus, theories for the nucleation process also need to be discussed in this chapter. Three suggested theories relating to this term will be derived. At the beginning, only a simple ansatz for this theory is applied. Deriving from phenomenology, two extended theories are proposed and are then employed in our problem. For the problem description at the microscale, there models: the original distribution function, $f(D, \rho)$, the modified distribution function, $\bar{f}(D, r)$, and the extended counterpart, $\tilde{f}(s, r)$, are here investigated. To investigate the reaction of materials in a test, the problem at the microscale should be linked to the problem at the macroscale. This chapter will end with the mathematical model of the macroscale. The basic thermodynamic problem, a general viscoplastic problem, is used at the macroscale in our model.

3.1 Variational approach for dynamic recrystallization

To derive the mathematical framework for dynamic recrystallization, the observable variables are proposed. To describe the system, the state variables $\mathbf{z} = \mathbf{z}(\mathbf{X}, \mathbf{x})$, where \mathbf{X} is a set of external variables and \mathbf{x} collects internal variables. The thermodynamic fluxes are defined by

$$\mathbf{V} = \dot{\mathbf{X}}, \quad \mathbf{v} = \dot{\mathbf{x}}, \quad (3.1)$$

where $\dot{\mathbf{X}}$, and $\dot{\mathbf{x}}$ are the material time derivative of \mathbf{X} , and \mathbf{x} , respectively. In our approach, the set of external variables is $\mathbf{X} = \boldsymbol{\varepsilon}$, the total strain, and internal variables are $\mathbf{x} = \{\rho, D, \boldsymbol{\varepsilon}_p, \boldsymbol{\varepsilon}_d\}$, where ρ is dislocation density, D is grain size, $\boldsymbol{\varepsilon}_p$ is plastic strain and $\boldsymbol{\varepsilon}_d$ is dislocation strain. For a polycrystalline aggregate, Hackl and Renner introduced a distribution function, $f(\mathbf{z}, t)$, characterizing individual grains by observable variables. Then $f(\mathbf{z}, t)d\Omega$ gives the probability to locate a grain in the subset $d\Omega \subset \Omega$. The representative value of a property g (denoted as $\langle \cdot \rangle$) is defined as

$$\langle g \rangle = \int_{\Omega} g f d\Omega. \quad (3.2)$$

Assuming spherical grains with diameter D , the average or representative volume $\langle \Pi D^3/6 \rangle$ is calculated as

$$V = \frac{\Pi}{6} \int_{\Omega} D^3 f d\Omega. \quad (3.3)$$

Consequently, the total amount of grains is calculated by

$$N = \int_{\Omega} f d\Omega. \quad (3.4)$$

The rate of this total amount is determined by the subtraction of the source function h , the number of grains in nucleation process, and the surface integral amount which goes into or leaves its boundary $\partial\Omega$. We obtain

$$\dot{N} = \int_{\Omega} \dot{f} d\Omega = \int_{\Omega} h d\Omega - \int_{\partial\Omega} f \dot{\mathbf{z}} \cdot d\mathbf{A}. \quad (3.5)$$

Employing Gauss' theorem and the localization theorem yields

$$\dot{f} + \nabla \cdot (f \dot{\mathbf{z}}) = h. \quad (3.6)$$

This equation plays an important role in our research since this differential equation is the main equation of the microscale problem solved numerically. Within our variational approach, the evolution equations are obtained by applying and adopting the principle of the minimum of the dissipation potential (PMDP), so that energy is minimized as well as dissipation is maximized. The formulations of free energy and dissipation are listed. The free energy of dynamic recrystallization process is obtained from

$$\Psi = \frac{\Pi}{6} \langle D^3 \psi \rangle, \quad (3.7)$$

where ψ is the specific free energy separating as

$$\psi(D, \rho, \boldsymbol{\varepsilon}_e) = \psi_e(\boldsymbol{\varepsilon}_e) + \psi_{\text{dis}}(D, \rho) + \psi_{\text{gb}}(D). \quad (3.8)$$

The member energies are given by

$$\begin{cases} \psi_e(\boldsymbol{\varepsilon}_e) &= \frac{1}{2} \boldsymbol{\varepsilon}_e : \mathbb{D} : \boldsymbol{\varepsilon}_e, \\ \psi_{\text{dis}}(D, \rho) &= \frac{6\gamma}{D}, \\ \psi_{\text{gb}}(D) &= \mu b^2 \rho, \end{cases} \quad (3.9)$$

where ψ_e is the linear elastic energy, ψ_{gb} is the grain boundary energy, and ψ_{dis} is the dislocation energy. Other parameters are mentioned in Table 3.1. The total strain of a grain, $\boldsymbol{\varepsilon}$, is decomposed into the elastic part $\boldsymbol{\varepsilon}_e$ and the inelastic part $\boldsymbol{\varepsilon}_i$. Then the total strain rate, $\dot{\boldsymbol{\varepsilon}}$, equals the summation

$$\dot{\boldsymbol{\varepsilon}} = \dot{\boldsymbol{\varepsilon}}_i + \dot{\boldsymbol{\varepsilon}}_e. \quad (3.10)$$

Moreover, the inelastic strain is also split into two components, one for crystal plasticity, $\boldsymbol{\varepsilon}_p$, and one due to transport of matter, $\boldsymbol{\varepsilon}_d$. Taking the time derivative of the inelastic strain, we have

$$\dot{\boldsymbol{\varepsilon}}_i = \dot{\boldsymbol{\varepsilon}}_p + \dot{\boldsymbol{\varepsilon}}_d. \quad (3.11)$$

The volume conservation requires

$$\text{tr}(\dot{\boldsymbol{\varepsilon}}_p) = \text{tr}(\dot{\boldsymbol{\varepsilon}}_d) = 0. \quad (3.12)$$

The change in dislocation density is divided into the change caused by deformation and the change for thermal process by deformation as follows

$$\dot{\rho} = \dot{\rho}_{\boldsymbol{\varepsilon}_e} + \dot{\rho}_T. \quad (3.13)$$

The dissipation Δ has three constituents: the dissipation Δ_p related to plastic deformation, the diffusion-related dissipation Δ_d , the dissipation Δ_D associated with grain coarsening, and the dissipation Δ_ρ associated with a change in dislocation density:

$$\Delta = \Delta_p + \Delta_d + \Delta_D + \Delta_\rho. \quad (3.14)$$

The detail of dissipation associated with the internal variables v_i , derived for a spherical grain are

$$\Delta_D = -\frac{\Pi}{6} \int_{\Omega} 3D^2 \psi_D \dot{D} f d\Omega, \quad (3.15)$$

$$\Delta_\rho = -\frac{\Pi}{6} \int_{\Omega} D^3 \frac{\partial \psi_{\text{dis}}}{\partial \rho} \dot{\rho}_T f d\Omega, \quad (3.16)$$

$$\Delta_p = \frac{\Pi}{6} \int_{\Omega} D^3 \left(\boldsymbol{\sigma}^d \cdot \dot{\boldsymbol{\epsilon}}_p - \frac{\partial \psi_{\text{dis}}}{\partial \rho} Q_p \right) f d\Omega, \quad (3.17)$$

$$\Delta_d = \frac{\Pi}{6} \int_{\Omega} D^3 \boldsymbol{\sigma}^d \cdot \dot{\boldsymbol{\epsilon}}_d f d\Omega, \quad (3.18)$$

where the deviatoric part of stress is defined as

$$\boldsymbol{\sigma}^d := \boldsymbol{\sigma} - \frac{1}{3} \mathbf{I} \text{tr} \boldsymbol{\sigma}. \quad (3.19)$$

Moreover, in accordance to [Hackl and Renner, 2013], $\psi_D = \psi_e + \psi_{\text{dis}} + \psi_{\text{gb}} + D/3 \partial(\psi_{\text{dis}} + \psi_{\text{gb}})/\partial D$ is the energy contributing to the total driving force for grain boundary migration. As mentioned in the principle of the minimum of the dissipation potential (PMDP), the next step, we need to discuss about the constraints concerning the dissipation. These constraints were proposed as

$$\hat{\Delta}_p = \frac{\Pi}{6} \int_{\Omega} R_p(D, \rho, \dot{\boldsymbol{\epsilon}}_p) D^3 f d\Omega, \quad (3.20)$$

$$\hat{\Delta}_\rho = \frac{\Pi}{6} \int_{\Omega} \frac{\nu_{\text{dis}}^2}{M_{\text{dis}}(D, \rho)} D^3 f d\Omega \quad \text{or} \quad \hat{\Delta}_p = \frac{\Pi}{6} \int_{\Omega} \frac{\dot{\rho}_T^2}{B_{\text{dis}}(D, \rho)} D^3 f d\Omega, \quad (3.21)$$

$$\hat{\Delta}_d = \frac{\Pi}{6} \int_{\Omega} \frac{1}{M_{\text{eff}}} D^5 \|\dot{\boldsymbol{\epsilon}}_d\|^2 f d\Omega, \quad \text{and} \quad (3.22)$$

$$\hat{\Delta}_D = \frac{\Pi w}{4M_\perp} \int_{\Omega} D^2 \dot{D}^2 f d\Omega, \quad (3.23)$$

where Q_p represents activation of dislocation sources by deviatoric stresses but also annihilation events when dislocations with opposite signs encounter each other on the same glide plane [Hackl and Renner, 2013]. The specific dissipation due to dislocation motion is R_p , and $M_{\text{dis}}(D, \rho)$ denotes the dislocation mobility. B_{dis} is the mobility function for dislocations. Furthermore, one more assumption concerning the representative or control volume kept to be constant during dynamic recrystallization. Let us assume to take the volume which is large enough. Then it is possible to neglect the travel of grains across the boundary of the control volume. The volume conservation is given by

$$V = \text{const.} \quad (3.24)$$

Consequently, the rate form of this conservation law has the form

$$\dot{V} = 0. \quad (3.25)$$

The optimization problem of the recrystallization model, subject to the above constraints, is summarized as follows

$$\begin{aligned} \dot{\Psi} &\rightarrow \min_{\dot{\mathbf{z}}}, & (3.26) \\ \text{s.t. } \Delta_i &= \hat{\Delta}_i, \\ \dot{V} &= 0, \end{aligned}$$

where $i = \{p, D, d, \rho\}$. Thus, the Lagrange functional for the optimization problem (3.26) can reads

$$\mathcal{L} = \dot{\Psi} + \sum_{i=1}^k \lambda_i (\Delta_i - \hat{\Delta}_i) + \lambda_V \dot{V}, \quad (3.27)$$

where λ_i and λ_V are Lagrange multipliers. Dealing with the stationarity condition helps us to obtain the critical points. Before doing this task, let us expand the Lagrange functional as well as the volume constraint. Using Eqs. (3.5) and (3.6), the rate form of the volume constraint is

$$\dot{V} = \int_{\Omega} V f d\Omega = \int_{\Omega} V h(\mathbf{z}) d\Omega - \int_{\Omega} V \nabla \cdot (f \dot{\mathbf{z}}) d\Omega. \quad (3.28)$$

The divergence theorem for the term $\int_{\Omega} V \nabla \cdot (f \dot{\mathbf{z}}) d\Omega$ reads

$$\dot{V} = \int_{\Omega} V h(\mathbf{z}) d\Omega - \int_{\partial\Omega} V (f \dot{\mathbf{z}}) \cdot d\mathbf{A} + \int_{\Omega} \nabla V \cdot (f \dot{\mathbf{z}}) d\Omega. \quad (3.29)$$

For spherical grains, the specific form of the time derivative of the volume conservation is rewritten as follows

$$\begin{aligned} \dot{V} &= \int_{\Omega} \frac{\pi}{6} D^3 h d\Omega + \int_{\Omega} \frac{\pi}{6} \frac{\partial D^3}{\partial \mathbf{X}} \cdot \mathbf{V} f d\Omega + \int_{\Omega} \frac{\pi}{6} \frac{\partial D^3}{\partial \mathbf{x}} \cdot \mathbf{v} f d\Omega \\ &\quad - \int_{\partial\Omega} \frac{\pi}{6} D^3 f \left(\frac{\partial \mathbf{z}}{\partial \mathbf{X}} \cdot \mathbf{V} \right) \cdot d\mathbf{A} - \int_{\partial\Omega} \frac{\pi}{6} D^3 f \left(\frac{\partial \mathbf{z}}{\partial \mathbf{x}} \cdot \mathbf{v} \right) \cdot d\mathbf{A}. \end{aligned} \quad (3.30)$$

In a similar way, the derivative of Helmholtz free energy with respect to time is

$$\begin{aligned} \dot{\Psi} &= \int_{\Omega} \frac{\pi}{6} (D^3 \psi) h d\Omega + \int_{\Omega} \frac{\pi}{6} \frac{\partial (D^3 \psi)}{\partial \mathbf{X}} \cdot \mathbf{V} f d\Omega + \int_{\Omega} \frac{\pi}{6} \frac{\partial (D^3 \psi)}{\partial \mathbf{x}} \cdot \mathbf{v} f d\Omega \\ &\quad - \int_{\partial\Omega} \frac{\pi}{6} (D^3 \psi) f \left(\frac{\partial \mathbf{z}}{\partial \mathbf{X}} \cdot \mathbf{V} \right) \cdot d\mathbf{A} - \int_{\partial\Omega} \frac{\pi}{6} (D^3 \psi) f \left(\frac{\partial \mathbf{z}}{\partial \mathbf{x}} \cdot \mathbf{v} \right) \cdot d\mathbf{A}, \end{aligned} \quad (3.31)$$

By defining $\Delta = (-\partial\Psi/\partial\mathbf{x}) \cdot \mathbf{v}$, the following terms of Eq. (3.31) are the dissipation of the free energy's rate

$$\Delta = - \int_{\Omega} \frac{\pi}{6} \frac{\partial (D^3 \psi)}{\partial \mathbf{x}} \cdot \mathbf{v} f d\Omega + \int_{\partial\Omega} \frac{\pi}{6} D^3 \psi f \left(\frac{\partial \mathbf{z}}{\partial \mathbf{x}} \cdot \mathbf{v} \right) \cdot d\mathbf{A} = \Delta_1 + \Delta_2, \quad (3.32)$$

where Δ_1 and Δ_2 are the dissipative terms within the control volume and the dissipation at the boundary, respectively. Substituting Eq. (3.31) into Eq. (3.27) yields the Lagrange functional for the recrystallization model as

$$\begin{aligned} \mathcal{L} &= \frac{\pi}{6} \left(\int_{\Omega} \frac{\partial D^3 (\psi + \lambda_V)}{\partial \mathbf{X}} \cdot \mathbf{V} f d\Omega + \int_{\Omega} D^3 (\psi + \lambda_V) r d\Omega \right. \\ &\quad \left. - \int_{\partial\Omega} D^3 (\psi + \lambda_V) f \left(\frac{\partial \mathbf{z}}{\partial \mathbf{X}} \cdot \mathbf{V} \right) \cdot d\mathbf{A} - \int_{\partial\Omega} D^3 (\psi + \lambda_V) f \left(\frac{\partial \mathbf{z}}{\partial \mathbf{x}} \cdot \mathbf{v} \right) \cdot d\mathbf{A} \right. \\ &\quad \left. + \sum_{i=1}^k \left[(1 - \lambda_i) \int_{\Omega} \frac{\partial (D^3 \psi)}{\partial \mathbf{x}_i} \cdot \mathbf{v}_i f d\Omega - \lambda_i \hat{\Delta}_i \right] + \int_{\Omega} \frac{\partial D^3}{\partial \mathbf{x}} \cdot \mathbf{v} f d\Omega \right). \end{aligned} \quad (3.33)$$

Basing on the steps of the principle of the minimum of the dissipation potential (PMDP), the next step is necessary to obtain the stationary points by taking the derivative of \mathcal{L} with respect to $v = \{\dot{\epsilon}_d, \dot{\epsilon}_p, \dot{D}, \dot{\rho}\}$. Then the evolution equations are obtained as

$$\dot{D} = M_{\perp} \frac{\lambda_V + (1 - \lambda_D)\psi_D}{\lambda_D w}, \quad (3.34)$$

$$\boldsymbol{\sigma}^d = \frac{\pi}{6V} \left\langle D^3 \left(\frac{\lambda_p}{\lambda_p - 1} \frac{\partial R_p}{\partial \dot{\epsilon}_p} + \frac{1}{1 - \lambda_p} \frac{\partial \psi_{dis}}{\partial \rho} \frac{\partial Q_p}{\partial \dot{\epsilon}_p} \right) \right\rangle, \quad (3.35)$$

$$\dot{\epsilon}_d = \frac{V}{\left\langle \frac{D^5}{M_{eff}} \right\rangle} \boldsymbol{\sigma}^d, \quad (3.36)$$

$$\dot{\rho} = Q_p - \frac{\lambda_p}{2\lambda_p} B_{dis} \frac{\partial \psi_{dis}}{\partial \rho}. \quad (3.37)$$

Equation (3.36) is called the flow law for diffusion creep, which will be used later in the mathematical model at the macroscale. Actually, for the grain boundaries, the diffusion of defects (e.g. vacancies) is the main mechanism. Generally, matter is actually transported in the opposite direction, for example, vacancies will transfer from low to high (compressive) stresses. When matter is transported, the shape of the crystal is changed and then the crystal will deform. For smaller grains, the length of diffusion paths is smaller than for the larger grains. After obtaining the evolution equations for internal variables, the Lagrange multipliers are calculated by using the dissipation constraints

$$\lambda_D^2 = 1, \quad (3.38)$$

$$\lambda_p = \frac{\left\langle D^3 \frac{\partial \psi_{dis}}{\partial \rho} \frac{\partial Q_p}{\partial \dot{\epsilon}_p} \right\rangle \cdot \dot{\epsilon}_p - \langle D^3 R_p \rangle}{\left\langle D^3 \frac{\partial R_p}{\partial \dot{\epsilon}_p} \right\rangle \cdot \dot{\epsilon}_p - \langle D^3 R_p \rangle}, \quad (3.39)$$

$$\lambda_d = -1, \quad (3.40)$$

$$\lambda_V = \frac{(\lambda_D - 1) \langle D^2 \psi_D \rangle}{\langle D^2 \rangle} = -2 \frac{\langle D^2 \psi_D \rangle}{\langle D^2 \rangle} \quad \text{for } \lambda_D = -1. \quad (3.41)$$

Upon insertion of the result for the Lagrangian multipliers, the formulation of the evolution for grain size is

$$\dot{D} = \frac{2M_{\perp}}{w} \left(\frac{\langle D^2 \psi_D \rangle}{\langle D^2 \rangle} - \psi_D \right) \quad \text{for } \lambda_D = -1. \quad (3.42)$$

Since at high temperatures, migration of dislocations (creep) is the main mechanism causing deformation, the change in dislocation density is assumed to be neglected. With this assumption, the deviator stress $\boldsymbol{\sigma}^d$ and λ_p are approximated as below

$$\boldsymbol{\sigma}^d \approx \frac{\pi}{6V} \left\langle D^3 \left(\frac{\lambda_p}{\lambda_p - 1} \frac{\partial R_p}{\partial \dot{\epsilon}_p} \right) \right\rangle, \quad (3.43)$$

$$\lambda_p \approx \frac{-\langle D^3 R_p \rangle}{\left\langle D^3 \frac{\partial R_p}{\partial \dot{\epsilon}_p} \cdot \dot{\epsilon}_p \right\rangle - \langle D^3 R_p \rangle}. \quad (3.44)$$

Substituting Eq. (3.44) into Eq. (3.43) and employing Orowan's relation, we arrive at

$$\boldsymbol{\sigma}^d = \frac{\pi}{6V} \frac{\langle D^3 R_p \rangle}{\left\langle D^3 \frac{\partial R_p}{\partial \dot{\epsilon}_p} \right\rangle \cdot \dot{\epsilon}_p} \left\langle D^3 \frac{\partial R_p}{\partial \dot{\epsilon}_p} \right\rangle = \frac{\pi}{6V} \left\langle \frac{D^3}{\rho^m} \right\rangle \frac{\|\dot{\epsilon}_p\|^{m-1}}{k_p^m} \dot{\epsilon}_p. \quad (3.45)$$

The evolution equation relating, i.e the flow law for dislocation creep, is formulated by

$$\dot{\epsilon}_p = \left[\frac{6V}{\pi} \frac{1}{\langle \frac{D^3}{\rho^m} \rangle} \right]^{\frac{1}{m}} k_p \|\sigma^d\|^{\frac{1-m}{m}} \sigma^d. \quad (3.46)$$

In our variational approach, the evolution equations for grain size and dislocation density are needed, ingredients for calculation of the distribution function. Now let us discuss how to get the evolution of the grain size. We call an aggregate quasi-homogeneous aggregate when new grains are nucleated with the grain size which is small enough to be neglected to compare the average grain size of aggregate. In addition, it is assumed that all the grains with the same dislocation density have identical grain size, i.e. $D = \bar{D}(\rho)$. There is an decrease in the grain size if the assemble energy is larger than the energy of the grain. According to [Urai et al., 1986; Hackl and Renner, 2013], small grains are mainly influenced by the grain boundary energy, the impacted dislocation density can be neglected. It also means that large grains are not affected by the grain boundary energy. Large grains with a higher dislocation density will make the grain to shrink. Let us consider the case with $\psi_{\text{dis}} = \mu b^2 \rho$ and $\psi_{\text{gb}} = 6\gamma/D$, then the below result will be obtained

$$\begin{aligned} \frac{\dot{D}}{\dot{\rho}} &= \frac{2M_{\perp}}{wQ_p} \left[\mu b^2 \left(\frac{\langle D^2 \rho \rangle}{\langle D^2 \rangle} - \rho \right) + 4\gamma \left(\frac{\langle D \rangle}{\langle D^2 \rangle} - \frac{1}{D} \right) + \frac{\langle D^2 \psi_e \rangle}{\langle D^2 \rangle} - \psi_e \right] \\ &= \frac{2M_{\perp}}{w} \left(\lambda - \mu b^2 \rho - \frac{4\gamma}{D} \right), \end{aligned} \quad (3.47)$$

with

$$\lambda = \frac{\langle D^2 \psi_i \rangle}{\langle D^2 \rangle} - \psi_e. \quad (3.48)$$

The full description of how to derive of this relation can be referred to [Hackl and Renner, 2013]. Here λ could be understood the average values which are constant at steady state. This is elastic strain energy at the macroscale. The energy of grain boundary is mainly used for driving force in the nucleation process of new grains. When dislocation density raises, this energy is locally negligible. As discussed above, in polycrystal, many new grains are formed, then the grain boundary energy becomes larger than dislocation energy. Consequently, the interfacial energy γ is able to be neglected. From this condition, we have

$$\dot{D} = \frac{2M_{\perp}}{w} (\lambda - \mu b^2 \rho). \quad (3.49)$$

$$\dot{\rho} = \frac{a_p}{b} \sqrt{\rho} \|\dot{\epsilon}_p\|, \quad (3.50)$$

Solving Eq. (3.49) analytically by using initial condition $\bar{D}(0) = 0$, then we arrive at

$$\bar{D}(\rho) = \frac{4bM_{\perp}}{3a_p w \|\dot{\epsilon}_p\|} \sqrt{\rho} (3\lambda - \mu b^2 \rho). \quad (3.51)$$

This relationship between grain size and dislocation density is depicted in Figure 3.1. Clearly, the aggregate of all grains is characterized by a life cycle of grains. Let us call it the life cycle or age of grains. A grain, having zero dislocation density, will nucleate. Its grain size will be larger to reach maximum value by accumulating dislocation density. As based on Eq. (3.51), the maximum value of dislocation density and grain size

$$\rho_{\text{max}} = \frac{3\lambda}{\mu b^2}, \quad (3.52)$$

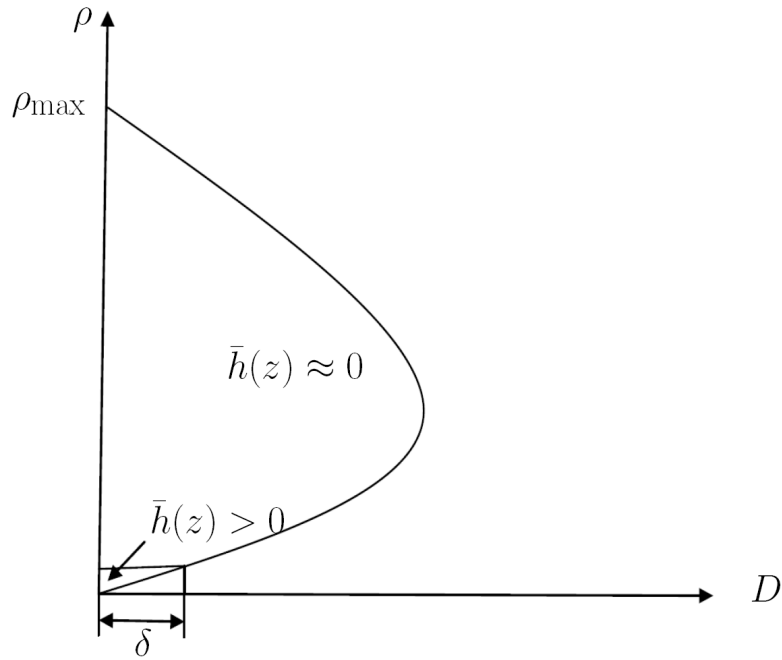


Figure 3.1: Evolution of a nucleated grain.

$$D_{max} = \frac{8bM_{\perp}\mu b^2}{3a_p w \|\dot{\epsilon}_p\|} \left(\frac{\lambda}{\mu b^2} \right)^{3/2}, \quad (3.53)$$

which occurs at

$$\rho_{D_{max}} = \sqrt{\frac{\lambda}{\mu b^2}}. \quad (3.54)$$

3.2 Microscale

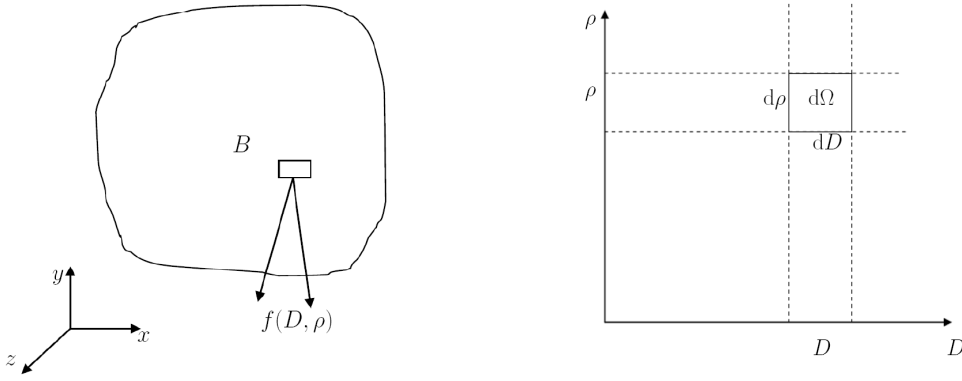
The generally consistent set of microstructural evolution equations for inelastic materials for dynamic recrystallization was discussed in the previous part. We also introduced the distribution function in polycrystalline aggregate. This part is devoted to deriving the mathematical framework for the problem at the microscale.

3.2.1 The original model for the distribution function $f(D, \rho)$

An assumption is made in our model, the elastic strain, ϵ_e , is assumed to be a constant during dynamic recrystallization. Then the variation in elastic strain is neglected. At this time, a grain of body B , its distribution function is characterized by only grain size and dislocation density as in Figure 3.1. Let us consider a subset $d\Omega = dDd\rho$. Being above introduced, the continuity condition has to be fulfilled by the probability distribution function $f(D, \rho)$ as below

$$\dot{f} + \nabla \cdot (f\dot{\mathbf{x}}) = h, \quad (3.55)$$

where the state variable $\mathbf{x} = \{D, \rho\}$ and h is grain production. Since h is for the nucleation process, then h is only different from 0 in small area dA . As illustrated in Figure 3.1, this region is around of the boundary $\rho = 0$ or $r = 0$. Consequently, in a large domain of $D - r$, let us assume $h = 0$. In dynamic recrystallization, the rate of f is equal to zero, i.e. $\dot{f} = 0$.

Figure 3.2: Subset $d\Omega$ of the entire space, Ω .

Employing these assumptions and making an expansion for the continuity equation, we have the continuity equation (or the mass conservation) as follows

$$\frac{\partial}{\partial D}(\dot{D}f) + \frac{\partial}{\partial \rho}(\dot{\rho}f) = 0. \quad (3.56)$$

Moreover, the aggregate volume has to be preserved, yielding for spherical grains of diameter D the constraint results to

$$V = \frac{\pi}{6} \iint_{\Omega} D^3 f(D, \rho) dD d\rho = \text{const}. \quad (3.57)$$

Parameter	Unit	Physical meaning
γ	J m^{-2}	Specific grain boundary energy
δ	m	Width of grain boundary
μ	N m^{-2}	Shear modulus
b	m	Norm of the Burger's vector
a_p	-	Material parameter related to the generation of dislocations
M_{\perp}	$\text{m}^3 \text{s kg}^{-1}$	Diffusion mobility
λ	-	Undetermined constant related to the Lagrange multiplier

Table 3.1: Material parameters information

Inserting evolution equations Eq. (3.49) and Eq. (3.50) into the continuity equation gives us

$$\frac{\partial}{\partial D} \left[\frac{2M_{\perp}}{\delta} \left(\lambda - \mu b^2 \rho - \frac{4\gamma}{D} \right) f \right] + \frac{\partial}{\partial \rho} \left[\left(\frac{a_p}{b} \sqrt{\rho} \|\dot{\epsilon}_p\| \right) f \right] = 0. \quad (3.58)$$

Then the mass conservation is reformulated as

$$\frac{2M_{\perp}}{\delta} \frac{\partial}{\partial D} \left[\left(\lambda - \mu b^2 \rho - \frac{4\gamma}{D} \right) f \right] + \frac{a_p}{b} \|\dot{\epsilon}_p\| \frac{\partial}{\partial \rho} (\sqrt{\rho} f) = 0. \quad (3.59)$$

Introducing $\beta = \mu b^2$, $\eta = 4\gamma$ and $v = a_p \delta \|\dot{\epsilon}_p\| / 4bM_{\perp}$, the continuity equation of the original model can be reduced as follows

$$\frac{\partial}{\partial D} \left[\left(\lambda - \beta \rho - \frac{\eta}{D} \right) f \right] + 2v \frac{\partial}{\partial \rho} (\sqrt{\rho} f) = 0. \quad (3.60)$$

We already considered that all grains are born with the dislocation-free nuclei. Thus, the nucleation condition is very important in modelling dynamic recrystallization in polycrystalline materials. For this model, we only use the nucleation condition or initial condition as follows

$$f(D, 0) = g(D) = De^{-kD}, \quad (3.61)$$

where k is a new material parameter. More information about the nucleation will be made clearly in Section 2.3. Lastly, the original form of our problem has the ansatz as follows

$$\begin{cases} \frac{\partial}{\partial D} \left[\left(\lambda - \beta\rho - \frac{\eta}{D} \right) f \right] + 2v \frac{\partial}{\partial \rho} (\sqrt{\rho} f) = 0, \\ \frac{\Pi}{6} \int D^3 f(D, \rho) dD d\rho = \text{const}, \\ f(D, 0) = De^{-kD} \end{cases} \quad (3.62)$$

3.2.2 The standard model for the distribution function $\bar{f}(D, r)$

As can be observed that equation (3.62) can face the singularity problem because of the term $\partial(\sqrt{\rho}f)/\partial\rho$. Let us introduce a new variable, rescaled dislocation density, r in order to avoid this problem as

$$r = \sqrt{\rho}. \quad (3.63)$$

In parallel with proposing the new variable r , an introduction of the new distribution function \bar{f} corresponding to r , the volume conservation is employed as

$$\int_{\Omega} f dD d\rho = \int_{\Omega} \bar{f} dD dr \quad (3.64)$$

Since this equation is correct for the whole body B , then we obtain $\bar{f} dr = f d\rho$. The continuity equation is rewritten as

$$\frac{\partial}{\partial D} \left[\left(\lambda - \beta r^2 - \frac{\eta}{D} \right) \frac{\bar{f}}{2r} \right] + 2v \frac{\partial r}{\partial \rho} \frac{\partial}{\partial r} \left(\sqrt{\rho} \frac{\bar{f}}{2\sqrt{\rho}} \right) = 0, \quad (3.65)$$

By inserting $\bar{\lambda} = \lambda/\beta$, $\bar{\mu} = \mu/\beta$, $\bar{v} = v/\beta$ into equation (3.59), this equation can be simplified

$$\frac{1}{2r} \frac{\partial}{\partial D} \left[\left(\bar{\lambda} - \bar{\beta} r^2 - \frac{\bar{\eta}}{D} \right) \bar{f} \right] + 2\bar{v} \frac{1}{2r} \frac{\partial}{\partial r} \left(\frac{\bar{f}}{2} \right) = 0. \quad (3.66)$$

Lastly, the distribution function is determined by solving the new continuity equation which is given by

$$\frac{\partial}{\partial D} \left[\left(\bar{\lambda} - r^2 - \frac{\bar{\eta}}{D} \right) \bar{f} \right] + \bar{v} \frac{\partial \bar{f}}{\partial r} = 0. \quad (3.67)$$

The initial condition or the nucleation is reformulated by the variables transformation

$$g(D) = \dot{r} \bar{f}(D, 0) = \frac{a_p}{2b} \|\dot{\epsilon}_p\| \bar{f}(D, 0). \quad (3.68)$$

The summary of the new system of the mathematical problem at the microscale which includes the volume conservation and the continuity equation is

$$\begin{cases} \frac{\partial}{\partial D} \left[\left(\bar{\lambda} - r^2 - \frac{\bar{\eta}}{D} \right) \bar{f} \right] + \bar{v} \frac{\partial \bar{f}}{\partial r} = 0, \\ \frac{\pi}{6} \iint_{\Omega} D^3 \bar{f}(D, r) dD dr = \text{const}. \end{cases} \quad (3.69)$$

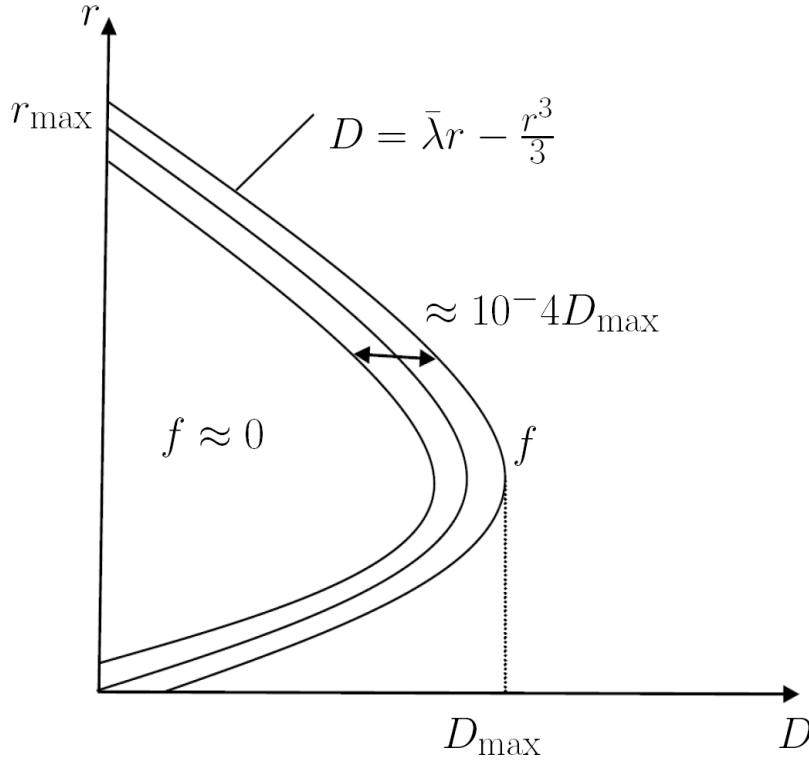


Figure 3.3: Evolution of a nucleated grain in $r - D$ domain.

3.2.3 The modified model for the distribution function $\tilde{f}(s, r)$

The curve created by $D = 1/\bar{v} (\bar{\lambda}r - 1/3r^3)$ is called the characteristic curve. Actually, the dynamic recrystallization takes place not only along this curve but also in its neighbor as plotted in Figure 3.1. We suspect that distribution function f will have larger values only in the neighborhood of the characteristic curve. Let us therefore introduce a new variable s by

$$D = s + \frac{1}{\bar{v}} \left(\bar{\lambda}r - \frac{1}{3}r^3 \right). \quad (3.70)$$

This leads $dD = ds$. Let us transfer from $\bar{f}(D, r)$ to $\tilde{f}(s, r)$ by

$$\frac{\partial \bar{f}(D, r)}{\partial r} = \frac{\partial \tilde{f}(s, r)}{\partial r} + \frac{\partial \tilde{f}(s, r)}{\partial s} = \frac{\partial \tilde{f}(s, r)}{\partial r} - \frac{1}{\bar{v}} (\bar{\lambda} - r^2) \frac{\partial \tilde{f}(s, r)}{\partial s}. \quad (3.71)$$

Inserting this equation into the mass conservation, we obtain

$$\frac{\partial}{\partial s} \left[\left(\bar{\lambda} - r^2 - \frac{\bar{\eta}}{s + \frac{1}{\bar{v}} (\bar{\lambda}r - \frac{1}{3}r^3)} \right) \tilde{f} \right] + \bar{v} \frac{\partial \tilde{f}}{\partial r} - (\bar{\lambda} - r^2) \frac{\partial \tilde{f}}{\partial s} = 0. \quad (3.72)$$

Expanding this equation gives us the result

$$(\bar{\lambda} - r^2) \frac{\partial \tilde{f}}{\partial s} - \frac{\partial}{\partial s} \left[\left(\frac{\bar{\eta}}{s + \frac{1}{\bar{v}} (\bar{\lambda}r - \frac{1}{3}r^3)} \right) \tilde{f} \right] + \bar{v} \frac{\partial \tilde{f}}{\partial r} - (\bar{\lambda} - r^2) \frac{\partial \tilde{f}}{\partial s} = 0. \quad (3.73)$$

By simplifying, we finally obtain

$$\frac{\partial}{\partial s} \left[\left(\frac{\bar{\eta}}{s + \frac{1}{\bar{v}} (\bar{\lambda}r - \frac{1}{3}r^3)} \right) \tilde{f} \right] = \bar{v} \frac{\partial \tilde{f}}{\partial r}. \quad (3.74)$$

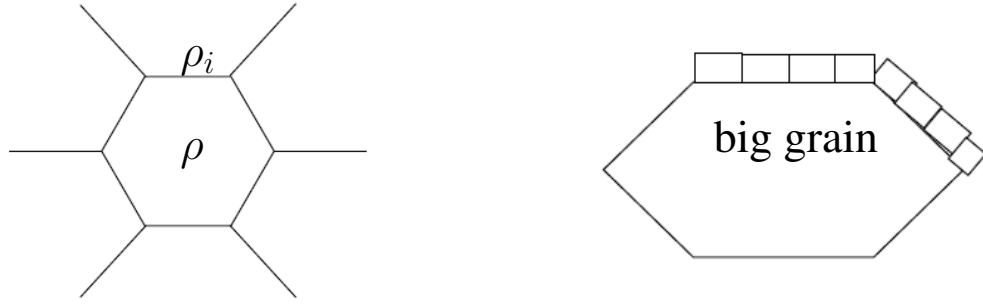


Figure 3.4: Grain and its surrounding for the distribution function $f(p, D, r)$.

The volume conservation is reformulated as

$$\frac{\Pi}{6} \int_0^\infty \int_{s_{\min}}^\infty D^3 f ds dr = 1, \quad (3.75)$$

where $s_{\min} < 0$ is an appropriate bound. The variational problem for dynamic recrystallization is rewritten as

$$\left\{ \begin{array}{l} \frac{\partial}{\partial s} \left[\left(\frac{\bar{\eta}}{s + \frac{1}{v} (\bar{\lambda}r - \frac{1}{3}r^3)} \right) \tilde{f} \right] = \bar{v} \frac{\partial \tilde{f}}{\partial r}, \\ \bar{g}(s) = \bar{v} f(s, 0), \\ \frac{\Pi}{6} \int_0^\infty \int_{s_{\min}}^\infty D^3 f ds dr = 1. \end{array} \right. \quad (3.76)$$

From here, many versions of distribution function will make us feel confused. Therefore, we only care the dependent variables of distribution function in stead of f or \bar{f} or \tilde{f} . Then, in this thesis, f sometimes will be used for \bar{f} and \tilde{f} .

3.2.4 The extended model with the distribution function $f(p, D, r)$

We will consider the surrounding region of grains. A grain with its dislocation density ρ has some neighboring grains. These grains will have different dislocation density ρ_i as can be seen in Figure 3.4.

Extended energy for small grains

Within this theory, we assume that grains are nucleated on triple lines with cylindrical shape having a characteristic diameter D_0 as in Figure 3.5. Thus, we have formulations for volume V and surfaces S as follows

- (1) Large grains: $V = \frac{\Pi}{6} D^3, S = \frac{\Pi}{2} D^2$.
- (2) Small grains: $V = \frac{\Pi}{4} D_0^2 D, S = \frac{\Pi}{2} D_0 D + \frac{\Pi}{8} D_0^2$.

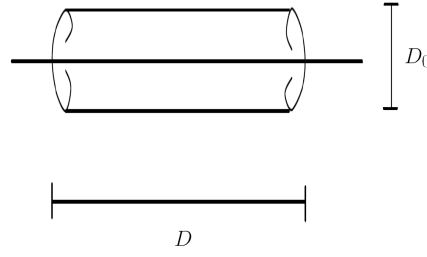


Figure 3.5: Nucleation on triple lines.

The surface S has the above forms since the surface of one new grain is formed from two grains. The right limiting behavior we get by first summing up the expressions as

$$V = \frac{\Pi}{6}D^3 + \frac{\Pi}{4}D_0^2D, \quad (3.77)$$

$$S = \frac{\Pi}{2}D^2 + \frac{\Pi}{2}D_0D + \frac{\Pi}{8}D_0^2. \quad (3.78)$$

Let's denote by p the average dislocation density outside the grain, then the Gibbs energy of the grain is

$$G = \gamma S - \mu b^2(p - r^2)V. \quad (3.79)$$

Evolution equations

We assume a dissipation potential of the form

$$Q = \frac{1}{2M_{\text{gb}}}S\dot{D}^2, \quad (3.80)$$

where $M_{\text{gb}} = 2M_{\perp}/\delta$, and make use of the minimum principle

$$\text{argmin} \left\{ \dot{G} + Q|\dot{D} \right\}. \quad (3.81)$$

Then the Lagrange function is built as $\mathcal{L} = \dot{G} + Q$. The evolution equation for \dot{D} is obtained by taking derivative of the Lagrange function with respect to \dot{D} .

$$\frac{\partial \mathcal{L}}{\partial \dot{D}} = \frac{\partial \dot{G}}{\partial \dot{D}} + \frac{\partial Q}{\partial \dot{D}}. \quad (3.82)$$

We obtain the evolution of grain size

$$\dot{D} = -\frac{M_{\text{gb}}}{S} \frac{\partial G}{\partial D}. \quad (3.83)$$

As usual, we assume

$$\dot{r} = \frac{a_p}{2b} \|\dot{\epsilon}_p\| = v = \text{const}. \quad (3.84)$$

After inserting the derivative of G with respect to D , the evolution of grain size is rewritten as

$$\dot{D} = -M_{\text{gb}} \left[\frac{4\gamma}{2D + D_0} - \mu b^2(p - r^2) \frac{4D^2 + 2D_0^2}{(2D + D_0)^2} \right]. \quad (3.85)$$

Consequently, we have the ratio between the evolution of grain size and the evolution of dislocation density

$$\frac{\dot{D}}{\dot{r}} = -\frac{M_{\text{gb}}}{v} \left[\frac{4\gamma}{2D + D_0} - \mu b^2 (p - r^2) \frac{4D^2 + 2D_0^2}{(2D + D_0)^2} \right]. \quad (3.86)$$

Let us denote $h = \dot{D}/\dot{r}$. The neighboring dislocation density p is probability distributed. However, large grains will experience an average value \bar{p} . This effect can be taken into account by postulating an evolution equation

$$\dot{p} = -k(p - \bar{p})\dot{D}, \quad (3.87)$$

which can be integrated up to

$$p = \bar{p} + (p_0 - \bar{p})e^{-kD}, \quad (3.88)$$

where $p_0 = p|_{D=0}$.

Evolution of distribution function

We assume that grains are nucleated with $D = 0$, $r = 0$ with a distribution function $g(p_0)$. This means we are looking for a distribution function $F(p, D, r)$ satisfying

$$\begin{cases} \frac{\partial}{\partial p}(\dot{p}F) + \frac{\partial}{\partial D}(\dot{D}F) + \frac{\partial}{\partial r}(\dot{r}F) = 0, \\ F(p_0, 0, 0) = g(p_0), \\ \frac{\Pi}{6} \int D^3 F(p, D, r) dp dD dr = 1. \end{cases} \quad (3.89)$$

The initial distribution g can be computed in different ways. For simplicity, we assume a surface average which is created by $r = \sqrt{p_0}$. Then the distribution $g(p_0)$ is computed by

$$g(p_0) = C \frac{\Pi}{2} \int D^2 p_0 F(p, D, \sqrt{p_0}) dD dp, \quad (3.90)$$

where C is given by the normalization

$$v \int g(p_0) dp_0 = \alpha. \quad (3.91)$$

α is the rate of grain nucleation per unit volume. Of course, eventually we will be interested in

$$f(D, r) = \int F(p, D, r) dp. \quad (3.92)$$

Rescaling

It's better to use the constant concerning initial values p_0 instead of p . Thus, we define an alternative distribution function by

$$\bar{F}(p_0, D, r) dp_0 = F(p, D, r) dp, \quad (3.93)$$

and get

$$\bar{F}(p_0, D, r) = F(p, D, r) \frac{dp}{dp_0} = e^{-kD} F(p, D, r). \quad (3.94)$$

These equations Eqs. (3.90)-(3.94) just undergo the replacement $p \mapsto p_0$, $F \mapsto \bar{F}$

$$F(p_0, 0, 0) = g(p_0) = \bar{F}(p_0, D, r), \quad (3.95)$$

$$\bar{F}(p_0, 0) = e^{-k \cdot 0} F(p_0, 0, 0), \quad (3.96)$$

$$\frac{\Pi}{6} \int D^3 \bar{F}(p_0, D, r) dp_0 dD dr = 1, \quad (3.97)$$

$$g(p_0) = \frac{\Pi}{2} \int CD^2 p_0 \bar{F}(p_0, D, \sqrt{p_0}) dp_0 dD, \quad (3.98)$$

$$f(D, r) = \int \bar{F}(p_0, D, r) dp_0. \quad (3.99)$$

Solution using characteristic

Using Eq. (3.84), we can introduce r as a new independent variable. Substitution of Eq. (3.83) into Eq. (3.88) then gives an evolution equation of the form

$$\frac{dD}{dr} = h(p_0, D, r), \quad (3.100)$$

which using the initial condition $D = 0$ for $r = 0$, can be numerically solved for

$$D = \hat{D}(p_0, r). \quad (3.101)$$

Let us assume that there is a similar function $\hat{F}(p_0, r)$ such that \bar{F} can be represented by

$$\bar{F}(p_0, D, r) = \hat{F}(p_0, r), \quad (3.102)$$

where $D = \hat{D}(p_0, r)$, we will call the patch $(\hat{D}(p_0, r), \hat{F}(p_0, r))$ a characteristic. \hat{F} can be calculated via the following argument

$$\int \hat{F}(p_0, r) dD = \int \hat{F}(p_0, r) \frac{d\hat{D}}{dp_0} dp_0. \quad (3.103)$$

An assumption is made as follows

$$\int \hat{F}(p_0, r) dD = \int g(p_0) dp_0 = \text{const in } r. \quad (3.104)$$

Hence, we get

$$\hat{F}(p_0, r) = \frac{g(p_0)}{\frac{d\hat{D}}{dp_0(p_0, r)}}. \quad (3.105)$$

The function $d\hat{D}/dp_0$ can be found by numerically integrating the

$$\frac{d}{dr} \frac{d\hat{D}}{dp_0} = \frac{d}{dr} h(\hat{D}(p_0, r), r). \quad (3.106)$$

Finally, we get

$$f(D, r) = \hat{F}(p_0, r), \quad (3.107)$$

where $D = \hat{D}(p_0, r)$. The volume conservation integral now becomes

$$\frac{\Pi}{6} \int \hat{D}(p_0, r)_+^3 \hat{F}(p_0, r) \frac{d\hat{D}}{dp_0} dp_0 dr = 1, \quad (3.108)$$

where $+$ denotes the positive part, i.e.

$$\hat{D}(p_0, r)_+ = \begin{cases} \hat{D}(p_0, r) & \text{if } \hat{D}(p_0, r) \geq 0, \\ 0 & \text{else} \end{cases}. \quad (3.109)$$

Using (3.102) and (3.108) simplifies to

$$\frac{\Pi}{6} \int \hat{D}(p_0, r)_+^3 g(p_0) dp_0 dr = 1. \quad (3.110)$$

The distribution $g(p_0)$ of grains when they are nucleated is reformulated as

$$g(p_0) = C \frac{\Pi}{2} \int \hat{D}(p, \sqrt{p_0})_+^2 p_0 g(p) dp. \quad (3.111)$$

3.3 Macroscale

The general viscoplastic problem without the yield function

- (i) With the displacement vector $\mathbf{u} = (u_1, u_2, u_3)^T$, the infinitesimal strain tensor is given

$$\boldsymbol{\varepsilon} = \Delta^s \mathbf{u} = \frac{1}{2} (\nabla \mathbf{u} + (\nabla \mathbf{u})^T). \quad (3.112)$$

As mentioned above, the total strain is divided into three parts

$$\boldsymbol{\varepsilon} = \boldsymbol{\varepsilon}_e + \boldsymbol{\varepsilon}_p + \boldsymbol{\varepsilon}_d. \quad (3.113)$$

- (ii) Here we use Hook's law for an elastic material. According to the classic theory of small strains elasticity, the basic constitutive assumption is given as

$$\boldsymbol{\sigma} = \mathbb{C} : \boldsymbol{\varepsilon}_e = \mathbb{C} : (\boldsymbol{\varepsilon} - \boldsymbol{\varepsilon}_d - \boldsymbol{\varepsilon}_p), \quad (3.114)$$

where \mathbb{C} is the 4th-order tensor of elastic moduli, e.g. (linear isotropic elasticity). This is known as the linear elastic relationship. For isotropic material, we get

$$\boldsymbol{\sigma} = 2\hat{\mu}\boldsymbol{\varepsilon} + \hat{\lambda}(\text{tr}\boldsymbol{\varepsilon})\mathbf{I}, \quad (3.115)$$

where $\hat{\mu}$ and $\hat{\lambda}$ denote material constants known as the Lamé' coefficients and $\text{tr}\boldsymbol{\varepsilon} = \sum_{i=1,3} \varepsilon_{ii}$. In matrix form, we have

$$\begin{bmatrix} \sigma_{11} \\ \sigma_{22} \\ \sigma_{33} \\ \sigma_{12} \\ \sigma_{23} \\ \sigma_{13} \end{bmatrix} = \begin{bmatrix} 2\hat{\mu} + \hat{\lambda} & \hat{\lambda} & \hat{\lambda} & 0 & 0 & 0 \\ \hat{\lambda} & 2\hat{\mu} + \hat{\lambda} & \hat{\lambda} & 0 & 0 & 0 \\ \hat{\lambda} & \hat{\lambda} & 2\hat{\mu} + \hat{\lambda} & 0 & 0 & 0 \\ 0 & 0 & 0 & \hat{\mu} & 0 & 0 \\ 0 & 0 & 0 & 0 & \hat{\mu} & 0 \\ 0 & 0 & 0 & 0 & 0 & \hat{\mu} \end{bmatrix} \begin{bmatrix} \varepsilon_e^{11} \\ \varepsilon_e^{22} \\ \varepsilon_e^{33} \\ \varepsilon_e^{12} \\ \varepsilon_e^{23} \\ \varepsilon_e^{13} \end{bmatrix}. \quad (3.116)$$

(iii) Based on the result of Hackl and Renner [Hackl and Renner, 2013], we have the flow rules as

$$\dot{\boldsymbol{\varepsilon}}_d = \frac{V}{\langle D^5/M_{\text{eff}} \rangle} \boldsymbol{\sigma}^d, \quad (3.117)$$

$$\dot{\boldsymbol{\varepsilon}}_p = \left[\frac{6V}{\Pi} \frac{1}{\langle D^3/\rho^m \rangle} \right]^{\frac{1}{m}} k_p \|\boldsymbol{\sigma}^d\|^{\frac{1-m}{m}} \boldsymbol{\sigma}^d. \quad (3.118)$$

The total energy is calculated as follows

$$\Pi = \int_{\Omega} \Psi(\boldsymbol{\varepsilon}, \boldsymbol{\varepsilon}_p, \boldsymbol{\varepsilon}_d) - \int_{\Omega} \mathbf{u} \cdot \mathbf{b} dV - \int_{\Omega} \mathbf{u} \cdot \mathbf{t} d\Gamma, \quad (3.119)$$

with the boundary condition

$$\mathbf{u} = \bar{\mathbf{u}} \quad \text{on} \quad \Gamma_u, \quad (3.120)$$

$$\mathbf{t} = \bar{\mathbf{t}} \quad \text{on} \quad \Gamma_t. \quad (3.121)$$

3.4 Nucleation

The ability to predict the onset of nucleation is important for the arrangement of the grain structure. The rate of homogeneous nucleation is determined by the rate of formation of nuclei which maximizes the free energy. After a nucleus reaches this point, further growth becomes energetically. Due to the importance of nucleation in dynamic recrystallization, the nucleation theory should be proposed to predict the initial structure of grains at the microstructure.

3.4.1 A global nucleation theory

Let us look at grain nucleation more closely. We assume that grains are nucleated at $\rho = 0$, i.e, we have

$$h(D, \rho) = g(D)\delta(0), \quad (3.122)$$

Moreover, the mass conservation for dynamic recrystallization gives

$$\nabla \cdot (\dot{\mathbf{x}}f) = h. \quad (3.123)$$

We look at a small test region w around $\mathbf{x} = (D, 0)^T$ (Figure 3.6) and find the source term (nucleation production) as

$$\int_w h dV = g(D)\Delta D. \quad (3.124)$$

From Eqs. (3.6) and (3.55), we obtain

$$\int_w h dV = \int_w \nabla \cdot (\dot{\mathbf{x}}f) dV. \quad (3.125)$$

Employing Gauss's theorem leads to

$$\int_w h dV = \int_{\partial w} \mathbf{n} \cdot \dot{\mathbf{x}}f dA = \dot{\rho}(0)f(D, 0)\Delta D. \quad (3.126)$$

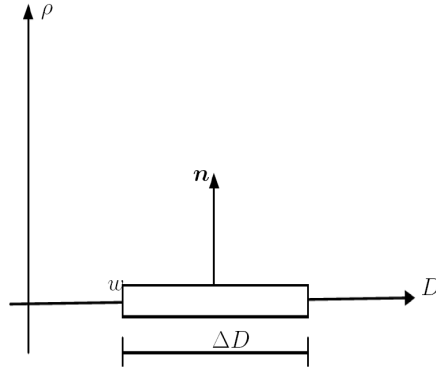


Figure 3.6: Nucleation test.

Eqs. (3.124) and (3.126) give

$$g(D) = \dot{\rho}(0)f(D, 0) \quad \text{or} \quad g(D) = \frac{a_p}{b} \|\dot{\epsilon}_p\| \sqrt{\rho} f(D, 0). \quad (3.127)$$

However, this means that the initial-value problem is ill-posed because for $\rho \rightarrow 0$ we have $f \rightarrow \infty$. Now let's look at the transformation

$$r = \sqrt{\rho}, \quad dr = \frac{1}{2\sqrt{\rho}} d\rho. \quad (3.128)$$

The volume conservation gives the relation between the distribution functions

$$f(D, \rho) d\rho = \bar{f}(D, r) dr, \quad \text{or} \quad \bar{f}(D, r) = 2\sqrt{\rho} f(D, \rho). \quad (3.129)$$

Consequently, the initial condition becomes well-posed as

$$\bar{g}(D) = \frac{a_p}{2b} \|\dot{\epsilon}_p\| \bar{f}(D, 0), \quad \text{or} \quad \bar{g}(D) = v \bar{f}(D, 0). \quad (3.130)$$

Within the standard form, $\bar{f}(D, r)$ the initial condition is given as follows

$$\bar{g}(D) = \bar{v} \bar{f}(D, 0). \quad (3.131)$$

After shifting the variable from D to s and doing the derivation as the variables transformation variables from D to s , the initial condition is changed to

$$\tilde{g}(s) = \bar{v} \tilde{f}(s, 0). \quad (3.132)$$

Since we will link the problem at the macroscale to the counterpart at the microscale, where the distribution function $\tilde{f}(s, 0)$ or $\bar{f}(D, 0)$ is used, it is essential to define the initial guess for this distribution function as

$$\tilde{f}(s, 0) = \bar{v} g(s). \quad (3.133)$$

From this equation, we can easily see that this initial distribution function is proportional to \bar{v} , depending on the plastic strain rate at the macroscale. Let us define the simple ansatz of the function g as below

$$g(s) = g_0 s \exp(-s/D_0), \quad (3.134)$$

here, g_0, D_0 are a material parameter and the initial grain size, respectively. Let us illustrate an example of this function $g(s)$ by Figure 3.7.

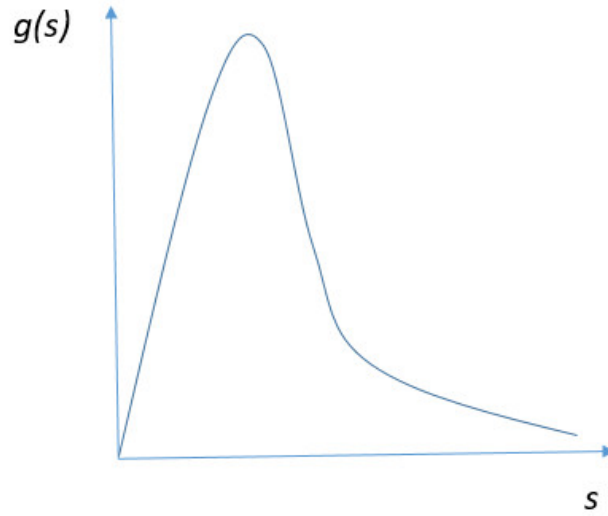


Figure 3.7: Nucleation function depending on s .

3.4.2 The production based nucleation theory

In the previous theory, $h(\mathbf{z})$ is assumed to be equal to zero. An alternative way to calculate the nucleation function g , we develop a theory to calculate the source term h or the nucleation rate. Let us recall the full continuity equation with the nucleation rate

$$\frac{\partial}{\partial D} \left[\left(\bar{\lambda} - r^2 + \frac{\bar{\eta}}{D} \right) f \right] + \bar{v} \frac{\partial f}{\partial r} = \bar{h}, \quad (3.135)$$

where

$$\bar{h} = \frac{h\delta}{4M_{\perp}\beta}. \quad (3.136)$$

The nucleation rate is determined by using the principle of the minimum of dissipations. Let us compute h by the variational principle. The rate of free energy as well as the dissipation concerning h are built. The rate of potential energy is given by

$$\dot{\psi}_h = \frac{\pi}{6} \int_{\Omega} D^3 \psi h d\Omega, \quad (3.137)$$

where $\psi = \mu b^2 r^2 + 4\gamma/D$ is the Helmholtz free energy. The dissipation potential for the source function takes the form

$$\hat{\Delta}_h = \frac{k\pi}{2} \int_{\Omega} D^2 h^2 d\Omega, \quad (3.138)$$

where k is a material parameter. Moreover, we have the constraint

$$\int_{\Omega} D^3 h d\Omega = 0. \quad (3.139)$$

Via this integral, the balance of spontaneous appearances are represented. Grains having a specific set of observable variables are disappeared in contrast to slow evolution of grain having one set of observable variables to a neighboring set due to diffusive processes. For example, a nucleus spontaneously occurring in a large strain also requires the spontaneous

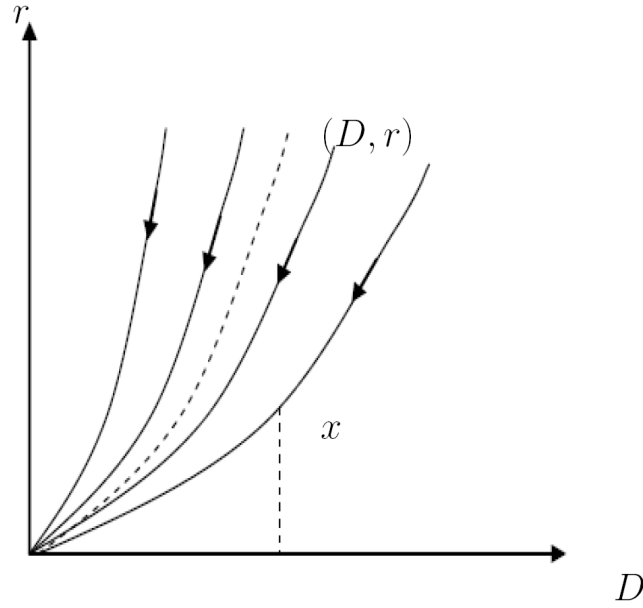


Figure 3.8: Arc curve.

disappearance of a large grain and the appearance of a grain with an intermediate size. These linked spontaneous processes are required to preserve volume. Then the minimization problem is given as

$$\operatorname{argmin} \left\{ \dot{\psi}_h + \hat{\Delta}_h | h : \frac{\Pi}{6} \int_{\Omega} D^3 h d\Omega = 0 \right\}. \quad (3.140)$$

We have the Lagrangian functional for the optimized problem (3.140) in the following form

$$\mathcal{L} = \frac{\Pi}{6} \int_{\Omega} D^3 \psi h d\Omega + \frac{k}{2} \frac{\Pi}{2} \int_{\Omega} D^2 h^2 d\Omega - \lambda \frac{\Pi}{6} \int_{\Omega} D^3 h d\Omega. \quad (3.141)$$

Applying the stationary conditions by solving $\partial \mathcal{L} / \partial h = 0$, we arrive at

$$\frac{\Pi}{6} D^3 \psi + k \frac{\Pi}{4} D^2 h - \lambda \frac{\Pi}{6} D^3 = 0, \quad (3.142)$$

therefore

$$h = \frac{2}{3k} D(\lambda - \Psi). \quad (3.143)$$

However, from this result, we realize that this is not realistic because it allows processes of the form. Actually, grains can not spontaneously get larger or loose dislocations. Thus, let us postulate that grains can only decompose into smaller ones and loose some of their dislocations this way. Let us suppose that this happens along axes $r = p(r_0, D) = r_0 D^\alpha$ as in Figure 3.8 . Then our variational problem has to be formulated on every arc curve separately; and we have the constraints

$$\int_0^\infty D^3 h dx, \quad \int_0^x h dx \geq 0, \quad (3.144)$$

where x is arclength, $dx = \sqrt{1 + (dp/dD)^2} dD$. This formulation can be simplified using

$$D^3 h = -\frac{dw}{dx}. \quad (3.145)$$

Then the constraints become:

$$w(0) = 0, \quad \lim_{x \rightarrow \infty} w(x) = 0, \quad w(x) \leq 0. \quad (3.146)$$

Two beginning terms are obtained from the first term of Eq.(3.144). Moreover, we have the constraint $h \geq 0$ for $f = 0$. Our variational problem has to be reformulated by introducing Kuhn-Tucker parameters κ, θ . The Lagrangian functional can be written in the following form

$$\mathcal{L} = -\frac{\Pi}{6} \int_0^\infty \psi \frac{dw}{dx} dx + \frac{k\Pi}{2 \cdot 2} \int_0^\infty \frac{1}{D^4} \left(\frac{dw}{dx}\right)^2 dx + \frac{\Pi}{6} \int_0^\infty \kappa w dx + \frac{\Pi}{6} \int_{f=0} \theta \frac{dw}{dx} dx, \quad (3.147)$$

with Kuhn-Tucker conditions

$$\kappa \geq 0, w \leq 0, \kappa w = 0 \text{ for all } x, \quad (3.148)$$

$$\theta \geq 0, \frac{dw}{dx} \leq 0, \theta \frac{dw}{dx} = 0 \text{ for all } f(x) = 0. \quad (3.149)$$

Then one solution of the minimization problem can be written as follows

$$h = \frac{2D}{3k}(C - \psi), \quad (3.150)$$

where C is the unknown Lagrange parameter.

3.4.3 The geometry based nucleation theory

As mentioned above, the sphere grain with the diameter D yields its volume and its change of volume with respect to time, respectively, as follows

$$V = \frac{\Pi}{6} D^3, \quad (3.151)$$

$$\dot{V} = \frac{\Pi}{2} D^2 \dot{D}_{\text{nuc}}, \quad (3.152)$$

where D_{nuc} and \dot{D}_{nuc} are the grain size when it is nucleated and its material time derivative, respectively.

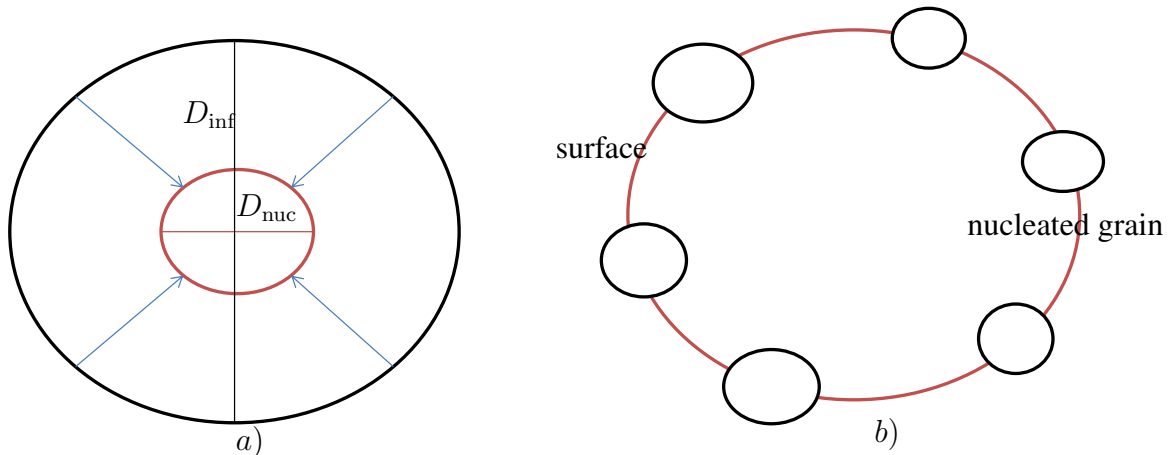


Figure 3.9: Size of nucleated grain

A new nucleated grain is formed by assembling of many other grains. Then we define an influence diameter D_{inf} , grains' diameter around one grain with size D . Moreover, basing in Figure ??, half of a newly nucleated grain belongs to the old grain, another half belongs to other grains. Half of the newly nucleated grain is created by accumulating dislocations of the old grains. Then the new grain is created by consuming dislocation at the interface or the surface. Therefore, the volume for the newly created grain is calculated by

$$V_{\text{nuc}} = -\frac{1}{2} \frac{\Pi}{6} D_{\text{nuc}}^3 \Pi D^2 g, \quad (3.153)$$

where g is the source function or the nucleation rate, presenting the density of nucleation sites at the neighbor of one grain. Since the change of volume in the nucleation process is caused by formation of the new grain, $\dot{V} = V_{\text{nuc}}$, $\dot{D}_{\text{nuc}} = -\frac{\Pi}{6} D_{\text{nuc}}^3 g$. Phenomena indicates that the change of surface area, including the new surface created by nucleation processes and vanished dislocations

$$\dot{S} = \frac{1}{2} \left(\frac{\Pi}{2} D_{\text{nuc}}^2 \Pi D^2 g + 2 \Pi D \dot{D}_{\text{nuc}} \right). \quad (3.154)$$

The area of surface (the change of surface's area) is given as

$$\delta S = \alpha b \delta R, \quad (3.155)$$

where δR is the change of dislocation's length. In addition, since dislocations are lost, then we have $\dot{R} = -\frac{1}{\alpha b} \dot{S}$. Let us specific the rate of Helmholtz free energy relating to the nucleation process

$$\dot{\psi}_{\text{nuc}} = \int_{\Omega} [\gamma \dot{S} + \mu b^2 \dot{R}] f d\Omega. \quad (3.156)$$

These formulations above yield the detailed form of $\dot{\psi}_{\text{nuc}}$ as follows

$$\dot{\psi}_{\text{nuc}} = \left(\gamma - \frac{\mu b^2}{\alpha b} \right) \int_{\Omega} \left(\frac{\Pi}{4} D_{\text{nuc}}^2 - \frac{\Pi}{6} \frac{D_{\text{nuc}}^3}{D} \right) \Pi D^2 g f d\Omega. \quad (3.157)$$

Moreover, the velocity of dislocation can be approximated (see Figure. ??) by

$$V_{\text{dis}} \approx \frac{1}{4} D_{\text{inf}} g, \quad (3.158)$$

where D_{inf} is calculated

$$D_{\text{inf}} = \left(\frac{6}{\alpha b} \right)^{\frac{1}{3}} D_{\text{nuc}}^{\frac{2}{3}}. \quad (3.159)$$

The velocity of dislocation is approximated as

$$V_{\text{dis}} \approx \frac{1}{4} D_{\text{inf}} g. \quad (3.160)$$

Inserting (3.159) into (3.160), we obtain

$$V_{\text{dis}} = \frac{1}{4} \left(\frac{6}{\alpha b} \right)^{\frac{1}{3}} \frac{D_{\text{nuc}}^{\frac{2}{3}}}{\rho^{\frac{1}{3}}} g. \quad (3.161)$$

Moreover, in accordance to [Hackl and Renner, 2013], the dissipation for dislocation is given by

$$\Delta_{\text{dis}} = \frac{1}{(m+1)M_{\text{dis}}} V_{\text{dis}}^{m+1}, \quad (3.162)$$

where M_{dis} is the mobility of dislocations. The result of Hackl and Renner [Hackl and Renner, 2013] also provided

$$\Delta_{\text{dis}} = M_{\text{dis}} \rho v_{\text{dis}}^{m+1}, \quad M_{\text{dis}} = \frac{\chi_p^{m+1}}{K_p^m} b^{m+1}. \quad (3.163)$$

The dissipation for the whole nucleation process is reformulated as

$$\Delta_{\text{nuc}} = \int_{\Omega} \Delta_{\text{dis}} \Pi D^2 f d\Omega \quad (3.164)$$

It becomes

$$\Delta_{\text{nuc}} = \frac{1}{(m+1)M_{\text{nuc}}} \int_{\Omega} \frac{D_{\text{nuc}}^{\frac{2(m+1)}{3}}}{r^{\frac{2(m-2)}{3}}} g^{m+1} \Pi D^2 f d\Omega, \quad (3.165)$$

where M_{nuc} is nucleation mobility. Consequently, we have the minimization problem for g as follows

$$\operatorname{argmin}\{\dot{\psi}_{\text{nuc}} + \Delta_{\text{nuc}}|g\}. \quad (3.166)$$

Thermodynamic principle PMD leads

$$g^m = M_{\text{nuc}} \left(\frac{\mu b}{\alpha} - \gamma \right) \frac{r^{\frac{2(m-2)}{3}}}{D_{\text{nuc}}^{\frac{2(m+1)}{3}}} \frac{\Pi}{6} \left(\frac{3}{2} D_{\text{nuc}}^2 - \frac{D_{\text{nuc}}^3}{D} \right). \quad (3.167)$$

Comparing to the nucleation theory which considers the source function h , dealing with the nucleation processes we already proposed, the benefits of this new direction are as follows

- The new approach is derived from physical phenomena.
- Its numerical algorithm is simpler than in the second theory regarding the nucleation process because the differential equation is now

$$\frac{\partial}{\partial D} \left[\left(\lambda - r^2 - \frac{\bar{\eta}}{D} \right) f \right] + \bar{v} \frac{\partial f}{\partial r} = 0, \quad (3.168)$$

where the previous counterpart was

$$\frac{\partial}{\partial D} \left[\left(\lambda - r^2 - \frac{\bar{\eta}}{D} \right) f \right] + \bar{v} \frac{\partial f}{\partial r} = \bar{h}. \quad (3.169)$$

Furthermore, in this new approach, it is not necessary to introduce the new rescaled variable s

$$D = s + \frac{1}{\bar{v}} \left(\lambda r - \frac{1}{3} r^3 \right) \quad (3.170)$$

- With the source function \bar{h} in the second nucleation theory, as mentioned before, the result is not compatible with the physical phenomena since grains can not spontaneously get larger and loose dislocation. Solving the nucleation process by the new theory can prevent this problem.

4 Numerical implementation

The mathematical model for dynamic recrystallization in polycrystalline materials was established in the previous chapter. In this chapter, a numerical treatment for this problem shall be discussed in detail. Since the problem is divided into two problems of a two-scale problem, two numerical methods are developed to solve two smaller problems. Firstly some numerical tools supporting us to deal numerically with our problems will be reviewed. These tools include a Simpson's rule and Newton-Raphson. We will implement numerical approach with finite element method (FEM) in Abaqus. Therefore, a short summary of FEM will be presented. The next part is a marching algorithm which is employed at the microscale. We utilize the return mapping at the macroscale. These are the components of a two-scale scheme which is employed to solve our model numerically.

4.1 Numerical scheme

4.1.1 Simpson's rule

In numerical analyses, Simpson's rule is a method to approximate a definite integral numerically. In the following part, we will use Simpson's rule to compute the numerical integrals over the domain. To get the approximated result of a definite integral, let us define integration points and then evaluate the integral at these points. For example, in one-dimensional space, the domain $[a, b]$ is divided into 2 small intervals. Consequently, the integral of the function f in $[a, b]$ is approximated as

$$\int_a^b f(x)dx \approx \frac{b-a}{6} \left[f(a) + 4f\left(\frac{a+b}{2}\right) + f(b) \right]. \quad (4.1)$$

Instead of two integration points, we use $(n+1)$ points. Let us divide $[a, b]$ into n small intervals, the integral is approximately computed by

$$\int_a^b f(x)dx \approx \frac{b-a}{3n} \left[f(x_0) + 2 \sum_{j=1}^{n/2-1} f(x_{2j}) + 4 \sum_{2j}^{n/2} f(x_{2j-1}) + f(x_n) \right], \quad (4.2)$$

where $x_j = a + jh$ for $j = 0, \dots, n$, $h = (b-a)/n$ and $x_0 = a$, $x_n = b$. In shorter expression, we have

$$\int_a^b f(x)dx \approx \frac{h}{3} \sum_i f(x_i)w_i. \quad (4.3)$$

In two-dimensional space \mathbb{R}^2 , in general, two domains $[a, b]$ and $[c, d]$ are separated into points, x_i and y_j , respectively. The vector, $\omega = (1, 4, 2, 4, 2, \dots, 2, 4, 2, 4, 1)$, is the vector collecting the weighting factors of Simpson's rule. Then the integral $\int_a^b \int_c^d f(x, y)dxdy$ is calculated approximately as

$$\int_a^b \int_c^d f(x, y)dxdy \approx \frac{h}{3} \frac{k}{3} \sum_{ij} f(x_i, y_j)w_iw_j, \quad (4.4)$$

where $k = (d - c)/n$.

4.1.2 Newton-Raphson scheme

In the numerical analysis, Newton-Raphson scheme is a method to obtain a good approximation to the exact solution of the root finding problem. In one-dimensional space \mathbb{R} , we need to find an approximated solution of the equation $f(y) = 0$. We assume that an initial guess, y_0 , is provided. This scheme will create an array $y_0, y_1, y_2, \dots, y_n$, that converges to the root solution. At an iterative step k , where $k = 1, \dots, n$, the value of the current step y_k is based on the counterpart of the previous step, y_{k-1} , as

$$y_k = y_{k-1} - \frac{f(y_{k-1})}{f'(y_{k-1})}. \quad (4.5)$$

In \mathbb{R}^n , we need to solve $f(\mathbf{y}) = 0$ with $\mathbf{y} = (y_1, y_2, \dots, y_n)^T$. Let us assume that \mathbf{y}_0 is an initial guess, then at step k

$$\mathbf{y}_k = \mathbf{y}_{k-1} - (\nabla f(\mathbf{y}_{k-1}))^{-1} \cdot f(\mathbf{y}_{k-1}). \quad (4.6)$$

In this scheme, the algorithm will end when the tolerance or the convergence criteria is reached. There are two kinds of convergence conditions: the absolute error is defined as $\|\mathbf{y}_k - \mathbf{y}_{k-1}\|$, and the absolute error is $\|(\mathbf{y}_k - \mathbf{y}_{k-1})/\mathbf{y}_{k-1}\|$.

4.2 Finite element method

4.2.1 FEM background

The equilibrium condition is obtained by minimizing the local form of conservation of linear momentum as

$$\nabla \cdot \boldsymbol{\sigma} + \mathbf{f} = \mathbf{0}, \quad (4.7)$$

where \mathbf{f} is external force vector. The detailed information how to derive this equation can be found in [Junker, 2011]. Hooke's law is used as the constitutive equation

$$\boldsymbol{\sigma} = \mathbb{C} : \boldsymbol{\varepsilon}, \quad (4.8)$$

the unknown variable of this problem is the displacement vector \mathbf{u} . This displacement is linked to the strain strain by the following relationship

$$\boldsymbol{\varepsilon} = \frac{1}{2}(\nabla \mathbf{u} + \mathbf{u} \nabla). \quad (4.9)$$

Normally we have two kinds of boundaries. For every physical body, displacements are known at some surfaces, for example, through supports or other prescribed non-zero displacements termed \mathbf{u}^* . The boundary where the displacements are known is indicated as $\partial\Omega_{\mathbf{u}}$. Then we have

$$\mathbf{u}(\mathbf{x}) = \mathbf{u}^* \quad \text{on} \quad \partial\Omega_{\mathbf{u}}. \quad (4.10)$$

Furthermore, the another constraint is satisfied

$$\boldsymbol{\sigma} \cdot \mathbf{n} = \mathbf{t}. \quad (4.11)$$

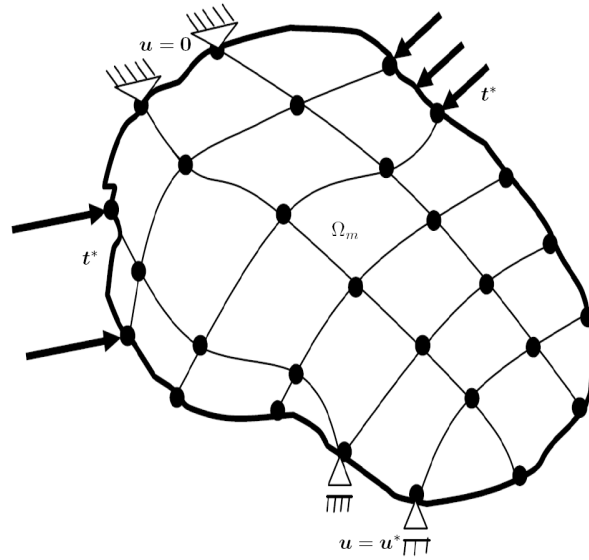


Figure 4.1: Discretized body.

This is Cauchy relation for surface force density. Actually, for an arbitrary body in three-dimensional space \mathbb{R}^3 , solving the problem with the differential equation as Eq. (4.7) accompanied by boundary conditions and Cauchy equation, to get the analytical solution is impossible, as a result, the proposal of a numerical method is offered. Let us first do some derivation from the equilibrium equation. After multiplying the equilibrium equation (4.7) by $\delta \mathbf{u}$ and integrating this equation over the domain, we gain

$$\int_{\Omega} \nabla \cdot \boldsymbol{\sigma} \delta \mathbf{u} d\Omega + \int_{\Omega} \mathbf{f} \delta \mathbf{u} d\Omega = \mathbf{0}. \quad (4.12)$$

Moreover, we have

$$\nabla \cdot (\boldsymbol{\sigma} \cdot \delta \mathbf{u}) = (\nabla \cdot \boldsymbol{\sigma}) \cdot \delta \mathbf{u} + \boldsymbol{\sigma} : \nabla \delta \mathbf{u}. \quad (4.13)$$

Eqs. (4.13), (4.12), and applying the divergence theorem lead

$$\int_{\Omega} \boldsymbol{\sigma} : \nabla \delta \mathbf{u} dV = \int_{\Omega} \mathbf{f} \cdot \delta \mathbf{u} dV + \int_{\partial \Omega} \mathbf{t} \cdot \delta \mathbf{u} dA \quad \forall \delta \mathbf{u}, \quad (4.14)$$

this equation is obtained because of the symmetry of $\boldsymbol{\sigma}$. The next step is to compare two equations, (4.7) and (4.14). Eq. (4.14) is an integral form. Comparing to Eq. (4.7), the divergence term $\nabla \cdot \boldsymbol{\sigma}$ should be given, i.e, the second derivative of the displacement vector \mathbf{u} . Because the two equations ((4.7), (4.14)) are equivalent, the advantage of first derivative in Eq. (4.14) is a centre point. Now the purpose is to find an approximated solution of Eq. (4.14). Let us divide the entire body, its volume Ω , into a certain number of smaller elements Ω_m (Figure 4.1). The elements are constructed by nodes. By interpolating the shape functions with the nodal values, the approximation for $\mathbf{u}(\mathbf{x})$ and $\delta \mathbf{u}$, can be calculated. Depending on the chosen kind of the shape functions, the accuracy of the approximated solution will be determined. The approximated solution can be obtained by using

$$\mathbf{u}(\mathbf{x}) \approx \mathbf{N}_u(\mathbf{x}) \cdot \hat{\mathbf{u}} = \mathbf{N}_u \cdot \hat{\mathbf{u}}, \quad \text{or} \quad \delta \mathbf{u}(\mathbf{x}) \approx \mathbf{N}_u(\mathbf{x}) \cdot \delta \hat{\mathbf{u}} = \mathbf{N}_u \cdot \delta \hat{\mathbf{u}}, \quad (4.15)$$

where \mathbf{N}_u , $\hat{\mathbf{u}}$ are shape functions, nodal values, respectively. Hence, the gradient of the solution function can be found according to

$$\nabla \mathbf{u} \approx \nabla \mathbf{N}_u \cdot \hat{\mathbf{u}} \quad \text{or} \quad \nabla \delta \mathbf{u} \approx \nabla \mathbf{N}_u \cdot \delta \hat{\mathbf{u}}. \quad (4.16)$$

In the small deformation theory, we have the relationship between strain and deformation as shown in Eq. (4.10). By defining a tensor \mathbf{B} in the three dimensional space \mathbb{R}^3 as follows

$$\mathbf{B} := \begin{bmatrix} \frac{\partial}{\partial x} & 0 & 0 \\ 0 & \frac{\partial}{\partial y} & 0 \\ 0 & 0 & \frac{\partial}{\partial z} \\ 0 & \frac{1}{2} \frac{\partial}{\partial z} & \frac{1}{2} \frac{\partial}{\partial y} \\ \frac{1}{2} \frac{\partial}{\partial z} & 0 & \frac{1}{2} \frac{\partial}{\partial x} \\ \frac{1}{2} \frac{\partial}{\partial y} & \frac{1}{2} \frac{\partial}{\partial x} & 0 \end{bmatrix}, \quad (4.17)$$

this relation can be expressed as

$$\boldsymbol{\varepsilon} = \mathbf{B} \cdot \mathbf{u} \Leftrightarrow \boldsymbol{\varepsilon} \approx \mathbf{B} \cdot \mathbf{N}_u \cdot \hat{\mathbf{u}}. \quad (4.18)$$

By denoting $\hat{\mathbf{B}} := \mathbf{B} \cdot \mathbf{N}_u$, Eq. (4.14) is rewritten as

$$\int_{\Omega} \hat{\mathbf{B}}^T \cdot \boldsymbol{\sigma} dV - \int_{\Omega} \mathbf{N}_u \cdot \mathbf{f} dV - \int_{\partial\Omega} \mathbf{N}_u \cdot \mathbf{t} dA = \mathbf{0}, \quad (4.19)$$

this equation should be solved numerically to get the unknown displacements. Furthermore, we knew how stress tensor is expressed in term of displacement

$$\boldsymbol{\sigma} = \mathbb{C} \cdot \boldsymbol{\varepsilon} \Leftrightarrow \boldsymbol{\sigma} = \mathbb{C} \cdot \hat{\mathbf{B}} \cdot \hat{\mathbf{u}} \quad (4.20)$$

By discretization, we arrive at

$$\sum_m \int_{\Omega_m} \hat{\mathbf{B}}^T \cdot \boldsymbol{\sigma} dV = \sum_m \int_{\Omega_m} \mathbf{N}_u \cdot \mathbf{f} dV + \sum_m \int_{\partial\Omega_m} \mathbf{N}_u \cdot \mathbf{t} dA \quad (4.21)$$

$$\Leftrightarrow \sum_m \int_{\Omega_m} \hat{\mathbf{B}}^T \cdot \mathbb{C} \cdot \hat{\mathbf{B}} dV \hat{\mathbf{u}} = \sum_m \int_{\Omega_m} \mathbf{N}_u \cdot \mathbf{f} dV + \sum_m \int_{\partial\Omega_m} \mathbf{N}_u \cdot \mathbf{t} dA \quad (4.22)$$

Let us define new tensors

$$\mathbf{K} = \sum_m \int_{\Omega_m} \hat{\mathbf{B}}^T \cdot \mathbb{C} \cdot \hat{\mathbf{B}} dV, \quad (4.23)$$

$$\mathbf{f}_f = \sum_m \int_{\Omega_m} \mathbf{N}_u \cdot \mathbf{f} dV, \quad (4.24)$$

$$\mathbf{f}_t = \sum_m \int_{\partial\Omega_m} \mathbf{N}_u \cdot \mathbf{t} dA. \quad (4.25)$$

Consequently, this leads to the result

$$\mathbf{K} \cdot \hat{\mathbf{u}} = \mathbf{f}_f + \mathbf{f}_t \quad (4.26)$$

where \mathbf{K} is called stiffness matrix, \mathbf{f}_f and \mathbf{f}_t denote internal force and external force, respectively. The volume of the element m is Ω_m and $\partial\Omega_m$ is its surface. The only remaining unknowns in Eq. (4.26) are the displacements at the nodes. Thus, the system of differential equations of Eq. (4.7) with the second derivative of displacements can be transformed to an algebraic system. Clearly, this system is easier to solve. For elastic materials, this system of equations is a linear one. Now to solve this system, the inverse tensor of \mathbf{K} is calculated.

4.2.2 FEM for non-linear materials

The non-linear term arises from two main reasons: a non-linear constitutive equations and a non-linear relation between displacements and strains due to large deformation. Now let us discuss the first cause of non-linearity. The constitutive equation is called non-linear when

$$\boldsymbol{\sigma} = \mathbb{D}(\boldsymbol{\varepsilon}) : \boldsymbol{\varepsilon}, \quad (4.27)$$

where $\mathbb{D}(\boldsymbol{\varepsilon})$ is not the elasticity tensor. Considering a potential as

$$\Pi = \int_{\Omega} \Psi dV - \int_{\Omega} \mathbf{f} \cdot \mathbf{u} dV - \int_{\partial\Omega} \mathbf{t} \cdot \mathbf{u} dA \rightarrow \min, \quad (4.28)$$

the finite element method (FEM) is applied in the problem to minimize this potential for linear elastic materials calculate the deformation of the physical system under external forces. According to the second law, the principle states that by applying forces on a system, the direction of deformation will be towards an state with the minimum potential energy along with the maximum wasting energy, i.e. dissipation. Then the next step is only to insert the corresponding energy into Eq. (4.28) and then to solve the equilibrium equations for every arbitrary material. In general, the variational form of Eq. (4.28) to obtain the optimized solutions has the form of

$$\int_{\Omega} \frac{\partial \Psi}{\partial \boldsymbol{\varepsilon}} : \delta \boldsymbol{\varepsilon} dV - \int_{\Omega} \mathbf{f} \cdot \delta \mathbf{u} dV - \int_{\partial\Omega} \mathbf{t} \cdot \delta \mathbf{u} dA = 0. \quad (4.29)$$

Furthermore, the constitutive equation for stress is given by

$$\boldsymbol{\sigma} = \frac{\partial \Psi}{\partial \boldsymbol{\varepsilon}}. \quad (4.30)$$

Substituting Eq. (4.30) into Eq. (4.29) yields

$$\int_{\Omega} \boldsymbol{\sigma} : \delta \boldsymbol{\varepsilon} dV - \int_{\Omega} \mathbf{f} \cdot \delta \mathbf{u} dV - \int_{\partial\Omega} \mathbf{t} \cdot \delta \mathbf{u} dA = 0. \quad (4.31)$$

In some literature, they define an internal energy and an external energy as below

$$\mathbf{f}_{int} = \int_{\Omega} \boldsymbol{\sigma} : \boldsymbol{\varepsilon} dV, \quad (4.32)$$

$$\mathbf{f}_{out} = - \int_{\Omega} \mathbf{f} \cdot \mathbf{u} dV - \int_{\partial\Omega} \mathbf{t} \cdot \mathbf{u} dA. \quad (4.33)$$

While \mathbf{f}_{int} is the energy which is stored in the material and belongs to the total free energy in the system, \mathbf{f}_{out} is the energy caused by a force through the displacement of a material point. Total potential energy only consists of the potential stored in the material, therefore, we have

$$\Pi = \mathbf{f}_{int} + \mathbf{f}_{out}. \quad (4.34)$$

With these definition, Eq. (4.31) is rewritten as

$$\delta \mathbf{f}_{int} + \delta \mathbf{f}_{out} = 0 \quad (4.35)$$

After discretization, by assembling all the elements, we have

$$\delta \mathbf{F}^{int} = \bigcup_{i=1}^{n_{el}} \delta \mathbf{f}_{int}, \quad (4.36)$$

$$\delta \mathbf{F}^{out} = \bigcup_{i=1}^{n_{el}} \delta \mathbf{f}_{out}, \quad (4.37)$$

here n_{el} is the total number of elements. The requirement is now to solve the equation, $\mathbf{R}_u = \delta \mathbf{F}^{int} - \delta \mathbf{F}^{out} = 0$, by an iteration method. In each time step, we change the external load $\delta \mathbf{F}^{out}$ based on its evolution over time, and the time increment Δt_n . the well known Newton-Raphson Method can be applied to find the solution of \mathbf{R}_u . Thus, we have

$$\mathbf{R}_u^{k+1} = \mathbf{R}_u^k + \frac{\partial \mathbf{R}_u^k}{\partial \mathbf{u}} \cdot \Delta \mathbf{u}^{k+1} = \mathbf{0} \quad (4.38)$$

where k is an iterator. The displacement increment is computed by the below equation

$$\Delta \mathbf{u}^{k+1} = -\left[\frac{\partial \mathbf{R}_u^k}{\partial \mathbf{u}}\right]^{-1} \cdot \mathbf{R}_u^k. \quad (4.39)$$

Then, the displacements are updated as

$$\mathbf{u}^{k+1} = \mathbf{u}^k + \Delta \mathbf{u}^{k+1}. \quad (4.40)$$

The full description of finite element method is summarized in algorithm 1.

Algorithm 1 Finite Element Method Algorithm

Specify the initial value \mathbf{u}

$$\mathbf{u}_{n+1}^0 = \mathbf{u}_n. \quad (4.41)$$

while convergence criterion is not satisfied **do**

1. Calculate of initial displacement and Update \mathbf{u}

$$\Delta \mathbf{u}_{n+1}^0 = - \left(\frac{\mathbf{R}_u}{\mathbf{u}} \right)^{-1} \mathbf{R}_u(\mathbf{u}_{n+1}^0), \quad (4.42)$$

$$\mathbf{u}_{n+1}^{m+1} = \mathbf{u}_{n+1}^m + \Delta \mathbf{u}^m. \quad (4.43)$$

2. Compute the strain tensor

$$\boldsymbol{\varepsilon}_p = \mathbf{B}_{n+1}^{m+1} \cdot \mathbf{u}_{n+1}^{m+1}. \quad (4.44)$$

3. Determine $\boldsymbol{\sigma}_{n+1}^{m+1}$ and tangent matrix \mathbf{D}_r

4. Calculate $\delta \mathbf{F}^{int}$ and $\delta \mathbf{F}^{ext}$

5. Calculate $\Delta \mathbf{u}_{n+1}^{m+1}$

$$\Delta \mathbf{u}_{n+1}^{m+1} = -\mathbf{K}_{n+1}^{e,m+1} \cdot \mathbf{R}_u(\mathbf{u}_{n+1}^{m+1}), \quad (4.45)$$

where $\mathbf{K}_{n+1}^{e,m+1} = \left. \frac{\partial \mathbf{R}_u}{\partial \mathbf{u}} \right|_{\mathbf{u}=\mathbf{u}_{n+1}^{m+1}}$.

end while

If the converged condition is reached, we need to update the values as

$$\mathbf{u}_{n+1} = \mathbf{u}_{n+1}^{m+1}, \quad (4.46)$$

$$\boldsymbol{\sigma}_{n+1} = \boldsymbol{\sigma}_{n+1}^{m+1}. \quad (4.47)$$

Let us now derive $\mathbf{K}_{n+1}^{e,m+1}$

$$\mathbf{K}_{n+1}^{e,m+1} = \frac{\partial}{\partial \mathbf{u}} (\delta \mathbf{F}^{int} - \delta \mathbf{F}^{ext}) = \int_{\Omega} \mathbf{B}^T \mathbf{D}_r \mathbf{B} \delta \mathbf{u} dV, \quad (4.48)$$

where \mathbf{D}_r and \mathbf{B} are calculated as follows

$$\mathbf{D}_r = \frac{\partial \boldsymbol{\sigma}_{n+1}^{m+1}}{\partial \boldsymbol{\varepsilon}_{p,n+1}^{m+1}}, \quad \text{and} \quad \mathbf{B} = \frac{\partial \boldsymbol{\varepsilon}_{p,n+1}^{m+1}}{\partial \mathbf{u}_{n+1}^{m+1}}. \quad (4.49)$$

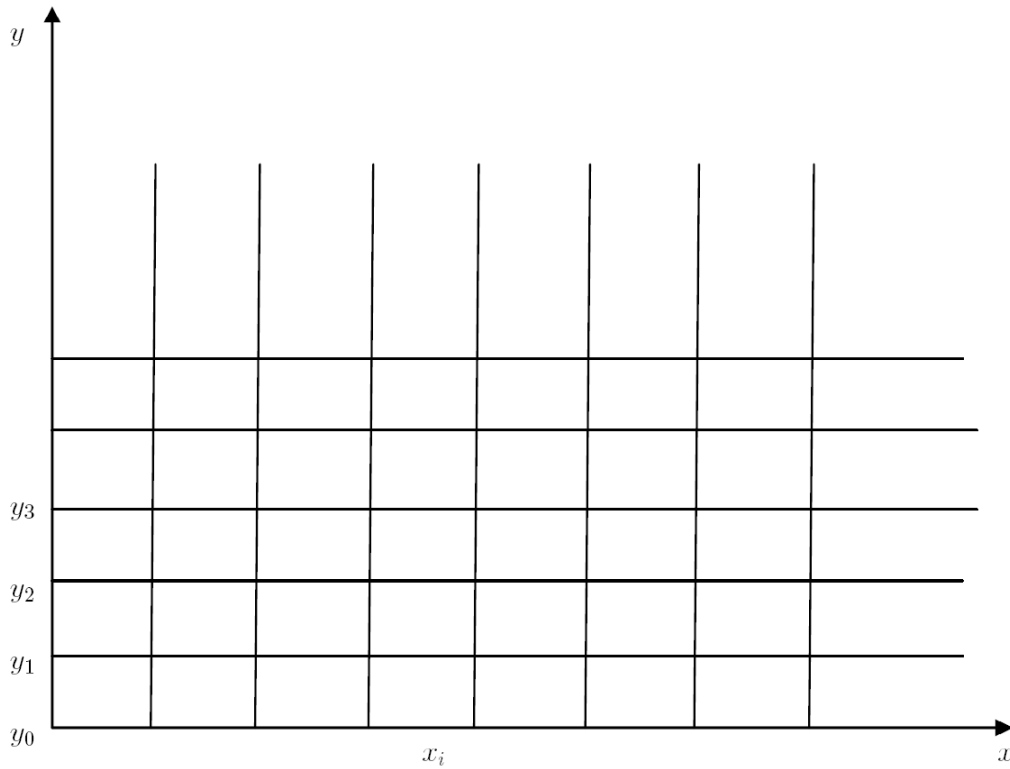


Figure 4.2: Uniformly meshed domain.

4.3 Marching algorithm

All the versions of the distribution function as well as of nucleation theory established for the problem at the microscale, discussed in Chapter 2, will need to be solved numerically. Hence, the discussion about the numerical approach to solve the differential equation as well as the volume conservation will be the main duty of this chapter. The algorithm which is applied to solve the problem at the microscale is called a marching algorithm. It is based on the Zienkiewicz-Zhu estimator. This algorithm is a mixture of finite element method, Euler-Backward method, Newton-Raphson method and integral approximations. Let us first discuss generally the marching algorithm and then the detailed algorithm with respect to each specific model will be presented. Since the distribution function is a function of two variables, we will consider a domain $x \times y$. This domain will be discretized uniformly. Let us implement the marching algorithm with non-uniform domain. If the readers are interested in this topic, please have a look at [Khai, 2014]. The maximum length in x direction and y direction are denoted l_x and l_y , respectively. The purpose of this algorithm is to find the numerically approximated solution of a function $f(x, y)$. The numerical solution is created step by step. With the initial value $f^0(x, 0)$, the value of f at the current step, corresponding to the line y_k , is computed from the previous value f^{k-1} . As can be seen in Figure 4.2, the domain is divided into m and n equal intervals, respectively. Δx and Δy are denoted as interval lengths of x and y , respectively. The discretization is defined as follows

$$x_{i+1} = x_i + \Delta x = x_0 + i\Delta x \quad (i = 0, m), \quad (4.50)$$

$$y_{j+1} = y_j + \Delta y = y_0 + j\Delta y \quad (j = 0, n). \quad (4.51)$$

The value of $f^k(x_i, y_k)$, where $i = \{0, \dots, m\}$ and $k = \{0, \dots, n\}$, is its value at the line y_k . The initial function is as bellow

$$f^0(x_i, y_0) = g(x_i), \quad (4.52)$$

where the value of $g(x_i)$ is required.

4.3.1 Marching algorithm for the distribution function $\bar{f}(D, r)$

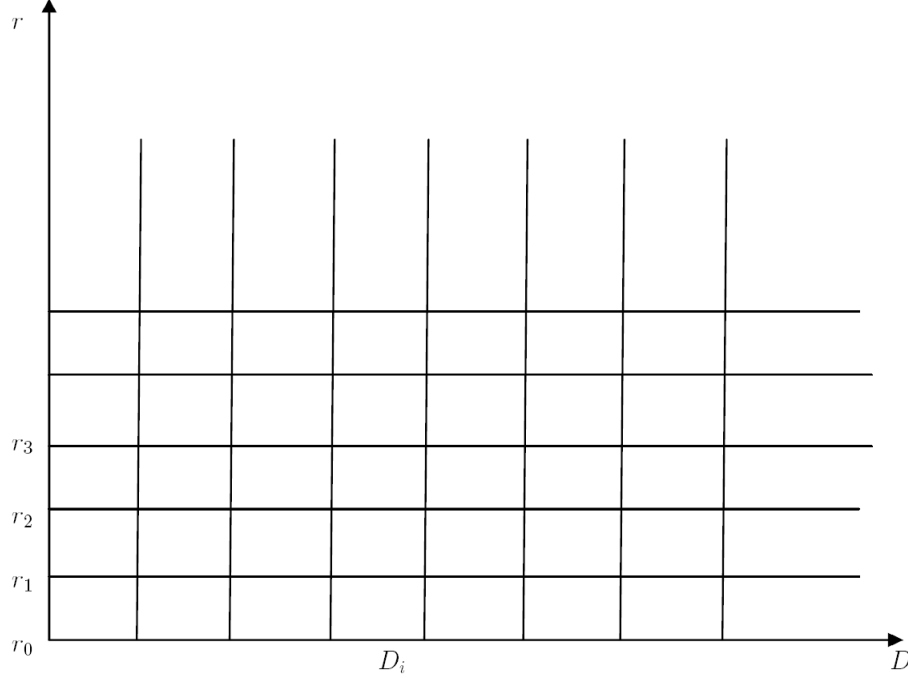


Figure 4.3: Uniformly meshed domain in $D \times r$.

Within this model, the domain $x \times y$ is $D \times r$ as can be seen in Figure ???. The maximum lengths of D and r are D_{\max} and r_{\max} , respectively. The differential equation as well as the volume constraint is reviewed again

$$\frac{\partial}{\partial D} \left[\left(-\bar{\lambda} + r^2 + \frac{\bar{\eta}}{D} \right) \bar{f} \right] = \bar{v} \frac{\partial \bar{f}}{\partial r}, \quad (4.53)$$

$$\frac{\pi}{6} \iint D^3 \bar{f}(D, r) \, dD dr = \text{const}, \quad (4.54)$$

where \bar{v} depends on ε_p from the problem at the macroscale. Now it is in turn that the detailed steps of the marching algorithm are established. Firstly, for the right-hand side of Eq. (4.53), the implicit Euler is employed. Consequently, the continuity equation can be recast into

$$\frac{\partial}{\partial D} \left[\left(-\bar{\lambda} + r_k^2 + \frac{\bar{\eta}}{D} \right) \bar{f}^k \right] = \bar{v} \frac{\bar{f}^k - \bar{f}^{k-1}}{\Delta r}. \quad (4.55)$$

Secondly, FEM with respect to D , $\bar{f}^k(D, r^k) \approx \mathbf{f}^k \cdot \boldsymbol{\varphi}$ is used in the left-hand side of Eq. (4.54), this leads

$$\frac{\partial}{\partial D} \left[\left(-\bar{\lambda} + r_k^2 + \frac{\bar{\eta}}{D_i} \right) \mathbf{f}^k \cdot \boldsymbol{\varphi} \right] = \bar{v} \frac{\mathbf{f}^k \cdot \boldsymbol{\varphi} - \mathbf{f}^{k-1} \cdot \boldsymbol{\varphi}}{\Delta r}. \quad (4.56)$$

By multiplying both sides of this equation by the shape function vector $\boldsymbol{\varphi}$ and then integrating this over the domain, the newly algebraic equation has the form of

$$\int \frac{\partial}{\partial D} \left[\left(-\bar{\lambda} + r_k^2 + \frac{\bar{\eta}}{D} \right) \mathbf{f}^k \cdot \boldsymbol{\varphi} \right] \otimes \boldsymbol{\varphi} \, dD = \int \left(\bar{v} \frac{\mathbf{f}^k \cdot \boldsymbol{\varphi} - \mathbf{f}^{k-1} \cdot \boldsymbol{\varphi}}{\Delta r} \right) \otimes \boldsymbol{\varphi} \, dD. \quad (4.57)$$

After simplification, the differential equation is rewritten as

$$\mathbf{f}^k(-\mathbf{A} \cdot \mathbf{H} + \frac{\bar{v}}{\Delta r} \cdot \mathbf{B}) = \frac{\bar{v}}{\Delta} \mathbf{f}^{k-1} \cdot \mathbf{B}, \quad (4.58)$$

where \mathbf{A} , $A_{ij} = \int \varphi_i(\varphi)_j dx$, is an operator approximating differentiation with respect to D and \mathbf{B} , $B_{ij} = \int \varphi_i(\varphi)_j dx$, is a smoothing operator projecting the result of numerical differentiation onto the space of shape functions. \mathbf{H} , diagonal matrix, is calculated by

$$H_{ii}^k = -\bar{\lambda} + \frac{\bar{\eta}}{D_i} + r_k^2. \quad (4.59)$$

After obtaining the value of the whole distribution function f , the next step is to compute the derivative of \bar{f} with respect to $\bar{\lambda}$. Taking derivative of the continuity equation (4.53) arrives

$$\mathbf{f}^k(-\mathbf{A} \cdot \mathbf{H} + \frac{\bar{v}}{\Delta r} \cdot \mathbf{B}) = \frac{\bar{v}}{\Delta} \mathbf{f}^{k-1} \cdot \mathbf{B}. \quad (4.60)$$

$$\mathbf{f}_{,\bar{\lambda}}^k(-\mathbf{A} \cdot \mathbf{H} + \frac{\bar{v}}{\Delta r} \cdot \mathbf{B}) - \mathbf{A} \cdot \mathbf{H}_{,\bar{\lambda}} \cdot \mathbf{f}^k = \frac{\bar{v}}{\Delta} \mathbf{f}_{,\bar{\lambda}}^{k-1} \cdot \mathbf{B}. \quad (4.61)$$

Now the distribution function is characterized by the value of all nodes in the discretized body. Doing the similar scheme as in getting f , the derivative of f with respect to $\bar{\lambda}$ is approximated by

$$\mathbf{f}_{,\bar{\lambda}}^k(-\mathbf{A} \cdot \mathbf{H} + \frac{\bar{v}}{\Delta r} \cdot \mathbf{B}) = -\mathbf{f}^k \cdot \mathbf{A} + \frac{\bar{v}}{\Delta r} \mathbf{f}_{,\bar{\lambda}}^{k-1} \cdot \mathbf{B}. \quad (4.62)$$

We assume that during the process to calculate f and $f_{,\bar{\lambda}}$, the value of $\bar{\lambda}$ is assumed to be given. The question is how to determine Lagrange multiplier $\bar{\lambda}$ ([Nguyen et al., 2013]). Let us base on the volume conservation to compute it. The assumption that the aggregate volume is unity during the dynamic recrystallization process. Let us firstly define two functions $F(\bar{\lambda})$ and $F(\bar{\lambda})_{,\bar{\lambda}}$ as follows

$$F(\bar{\lambda}) = \frac{\Pi}{6} \int D^3 \bar{f}(\bar{\lambda}) dD dr - 1, \quad F(\bar{\lambda})_{,\bar{\lambda}} = \frac{\Pi}{6} \int D^3 \bar{f}_{,\bar{\lambda}}(\bar{\lambda}) dD dr. \quad (4.63)$$

Then employing Newton-Raphson method, the value of $\bar{\lambda}$ at the current step $i+1$ is obtained by

$$\bar{\lambda}_{i+1} = \bar{\lambda}_i - \frac{1}{F_{,\bar{\lambda}}(\bar{\lambda}_i)} \cdot F(\bar{\lambda}_i). \quad (4.64)$$

It means that the value of $\bar{\lambda}_{i+1}$ is dependent on the value of $F(\bar{\lambda})$ and its derivative with respect to $\bar{\lambda}$. However, as in Eq. (4.63), these values will be impacted on the discretized values of \bar{f} . Therefore, the requirement to link the discretized values and $F(\bar{\lambda})$ and $F(\bar{\lambda})_{,\bar{\lambda}}$ by Simpson's rule as below

$$\begin{aligned} F &= \frac{\Pi}{6} \int \int D^3 \bar{f} dD dr - 1 \approx \sum_{i,j} \frac{\Pi}{54} \bar{f}(D_i, r_j) \Delta D \Delta r D_i^3 w_i w_j - 1, \\ F_{,\bar{\lambda}} &= \frac{\Pi}{6} \int \int D^3 \bar{f}_{,\bar{\lambda}} dD dr \approx \sum_{i,j} \frac{\Pi}{54} \bar{f}_{,\bar{\lambda}}(D_i, r_j) \Delta D \Delta r D_i^3 w_i w_j. \end{aligned} \quad (4.65)$$

Let us summarize the full description of marching algorithm

Algorithm 2 Marching Algorithm for $\bar{f}(D, r)$

Initialize values for t_{n+1}

$$\dot{\epsilon}_{p,n+1}^0 = \dot{\epsilon}_{p,n}, \quad \bar{\lambda}_{n+1}^0 = \bar{\lambda}_n \quad \text{and} \quad D_{\max}^0 = \frac{2}{3}(\bar{\lambda}_{n+1}^0)^{\frac{3}{2}} \frac{1}{\bar{v}}.$$

while convergence criterion is not satisfied **do**

Compute $\mathbf{f}(D, r)$ and $\mathbf{f}_{,\bar{\lambda}}(D, r)$ from Eqs. (4.62) and (4.58) for $\bar{\lambda}_{n+1}^u$

Calculate the value of $\bar{\lambda}$

$$\bar{\lambda}_{n+1}^{u+1} = \bar{\lambda}_{n+1}^u - \frac{F(\bar{\lambda}_{n+1}^u)}{F_{,\bar{\lambda}}(\bar{\lambda}_{n+1}^u)},$$

where $F(\bar{\lambda}_{n+1}^u)$ and $F_{,\bar{\lambda}}(\bar{\lambda}_{n+1}^u)$ are calculated by Eq.(4.65) and D_{\max}

$$D_{\max,n+1}^{u+1} = \frac{2}{3}(\bar{\lambda}_{n+1}^{u+1})^{\frac{3}{2}} \frac{1}{\bar{v}}.$$

end while

In our marching algorithm, the absolute convergence criterion has the below formulation

$$\frac{\bar{\lambda}_{n+1}^{u+1} - \bar{\lambda}_{n+1}^u}{\bar{\lambda}_{n+1}^u} \leq \mathbf{TOL}. \quad (4.66)$$

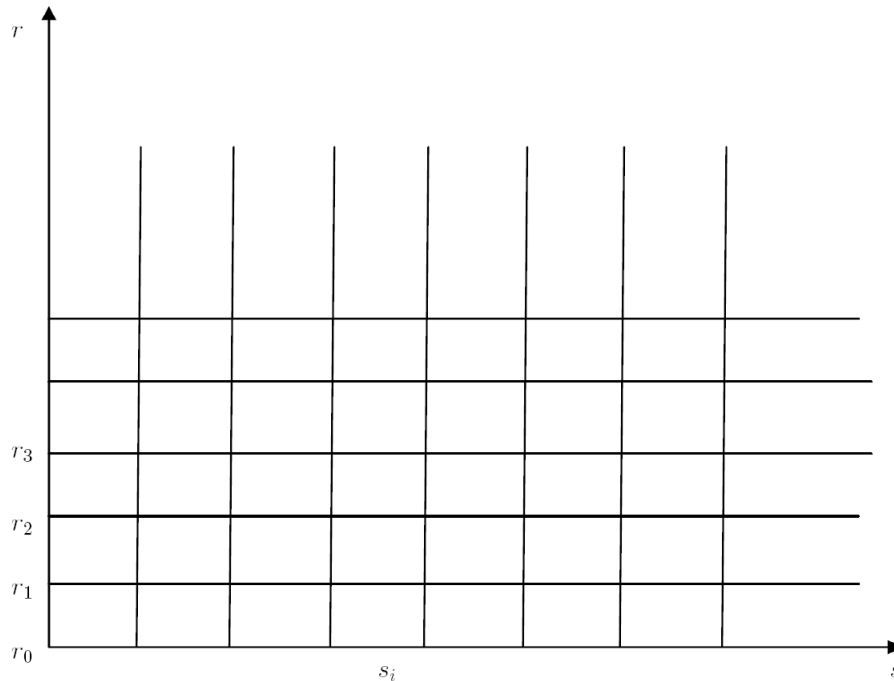
4.3.2 Marching algorithm for the distribution function $\tilde{f}(s, r)$ 

Figure 4.4: Uniformly meshed domain in $s \times r$.

Now we deal with the distribution function which is influenced by s and r . We implement the same steps as mentioned in the previous part. Firstly, the backward Euler method with

respect to r and FEM with respect to s are carried out in the differential equation as same as in the marching algorithm for $\bar{f}(D, r)$. It means that the first term is applied for the right-hand side and the second for the left-hand side of Eq. (3.76)(1). The mathematical model in Section 2.3 states that

$$\frac{\partial}{\partial s} \left[\left(\frac{\bar{\eta}}{s + \frac{1}{v} (\bar{\lambda}r - \frac{1}{3}r^3)} \right) \tilde{f} \right] = \bar{v} \frac{\partial \tilde{f}}{\partial r}. \quad (4.67)$$

Performing the implicit Euler for Eq. (4.67), it has the new form of

$$\frac{\partial}{\partial s} \left[\left(\frac{\bar{\eta}}{s + \frac{1}{v} (\bar{\lambda}r_{k+1} - \frac{1}{3}r_{k+1}^3)} \right) \tilde{f}^{k+1} \right] \approx \bar{v} \frac{\tilde{f}^{k+1} - \tilde{f}^k}{\Delta r}. \quad (4.68)$$

The unknown \tilde{f} and its derivative $\tilde{f}_{,\bar{\lambda}}$ with respect to $\bar{\lambda}$ at the line r^k can be linearly approximated based on FEM [Zienkiewicz and Taylor, 2005] as

$$\tilde{f}^k(s, r_k) \approx \mathbf{f}^k \cdot \boldsymbol{\varphi}, \quad \tilde{f}_{,\bar{\lambda}}^k(s, r_k) \approx \mathbf{f}_{,\bar{\lambda}}^k \cdot \boldsymbol{\varphi}, \quad (4.69)$$

where \mathbf{f}^k and $\mathbf{f}_{,\bar{\lambda}}^k$ are vectors containing nodal values, and $\boldsymbol{\varphi}$ is a vector containing the shape functions in variable s . Inserting Eq. (4.69) into Eq. (4.68) gives us

$$\frac{\partial}{\partial s} \left[\left(\frac{\bar{\eta}}{s_i + \frac{1}{v} (\bar{\lambda}r_{k+1} - \frac{1}{3}r_{k+1}^3)} \right) \mathbf{f}^{k+1} \cdot \boldsymbol{\varphi} \right] \approx \bar{v} \frac{\mathbf{f}^{k+1} \cdot \boldsymbol{\varphi} - \mathbf{f}^k \cdot \boldsymbol{\varphi}}{\Delta r}. \quad (4.70)$$

Due to the fact that \mathbf{f}^{k+1} is independent on s , it is possible to allow it out of the derivative. Then we have

$$\mathbf{f}^{k+1} \cdot \boldsymbol{\varphi}_{,s} \left(\frac{\bar{\eta}}{s_i + \frac{1}{v} (\bar{\lambda}r_{k+1} - \frac{1}{3}r_{k+1}^3)} \right) \approx \frac{\bar{v}}{\Delta r} \mathbf{f}^{k+1} \cdot \boldsymbol{\varphi} - \frac{\bar{v}}{\Delta r} \mathbf{f}^k \cdot \boldsymbol{\varphi}. \quad (4.71)$$

Furthermore, multiplying with $\boldsymbol{\varphi}$ and integrating over the whole length l_s of both sides yield

$$\mathbf{f}^{k+1} \cdot \int_{l_s} \boldsymbol{\varphi}_{,s} \otimes \boldsymbol{\varphi} ds \cdot \mathbf{H}^{k+1} \approx \frac{\bar{v}}{\Delta r} \mathbf{f}^{k+1} \cdot \int_{l_s} \boldsymbol{\varphi} \otimes \boldsymbol{\varphi} ds - \frac{\bar{v}}{\Delta r} \mathbf{f}^k \cdot \int_{l_s} \boldsymbol{\varphi} \otimes \boldsymbol{\varphi} ds, \quad (4.72)$$

Using the definition of the smoothing operator \mathbf{B} , the derivative operator \mathbf{A} , the distribution function value of nodes are calculated by

$$\mathbf{f}^{k+1} (-\mathbf{A} \cdot \mathbf{H} + \frac{v}{\Delta r} \cdot \mathbf{B}) = \frac{v}{\Delta} \mathbf{f}^k \cdot \mathbf{B}. \quad (4.73)$$

Let us call \mathbf{H} a diagonal matrix with its component

$$\begin{aligned} H_{ii}^{k+1} &= \frac{\bar{\eta}}{s_i + \frac{1}{v} (\bar{\lambda}r_{k+1} - \frac{1}{3}r_{k+1}^3)}, \\ H_{ij}^{k+1} &= 0 \quad \text{if } i \neq j, \end{aligned} \quad (4.74)$$

where $i, j = \{1, \dots, n\}$. The derivative of f^{n+1} with respect to $\bar{\lambda}$ is obtained by taking derivative of Eq. (4.73) with respect to $\bar{\lambda}$

$$\mathbf{f}_{,\bar{\lambda}}^{k+1} (-\mathbf{A} \cdot \mathbf{H} + \frac{v}{\Delta r} \cdot \mathbf{B}) = \mathbf{H}_{,\bar{\lambda}} \cdot \mathbf{f}^{k+1} \cdot \mathbf{A} + \frac{v}{\Delta r} \mathbf{f}_{,\bar{\lambda}}^k \cdot \mathbf{B}, \quad (4.75)$$

where $H_{,\bar{\lambda}}$ is the diagonal matrix concerning the derivative of H with respect to $\bar{\lambda}$ as

$$\begin{aligned} H_{ii,\lambda}^{k+1} &= \frac{\eta r_{k+1}}{v \left[s_i + \frac{1}{v} (\bar{\lambda} r_{k+1} - \frac{1}{3} r_{k+1}^3) \right]^2}, \\ H_{ij,\lambda}^{k+1} &= 0 \quad \text{if } i \neq j, \end{aligned} \quad (4.76)$$

As in Section 4.3.1, $\bar{\lambda}$ is approximated by using Simpson's rule in the volume conservation. The assumption that the aggregate volume is unity during the dynamic recrystallization process is provided as

$$\frac{\pi}{6} \iint_{\Omega} \left[s + \frac{1}{v} \left(\bar{\lambda} r - \frac{1}{3} r^3 \right) \right]^3 \tilde{f}(s, r) \, ds dr = 1. \quad (4.77)$$

The constraint of the preserved aggregate volume and its derivative with respect to $\bar{\lambda}$ are in the form of

$$V = \frac{\pi}{6} \iint_{\Omega} \left[s + \frac{1}{v} \left(\bar{\lambda} r - \frac{1}{3} r^3 \right) \right]^3 \tilde{f}(s, r) \, ds dr - 1, \quad (4.78)$$

$$V_{,\bar{\lambda}} = \frac{\pi}{6} \iint_{\Omega} \left\{ 3 \frac{r}{v} \left[s + \frac{1}{v} \left(\bar{\lambda} r - \frac{1}{3} r^3 \right) \right]^2 \tilde{f}(s, r) + \left[s + \frac{1}{v} \left(\bar{\lambda} r - \frac{1}{3} r^3 \right) \right]^3 \tilde{f}_{,\bar{\lambda}}(s, r) \right\} \, ds dr. \quad (4.79)$$

These constraints can be solved for the unknown $\bar{\lambda}$ by the Newton-Raphson method as following

$$\bar{\lambda}_{l+1} = \bar{\lambda}_l - \frac{V(\bar{\lambda}_l)}{V_{,\bar{\lambda}}(\bar{\lambda}_l)}. \quad (4.80)$$

The volume and its derivative with respect to λ are determined by the approximate method

$$V \approx \frac{\pi}{54} \left[s_j + \frac{1}{v} \left(\bar{\lambda} r_i - \frac{1}{3} r_i^3 \right) \right]^3 \tilde{f}(s_j, r_i) w_i w_j - 1, \quad (4.81)$$

$$\begin{aligned} V_{,\bar{\lambda}} \approx & \frac{\pi}{54} \left\{ 3 \frac{r_i}{v} \left[s_j + \frac{1}{v} \left(\bar{\lambda} r_i - \frac{1}{3} r_i^3 \right) \right]^2 \tilde{f}(s_j, r_i) \right. \\ & \left. + \left[s_j + \frac{1}{v} \left(\bar{\lambda} r_i - \frac{1}{3} r_i^3 \right) \right]^3 \tilde{f}_{,\bar{\lambda}}(s_j, r_i) w_i w_j \right\} \end{aligned} \quad (4.82)$$

The full marching algorithm corresponding to this version of our problem is summarized as

Algorithm 3 Marching Algorithm for $\tilde{f}(s, r)$

Initialize values for t_{n+1}

$$\dot{\epsilon}_{p,n+1}^0 = \dot{\epsilon}_{p,n}, \quad \bar{\lambda}_{n+1}^0 = \bar{\lambda}_n \quad D_{\max}^0 = \frac{2}{3}(\bar{\lambda}_{n+1}^0)^{\frac{3}{2}} \frac{1}{\bar{v}}.$$

while convergence criterion is not satisfied **do**

Compute $\mathbf{f}(s, r)$ and $\mathbf{f}_{,\bar{\lambda}}(s, r)$ based on Eqs. (4.73) and (4.75) for $\bar{\lambda}_{n+1}^u$

Update the value of $\bar{\lambda}$

$$\bar{\lambda}_{n+1}^{u+1} = \bar{\lambda}_{n+1}^u - \frac{F(\bar{\lambda}_{n+1}^u)}{F_{,\bar{\lambda}}(\bar{\lambda}_{n+1}^u)},$$

where $F(\bar{\lambda}_{n+1}^u)$ and $F_{,\bar{\lambda}}(\bar{\lambda}_{n+1}^u)$ are calculated by (4.78) and (4.79) and r_{\max}, D_{\max}

$$r_{\max,n+1}^{u+1} = \sqrt{3\bar{\lambda}_{n+1}^{u+1}}, \quad D_{\max,n+1}^{u+1} = \frac{2}{3}(\bar{\lambda}_{n+1}^{u+1})^{\frac{3}{2}} \frac{1}{\bar{v}}.$$

end while

As same as in the standard model, we use the absolute converge criterion as

$$\frac{\bar{\lambda}_{n+1}^{u+1} - \bar{\lambda}_{n+1}^u}{\bar{\lambda}_{n+1}^u} \leq \text{TOL}. \quad (4.83)$$

4.3.3 Marching algorithm for $\tilde{f}(s, r)$ and h

In this part, we will study how a marching algorithm is employed in the problem at the microscale when the distribution function in form of $\tilde{f}(s, r)$ and the extended nucleation theory are applied. Now, by inserting $D = s + \frac{1}{\bar{v}}(\bar{\lambda}r - \frac{1}{3}r^3)$ into Eq. (3.135), the continuity equation with the source function \bar{h} has the following form

$$\frac{\partial}{\partial s} \left[\left(\frac{\bar{\eta}}{s + \frac{1}{\bar{v}}(\bar{\lambda}r - \frac{1}{3}r^3)} \right) \tilde{f} \right] = \bar{v} \frac{\partial \tilde{f}}{\partial r} + \bar{h}. \quad (4.84)$$

The theory of \bar{h} is already mentioned in Section 2.3.3. Euler-Backward expression for the right hand side gives the result as

$$\frac{\partial}{\partial s} \left[\left(\frac{\bar{\eta}}{s + \frac{1}{\bar{v}}(\bar{\lambda}r_{n+1} - \frac{1}{3}r_{n+1}^3)} \right) \tilde{f}^{n+1} \right] = \bar{v} \frac{f^{n+1} - f^n}{\Delta r} + \bar{h}^{n+1}. \quad (4.85)$$

Comparing to other cases, in this case we need one more unknown variable. This is C , the unknown Lagrange multiplier relating to the source function. Therefore, at the microscale, the problem are solved to get $\bar{\lambda}$, \mathbf{f} and C . Following the steps of marching algorithm [Nguyen et al., 2015], the next step is to apply discretization for s and to approximate the derivative of $\tilde{f}(s, r)$, the differential equation has the below ansatz after simplification

$$\mathbf{f}^{n+1}(-\mathbf{A} \cdot \mathbf{H} + \frac{v}{\Delta r} \cdot \mathbf{B}) = \frac{v}{\Delta} \mathbf{f}^n \cdot \mathbf{B} + \mathbf{R}^{n+1}. \quad (4.86)$$

The derivative of distribution function fulfills the equation as follows

$$\mathbf{f}_{,\bar{\lambda}}^{n+1}(-\mathbf{A} \cdot \mathbf{H} + \frac{v}{\Delta r} \cdot \mathbf{B}) = \mathbf{R}_{,\bar{\lambda}} \cdot \boldsymbol{\varphi} + \mathbf{H}_{,\bar{\lambda}} \cdot \mathbf{f}^{n+1} \cdot \mathbf{A} + \frac{v}{\Delta r} \mathbf{f}_{,\bar{\lambda}}^n \cdot \mathbf{B}, \quad (4.87)$$

where \mathbf{H} and $\mathbf{H}_{,\bar{\lambda}}$ are computed by Eqs. (4.76) and (4.74). The index form of tensor \mathbf{R} is given by

$$R_{ii}^{n+1} = \bar{h}(r_{n+1}, s_i, \bar{\lambda}, C). \quad (4.88)$$

As can be seen in (4.88), the source function depends on values of $\bar{\lambda}$ and C . Let us discuss how to compute them. These unknown parameters are determined by Newton-Raphson method as below

$$\begin{pmatrix} \bar{\lambda}_{i+1} \\ C_{i+1} \end{pmatrix} = \begin{pmatrix} \bar{\lambda}_i \\ C_i \end{pmatrix} - \mathbf{J}^{-1} \begin{pmatrix} \bar{\lambda}_i \\ C_i \end{pmatrix} \cdot \mathbf{F} \begin{pmatrix} \bar{\lambda}_i \\ C_i \end{pmatrix}, \quad (4.89)$$

where $\mathbf{F} = (F_1, F_2)^T$. Firstly, let us define the vector \mathbf{F}

$$F_1 = \frac{\Pi}{6} \int \int D^3 \tilde{f} ds dr - 1, \quad (4.90)$$

$$F_2 = \frac{\Pi}{6} \int \int D^3 \bar{h} ds dr. \quad (4.91)$$

Then this vector's components are approximately calculated by Simpson's rule as in the below formulations

$$F_1 \approx \sum_{i,j} \frac{\Pi}{54} \tilde{f}(s_i, r_j) \Delta s \Delta r D^3(s_i, r_j) w_i w_j - 1, \quad (4.92)$$

$$F_2 \approx \sum_{i,j} \frac{\Pi}{54} D^3(s_i, r_j) \bar{h}(s_i, r_j) \Delta s \Delta r w_i w_j. \quad (4.93)$$

Moreover, \mathbf{J} is the gradient tensor of \mathbf{F} . Therefore, \mathbf{J} can be computed by

$$\mathbf{J} = \begin{bmatrix} F_{1,\lambda} & F_{1,C} \\ F_{2,\lambda} & F_{2,C} \end{bmatrix} \quad (4.94)$$

Of course, in this algorithm, we require the initial value of $\bar{\lambda}$ and C .

Algorithm 4 Marching Algorithm for $\tilde{f}(s, r)$ and h

Initialize values for t_{n+1}

$$\dot{\epsilon}_{p,n+1}^0 = \dot{\epsilon}_{p,n}, \quad \bar{\lambda}_{n+1}^0 = \bar{\lambda}_n \quad \text{and} \quad r_{\max,n+1}^0 = \sqrt{3\bar{\lambda}_{n+1}^0}, \quad D_{\max}^0 = \frac{2}{3}(\bar{\lambda}_{n+1}^0)^{\frac{3}{2}} \frac{1}{v}.$$

while convergence criteria not fulfilled **do**

Calculate $\mathbf{f}(s, r)$ and $\mathbf{f}_{,\bar{\lambda}}(s, r)$ based on Eq. (4.86) and Eq. (4.87) for $\bar{\lambda}_{n+1}^u$

Update the value of $\bar{\lambda}$ and C with Eq. (4.89)

where $\mathbf{F}(\bar{\lambda}_{n+1}^u)$ and $\mathbf{J}_{,\bar{\lambda}}^{-1}(\bar{\lambda}_{n+1}^u)$ are computed by Eq. (4.92), Eq. (4.93) and Eq.(4.94) and r_{\max}, D_{\max}

$$r_{\max,n+1}^{u+1} = \sqrt{3\bar{\lambda}_{n+1}^{u+1}}, \quad D_{\max,n+1}^{u+1} = \frac{2}{3}(\bar{\lambda}_{n+1}^{u+1})^{\frac{3}{2}} \frac{1}{v}.$$

end while

In our marching algorithm the absolute convergence criterion as follows

$$\frac{\bar{\lambda}_{n+1}^{u+1} - \bar{\lambda}_{n+1}^u}{\bar{\lambda}_{n+1}^u} \leq \mathbf{TOL}. \quad (4.95)$$

4.3.4 Fix-point algorithm

In order to find the distribution $g(p_0)$ of grains $g(p_0) = C \frac{\Pi}{2} \int \hat{D}(p, \sqrt{p_0})^2 p_0 g(p) dp$, the fix-point algorithm is applied. A point is called the fix-point of a function $g(x)$ when the condition, $x = g(x)$, is fulfilled. Fix-point iteration is an iterative method. The next iterative result is calculated as $x_{i+1} = g(x_i)$.

Algorithm 5 Fix-point algorithm

Choose the initial values for the initial step

while convergence criterion is not satisfied **do**

1. Solve differential equations to get $\hat{D}(p_0, r)$
2. Calculate the volume at the current step l

$$V = \frac{\Pi}{6} \int_{\Omega} \hat{D}^3(p_0, r) g(l, p_0) dp_0 dr. \quad (4.96)$$

3. Calculate $g(l + 1)$

- Determine $g^*(l + 1) = \int \frac{\Pi}{2} \hat{D}^2(p_0, \sqrt{p_0}) p_0 g(l, p_0) dp$
- Calculate $C(l + 1)$ by solving $v \int C(l + 1) g^*(l + 1) dp_0 = \alpha$
- Compute $g(l + 1) = C(l + 1) g^*(l + 1)$

4. Normalize by the formulation $g(l + 1) = g(l + 1)/V_0$

5. Update $k[l + 1] = [\int \hat{D}(p_0, r) g(l + 1) dp_0 dr]^{-1}$

6. Get the value of $\bar{p}(l + 1) = \frac{\Pi}{6} \int \hat{D}^3(p_0, r) p_0 dp_0 dr$

end while

4.4 Macroscopic simulation

As can be seen in the problem's description at the macroscale, in our model we assume that no hardening is considered and no yield function is analyzed. Moreover, another assumption was made in Hackl-Renner model that diffusion along grain boundaries is dominant, then

$M_{\text{eff}} = 720 (wM_{\parallel}/D\pi)$, where $M_{\parallel} = M_{\perp}$. The flow law multipliers for diffusion and dislocation creep, A_d and A_p , respectively, are introduced by

$$A_d = \frac{V}{\langle D^5/M_{\text{eff}} \rangle}, \quad \text{and} \quad (4.97)$$

$$A_p = \left[\frac{6V}{\Pi} \frac{1}{\langle D^3/\rho^m \rangle} \right]^{\frac{1}{m}} k_p. \quad (4.98)$$

The flow rules are rewritten as

$$\dot{\boldsymbol{\varepsilon}}_d = A_d \boldsymbol{\sigma}^d, \quad (4.99)$$

$$\dot{\boldsymbol{\varepsilon}}_p = A_p \|\boldsymbol{\sigma}^d\|^{\frac{1-m}{m}} \boldsymbol{\sigma}^d. \quad (4.100)$$

The differential equations are transformed into an incremental form using the time discretization. The algebraic equations are evaluated at the time instant t_{n+1}

$$\boldsymbol{\varepsilon}_d^{n+1} = \boldsymbol{\varepsilon}_d^n + A_d \boldsymbol{\sigma}^d \Delta t = \boldsymbol{\varepsilon}_d^n + Z^d(\boldsymbol{\sigma}^d) \cdot \Delta t, \quad (4.101)$$

$$\boldsymbol{\varepsilon}_p^{n+1} = \boldsymbol{\varepsilon}_p^n + A_p \|\boldsymbol{\sigma}^d\|^{\frac{1-m}{m}} \boldsymbol{\sigma}^d \Delta t = \boldsymbol{\varepsilon}_p^n + Z^p(\boldsymbol{\sigma}^d) \cdot \Delta t, \quad (4.102)$$

where $Z^d(\boldsymbol{\sigma}^d) = A_d \boldsymbol{\sigma}^d$ and $Z^p(\boldsymbol{\sigma}^d) = A_p \|\boldsymbol{\sigma}^d\|^{\frac{1-m}{m}} \boldsymbol{\sigma}^d$. In Voigt-notation, the constitutive equation is expressed implicitly as

$$\boldsymbol{\sigma}_{n+1} = \boldsymbol{\sigma}_n + \mathbb{C} \cdot (\Delta \boldsymbol{\varepsilon}^{n+1} - \Delta \boldsymbol{\varepsilon}_p^{n+1} - \Delta \boldsymbol{\varepsilon}_d^{n+1}). \quad (4.103)$$

The residual tensor is defined as

$$\mathbf{R}_{\boldsymbol{\sigma}} = \boldsymbol{\sigma}_{n+1} - \boldsymbol{\sigma}_n - \mathbb{C} \cdot \Delta \boldsymbol{\varepsilon}^{n+1} + \mathbb{C} \cdot (\Delta \boldsymbol{\varepsilon}_p^{n+1} + \Delta \boldsymbol{\varepsilon}_d^{n+1}). \quad (4.104)$$

Inserting (4.101) and (4.102) into (4.104) leads

$$\mathbf{R}_{\boldsymbol{\sigma}} = \boldsymbol{\sigma}_{n+1} - \boldsymbol{\sigma}_n - \mathbb{C} \cdot \Delta \boldsymbol{\varepsilon}^{n+1} + \mathbb{C} \cdot (Z^p(\boldsymbol{\sigma}^d)(\boldsymbol{\sigma}_d) + Z^d(\boldsymbol{\sigma}^d)(\boldsymbol{\sigma}_d)) \cdot \Delta t. \quad (4.105)$$

We solve the equation $\mathbf{R}_{\boldsymbol{\sigma}} = \mathbf{0}$ by the Newton-Raphson as follows

$$\boldsymbol{\sigma}_{n+1}^{k+1} = \boldsymbol{\sigma}_{n+1}^k - \left[\frac{\partial \mathbf{R}_{\boldsymbol{\sigma}}}{\partial \boldsymbol{\sigma}}(\boldsymbol{\sigma}_{n+1}^k) \right]^{-1} \cdot \mathbf{R}_{\boldsymbol{\sigma}}(\boldsymbol{\sigma}_{n+1}^k), \quad (4.106)$$

where

$$\frac{\partial \mathbf{R}_{\boldsymbol{\sigma}}}{\partial \boldsymbol{\sigma}}(\boldsymbol{\sigma}_{n+1}^k) = \mathbf{I} + \mathbb{C} \cdot \left(\frac{\partial Z^d(\boldsymbol{\sigma}^d)}{\partial \boldsymbol{\sigma}} + \frac{\partial Z^p(\boldsymbol{\sigma}^d)}{\partial \boldsymbol{\sigma}} \right) \Delta t, \quad (4.107)$$

and $\mathbf{I} = \delta_{ij} \mathbf{e}_i \mathbf{e}_j$. By denoting

$$\mathbf{A} = \frac{\partial \mathbf{R}_{\boldsymbol{\sigma}}}{\partial \boldsymbol{\sigma}}(\boldsymbol{\sigma}_{n+1}^k), \quad (4.108)$$

we obtain

$$\boldsymbol{\sigma}_{n+1}^{k+1} = \boldsymbol{\sigma}_{n+1}^k - \mathbf{A}^{-1} \cdot \mathbf{R}_{\boldsymbol{\sigma}}(\boldsymbol{\sigma}_{n+1}^k). \quad (4.109)$$

Given the increment in strain $\Delta \boldsymbol{\varepsilon}^{n+1} = \boldsymbol{\varepsilon}^{n+1} - \boldsymbol{\varepsilon}^n$ corresponding to an increment in time $[t_n, t_{n+1}]$, the state variables at time t_n are also given, for example, $\boldsymbol{\sigma}_n$. Then the corresponding initial value, $\Delta \boldsymbol{\sigma}_{n+1}^0$, is computed as

$$\boldsymbol{\sigma}_{n+1}^0 = \boldsymbol{\sigma}_n, \quad (4.110)$$

$$\Delta \boldsymbol{\sigma}_{n+1}^0 = -\mathbf{A}^{-1}(\boldsymbol{\sigma}_{n+1}^0) \cdot \mathbf{R}_{\boldsymbol{\sigma}}(\boldsymbol{\sigma}_{n+1}^0), \quad (4.111)$$

where $\mathbf{R}_\sigma(\sigma_{n+1}^0, \sigma_n^d)$ is computed based on Eq. (4.104):

$$\mathbf{R}_\sigma(\sigma_{n+1}^0, \sigma_n^d) = \sigma_n - \sigma_{n+1} - \mathbb{C} \cdot \Delta \epsilon^{n+1} + \mathbb{C} \cdot (\mathbf{Z}^p(\sigma_n^d) + \mathbf{Z}^d(\sigma_n^d)) \cdot \Delta t \quad (4.112)$$

$$= \mathbb{C} \cdot ((\mathbf{Z}^p(\sigma_n^d) + \mathbf{Z}^d(\sigma_n^d)) \cdot \Delta t - \Delta \epsilon^{n+1}). \quad (4.113)$$

taking the derivative of the implicit function (4.105) with respect to σ , \mathbf{A} is obtained by

$$\mathbf{A} = \left[\mathbf{I} + \mathbb{C} \cdot (A_d + A_p \|\sigma^d\|^{\frac{1-m}{m}}) \mathbf{I}^d + A_p \frac{1-m}{m} \|\sigma^d\|^{\frac{1-3}{m}} \sigma^d \otimes \sigma^d \Delta t \right]. \quad (4.114)$$

Therefore a consistent tangent operator (modulus), $\mathbf{D} = \frac{\partial \sigma_{n+1}}{\partial \epsilon^{n+1}}$, reads

$$\mathbf{D} = \left[\mathbf{I} + \mathbb{C} \cdot \left(\frac{\partial \mathbf{Z}^d(\sigma^d)}{\partial \sigma} + \frac{\partial \mathbf{Z}^p(\sigma^d)}{\partial \sigma} \right) \Delta t \right]^{-1} \cdot \mathbb{C} = \mathbf{A}^{-1} \cdot \mathbb{C}. \quad (4.115)$$

Box 1: Fully implicit algorithm of numerical integration for dynamic recrystallization .

1. Compute the distribution function $f(D, r)$, $\langle D^3/\rho^m \rangle$ and $\langle D^5/M_{\text{eff}} \rangle$, see the marching algorithm.
2. Given $\Delta \epsilon^{n+1}$ and the state variable at t_n , σ_n , evaluate the elastic initial state $\Delta \sigma_{n+1}^0$.
3. Return-Mapping with an iterative step k

- (i) Calculate the Newton step and update stress

$$\Delta \sigma_{n+1}^k = -\mathbf{A}^{-1}(\sigma)_{n+1}^k \cdot \mathbf{R}_\sigma(\sigma)_{n+1}^k, \quad (4.116)$$

$$\sigma_{n+1}^{k+1} = \Delta \sigma_{n+1}^k + \sigma_{n+1}^k. \quad (4.117)$$

- (ii) Check convergence criterion:

$$\|\mathbf{R}_\sigma(\sigma_n^{k+1})\| \leq \text{TOL}. \quad (4.118)$$

If this condition is fulfilled, go to step 4. If not, go to step 3.

4. Update the tangent matrix

$$\mathbf{D} = \mathbf{A}^{-1} \cdot \mathbb{C}, \quad (4.119)$$

and the necessary state-dependent variables (SDV), ϵ_p , ϵ_d , the effective inelastic strain norms together with the corresponding rate values

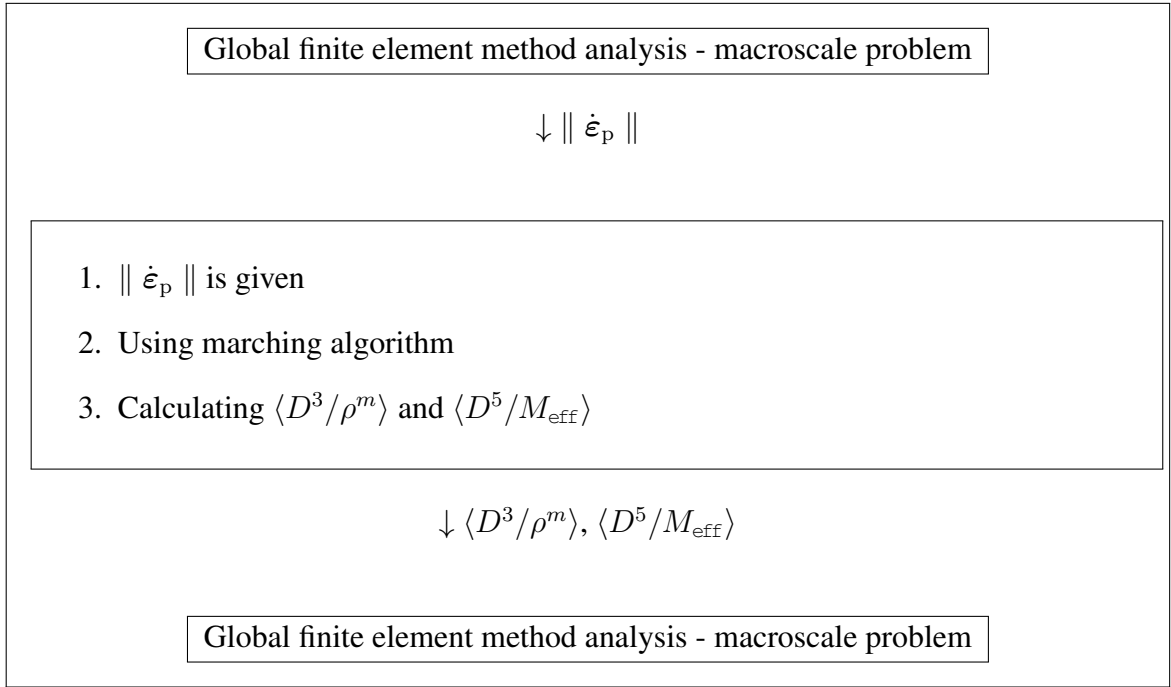
$$\epsilon_p = \sqrt{\frac{2}{3}} \|\epsilon_p\| \quad \text{and} \quad \dot{\epsilon}_p = \sqrt{\frac{2}{3}} \|\dot{\epsilon}_p\| \quad (4.120)$$

$$\epsilon_d = \sqrt{\frac{2}{3}} \|\epsilon_d\| \quad \text{and} \quad \dot{\epsilon}_d = \sqrt{\frac{2}{3}} \|\dot{\epsilon}_d\| \quad (4.121)$$

and also the converged $\bar{\lambda}$.

For more information about this algorithm, readers can refer to [Isfahani, 2014]. This is time to discuss how the microscale is linked to the macroscale. The connection between the microlevel and the macrolevel in the program code is shown as below,

Box 2: Connection of scales in the program code



As can be seen in this simplified flow chart, the calculation at the macroscale provides the rate of plastic strain, $\|\dot{\epsilon}_p\|$. The rate of plastic strain, $\|\dot{\epsilon}_p\|$ is understood as a given at the microscale. Solution of the differential equation accompanied by the volume constraint at this level results in the distribution function. From this result, the average values of $\langle D^3/\rho^m \rangle$, $\langle D^5/M_{\text{eff}} \rangle$ are calculated by (3.2).

5 Numerical results

During the research progress, we developed the modified theories regarding the nucleation process and the modified version of distribution function. Now it is in turn to discuss how these models, including a combination of a nucleation theory and of a kind of the distribution function, reacted after the numerical treatment. In this section, numerical results for all three material models are presented and discussed. Moreover, the advantages and disadvantages are discussed. To verify our models, we will compare our numerical results of our models with the existing Abaqus models. A brief introduction of Abaqus and Umat, a user subroutine to carry out an ABAQUS/Standard the user-defined material model, will be introduced. We will implement models by writing the Umat subroutine in Abaqus. Not only a comparison with Abaqus models but also a comparison of the present model with existing phenomenological ones is given. Via a creep test and a relaxation test, the differentiation and the similarity will be clarified. A simple discretization and geometry are observed in these tests. After numerical treatments, there will be a comparison via the total effective creep strain-time diagram. The stress is plotted over strain. Furthermore, a cycle life of a grain will be depicted in each case of our models to get the differences between the current model and phenomenological models.

5.1 Methods

Abaqus is a commercial CAE software which has several subroutines to be defined by user for different purposes. Umat subroutine can be used to define constitutive laws which enable user to implement any arbitrary material model. In this section, we introduce the procedure of an analysis in Abaqus using Umat.

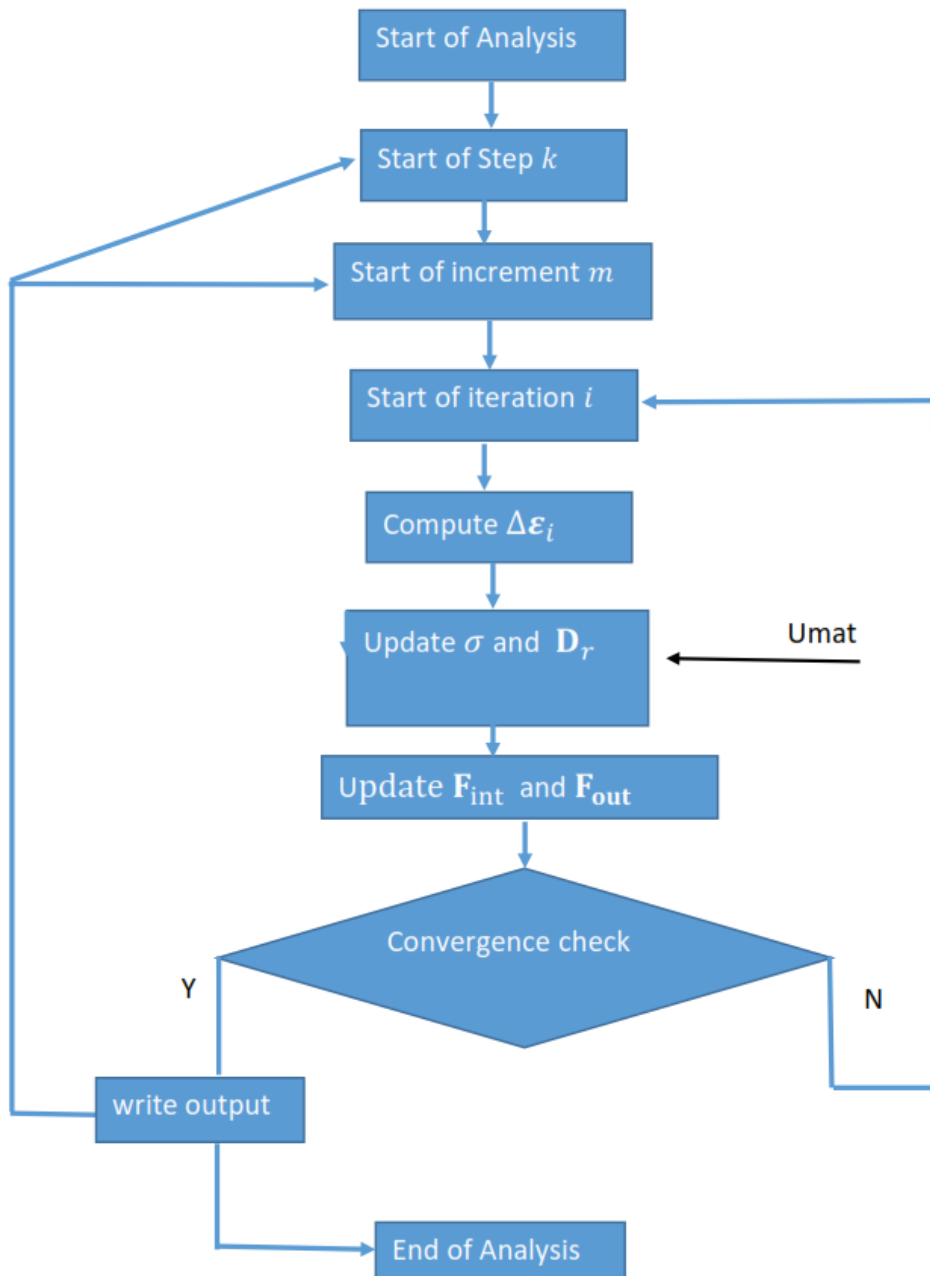


Figure 5.1: Typical analysis procedure in Abaqus.

A finite element procedure will be executed in Abaqus. This implementation is probably conducted several times (steps). The initial values of the next step are the values which are calculated in the current step. An increment into time step is used during a time span. Then each step will be solved within the time span. In every increment, as another finite element program, for example, FEAP, an increment in the plastic strain, ϵ_p , is reformed. This reformation is dependent on the time increment which is denoted Δt (*dtime*). The local internal and external force vectors are calculated at every single integration point of each element. Then the assemble force (or the global forces) is obtained and the algorithm is repeated until the condition is fulfilled. The time will increase step by step after the step time is gained. When the total time is finished, the implementation (the analysis) or a job in Abaqus is ended. This algorithm is conducted and will return the new stress and tangent

matrix whose formulations are given. One important part in Abaqus is the SDVs. These value are needed to be updated in each step. Abaqus should be connected to Intel Fortran and Microsoft Visual Studio.

5.2 Numerical results in the microscale

The numerical treatment was employed separately for the problem at the microscale. Moreover, for the distribution function in form of $\bar{f}(D, r)$ as well as $\tilde{f}(s, r)$, we also applied the numerical scheme to the whole problem at two scales. The result in only the problem at the microscale and the result after the two-scale scheme are same, then we discussed here only one result. With the distribution function, $f(p, D, r)$, until now, we haven't researched on how to further develop. This will be the next investigation. As a result, only the distinct microscale problem is solved numerically.

Parameter	Value	Unit	Physical interpretation
μ	$60 \times 10^{+9}$	Pa	Shear modulus
b	5.34000×10^{-10}	m	Burger's vector
a_p	$1.03154 \times 10^{+4}$	-	Material parameter
M_{\perp}	2.2×10^{-16}	$\text{m}^3 \text{s kg}^{-1}$	Diffusion mobility
δ	1.0×10^{-9}	m	Grain boundary thickness
γ	5.0×10^{-3}	Jm^{-2}	Interfacial energy
g_0	5.78845×10^{-12}	-	Material parameter for nucleation function
D_0	1.0×10^{-4}	m	Material parameter for nucleation function
$\ \dot{\epsilon}_p\ $	0.1407780×10^{-5}	1/s	Norm of the rate of plastic strain

Table 5.1: Material parameters for the model, $\bar{f}(D, r)$.

5.2.1 Results for the distribution function, $\bar{f}(D, r)$

Before implementing the two-scale model, we carried out numerically the problem at the microscale via the marching algorithm. The result of the distribution function is depicted in Figure 5.3. Its contour lines are drawn in Figure 5.2. These contour lines illustrate the “life cycle” of grains. Let us call the grains having small dislocation densities the young grains. These grains have the small energy. Other grains with the large dislocation densities are called old grains. The old grains have large energy. The “life cycle” of grains have some stages. The first stage is the formation of grains. The small-energy grains are nucleated. Then the grains grow up by an increase of the grain sizes. At the certain age, the grain size will reach the maximum grain size. Their energy also gets larger. The last stage is that the old grains will be consumed by the young grains or the newly formed grains. Lastly, the grains will be disappeared. This “life cycle” shows a good agreement with phenomenological ones. However, it can be shown in Figure 5.2, in contrast with the phenomenological ones, all grains will be “born” at the same dislocation density. In the reality, different grains will nucleate with different dislocation densities. However, in Figure 5.2, all grains are “born” with the same value of the dislocation density. This result is unreasonable. Furthermore, actually, only grains with small dislocation density participates in the nucleation process. As sketched in Figure 5.2, even large dislocation density grains are also nucleated.

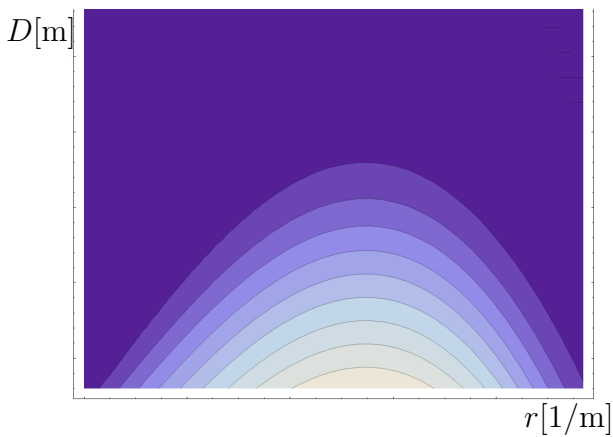


Figure 5.2: “Life cycle” of grains.

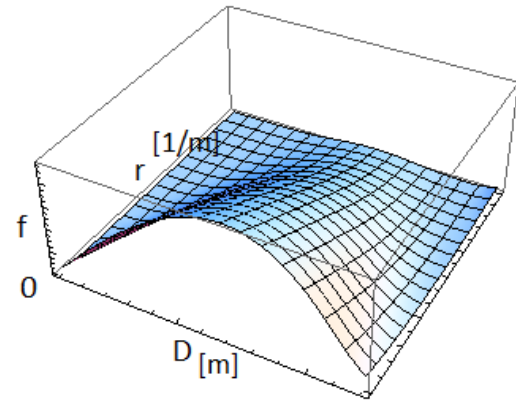
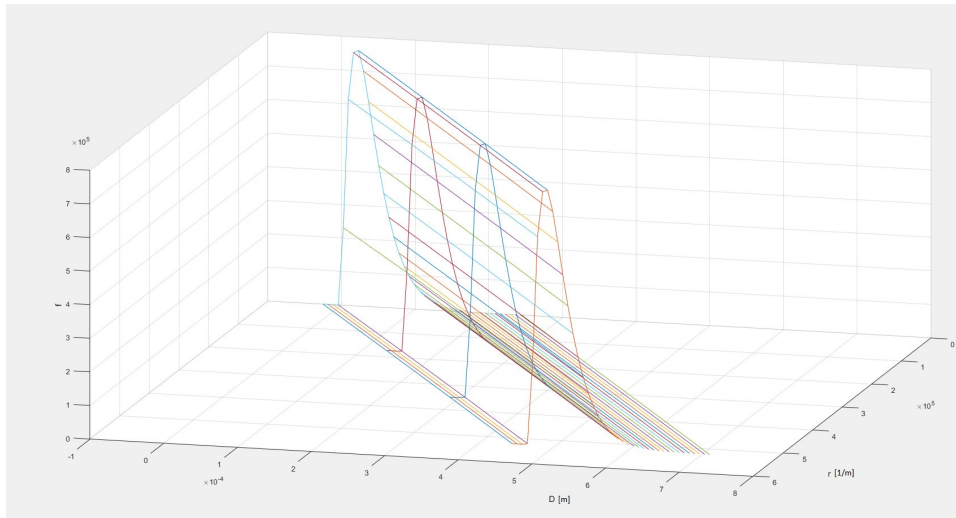


Figure 5.3: Distribution function.

Figure 5.4: A part of the distribution function, $\gamma = 5.0 \times 10^{-3}$.

5.2.2 Results for the distribution function, $\tilde{f}(s, r)$

In this part, we will discuss about the distribution function which is a function of two variables s and r . By using a variable transformation from D to s , s is introduced. Firstly, let me show the form of this distribution function and its contour line which depicts the relationship between “grain size” and rescaled dislocation density. We implemented the problem at the microscale with the set of parameters shown in the below table. With this set of parameters, the result of distribution function and its contour line are sketched in Figure 5.4 and in Figure 5.5. Since we want to have a closer look at the distribution function, a small part of this distribution function will be zoomed out. In order to investigate in the distribution function, the value of each parameter will be varied so that we can see the influence of these parameters on the distribution function. As a result, the modification of distribution function and of “life cycle” are considered. We can see their changes when γ is equal to 7.0 Jm^{-2} .

As can be plotted in Figures 5.6, the small part of the distribution functions has a large difference. Furthermore, the range of grain size for nucleation process will be bigger than it in $\gamma = 5.0 \times 10^{-3} \text{ Jm}^{-2}$. It means that less grains will be “born” (see Fig 5.7). Now let us alter the value μ from $60. \times 10^{+9} \text{ Pa}$. Then this value is continuously decreased again to $9. \times 10^{+8} \text{ Pa}$. The difference of distribution function in different values of μ will be shown

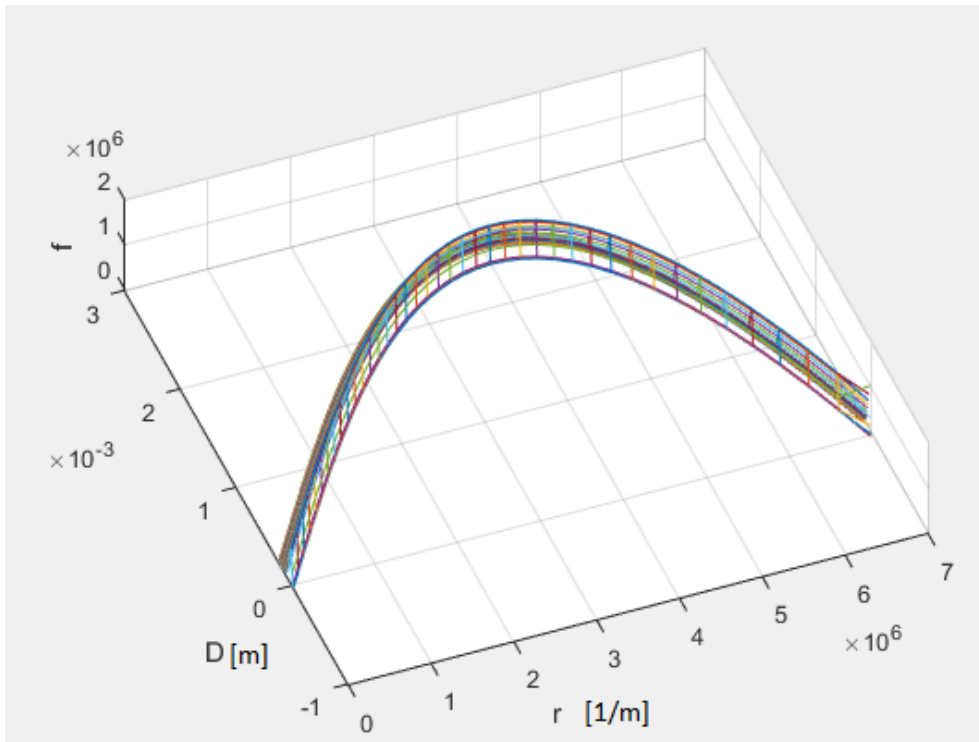


Figure 5.5: Full distribution function, $\gamma = 5.0 \times 10^{-3}$.

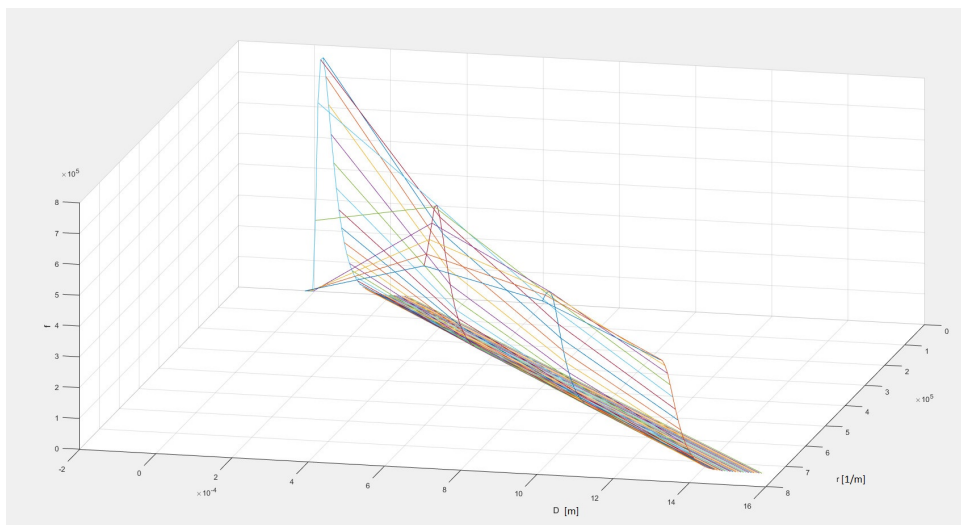


Figure 5.6: A part of the distribution function, $\gamma = 7.0 \times 10^{-0}$.

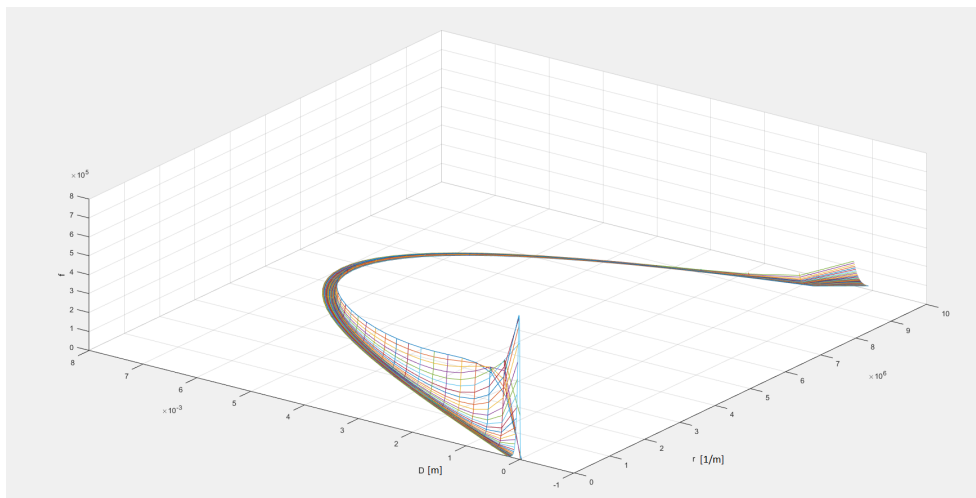


Figure 5.7: Full distribution function, $\gamma = 7.0 \times 10^{-0}$.

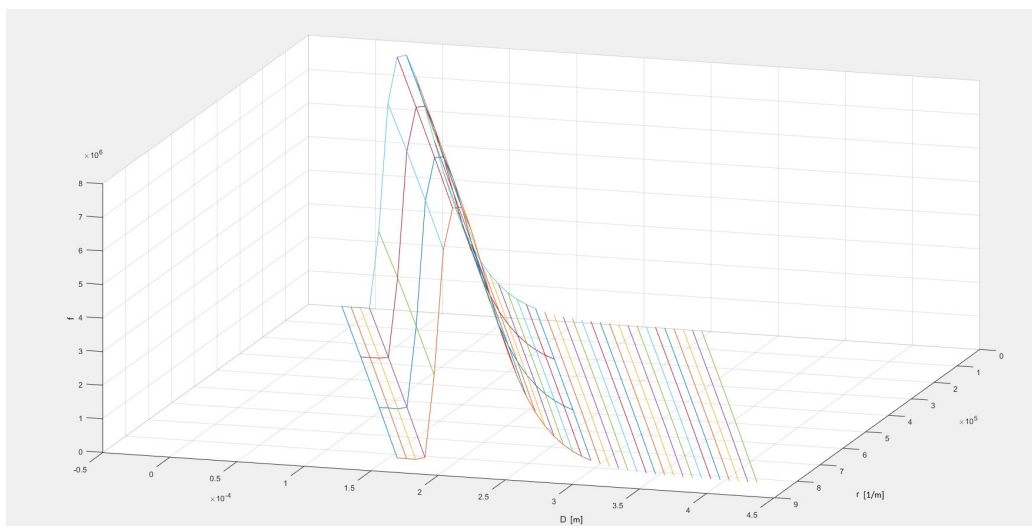


Figure 5.8: A part of the distribution function, $\mu = 6. \times 10^{+9}$.

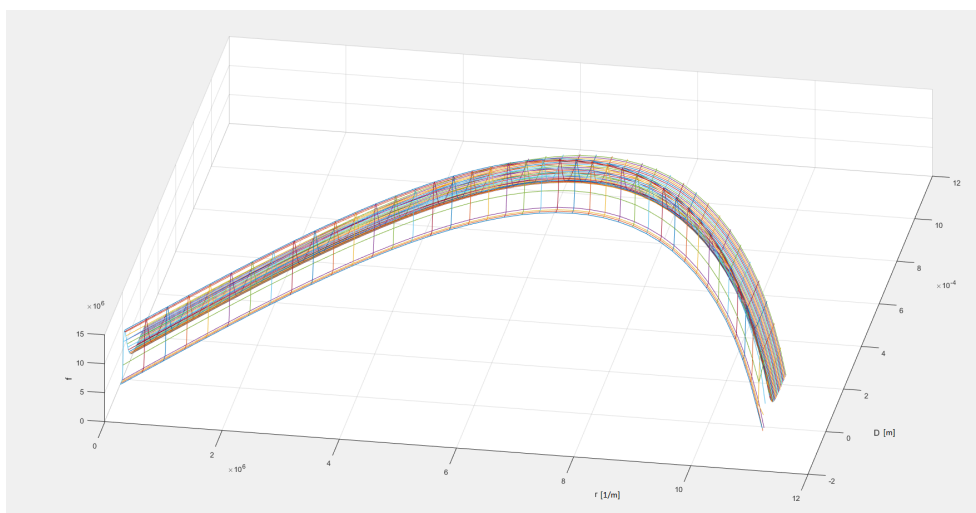
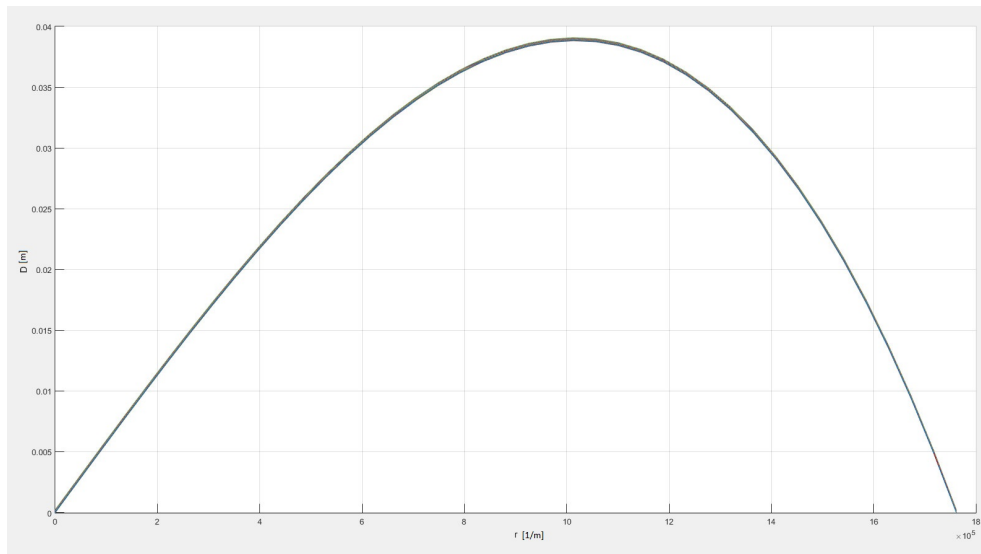
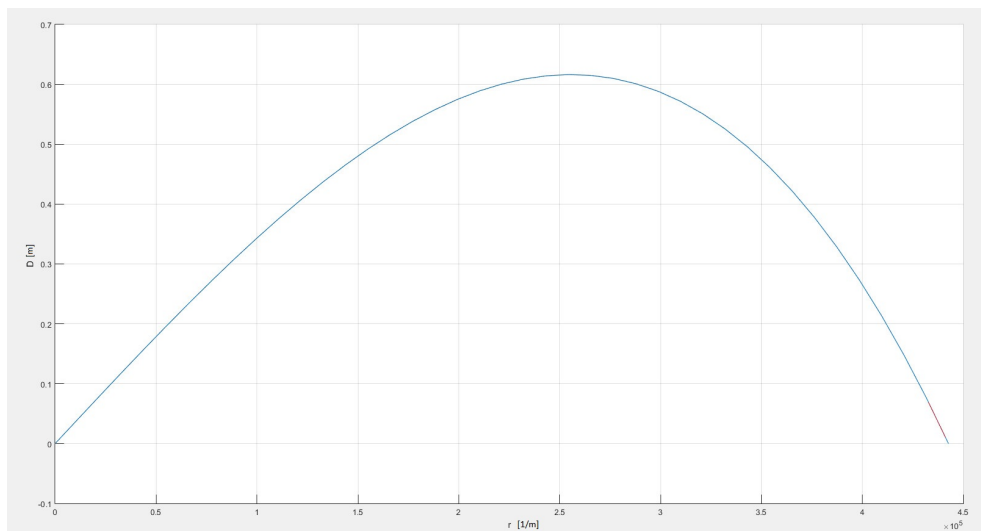


Figure 5.9: Full distribution function, $\mu = 6. \times 10^{+9}$.

Figure 5.10: “Life cycle” of grains, $b = 5.34 \times 10^{-9}$.Figure 5.11: “Life cycle” of grains, $b = 5.34 \times 10^{-8}$.

in Figure 5.8. From these figures, while μ decreases, the value of distribution function increases. In addition, responding to a reduction of μ , a raise of the number of “born” grains can be seen in Figure 5.9. The next step is to sketch the variation if b is 5.34×10^{-9} . When we apply the bigger norm of the plastic strain $\dot{\epsilon}_p$, with $\|\dot{\epsilon}_p\| = 0.1407780 \times 10^{-1}$, in Figure 5.13, the value of distribution function is larger than in the case $\|\dot{\epsilon}_p\| = 0.1407780 \times 10^{-5}$. Moreover, Figure 5.13 already sketched how many grains are nucleated. It means that the bigger plastic strain makes the dislocation be more active. Therefore, the disorganization of materials will increase. This will create a good condition for nucleation process. Then there will be more nucleated grains. In contrast to the case of plastic strain rate’s change, when a change in diffusion mobility raises, the range of grain size in which grains are nucleated will be smaller. This seems to match with the reality. Since diffusion mobility increases, this prevents dislocations from moving. Thus, the movement of dislocations will be slower. As a result, not many grains are “born” when M_{\perp} enlarges. Lastly, a change in material parameter a_p is employed. As same as in the case that plastic strain rate is modified, the distribution function’s value increases when a_p goes up (see Figure 5.15). The grains are nucleated as in Figure 5.19.

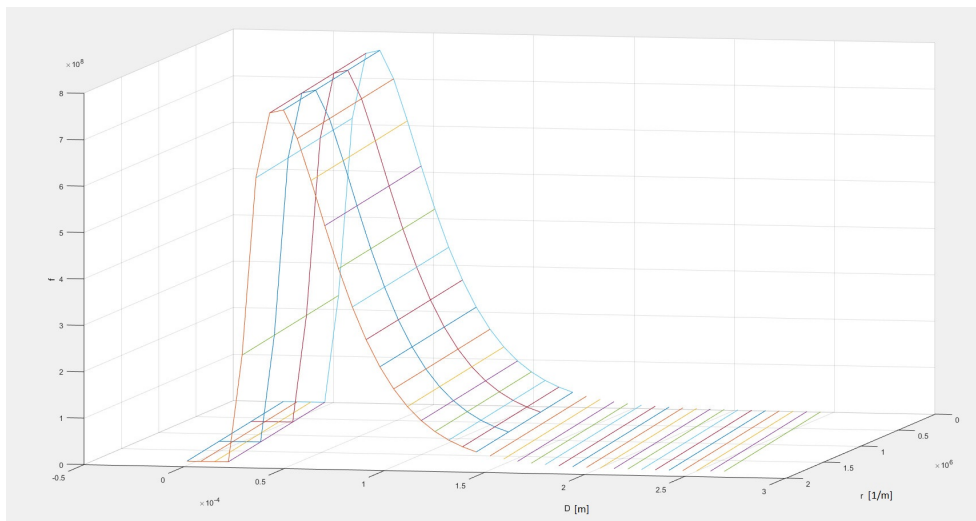


Figure 5.12: A part of the distribution function, $\|\dot{\epsilon}_p\| = 0.1407780 \times 10^{-1}$.

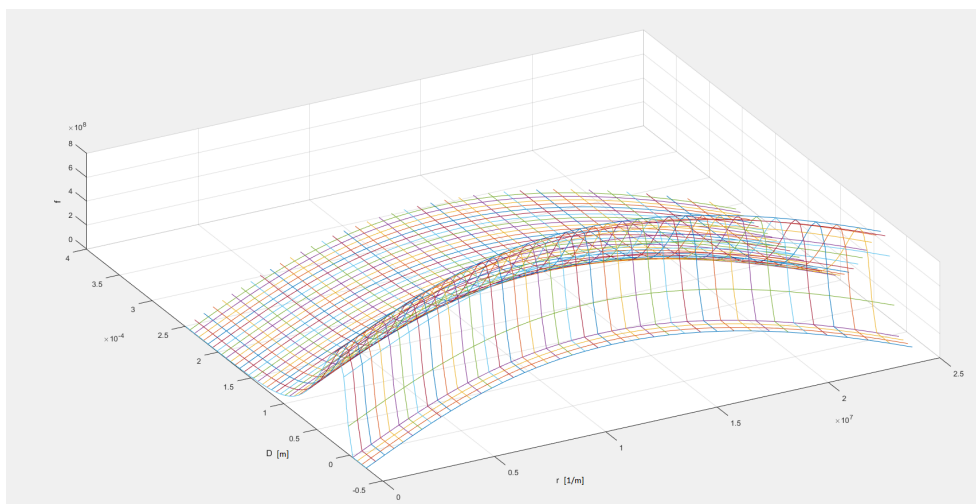


Figure 5.13: Full distribution function, $\|\dot{\epsilon}_p\| = 0.1407780 \times 10^{-1}$.

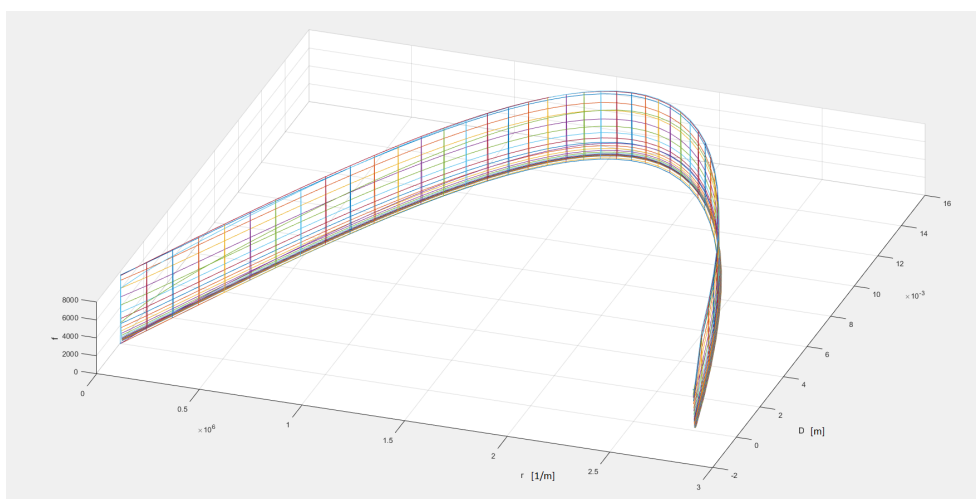


Figure 5.14: Full distribution function, $M_{\perp} = 2.2 \times 10^{-14}$.

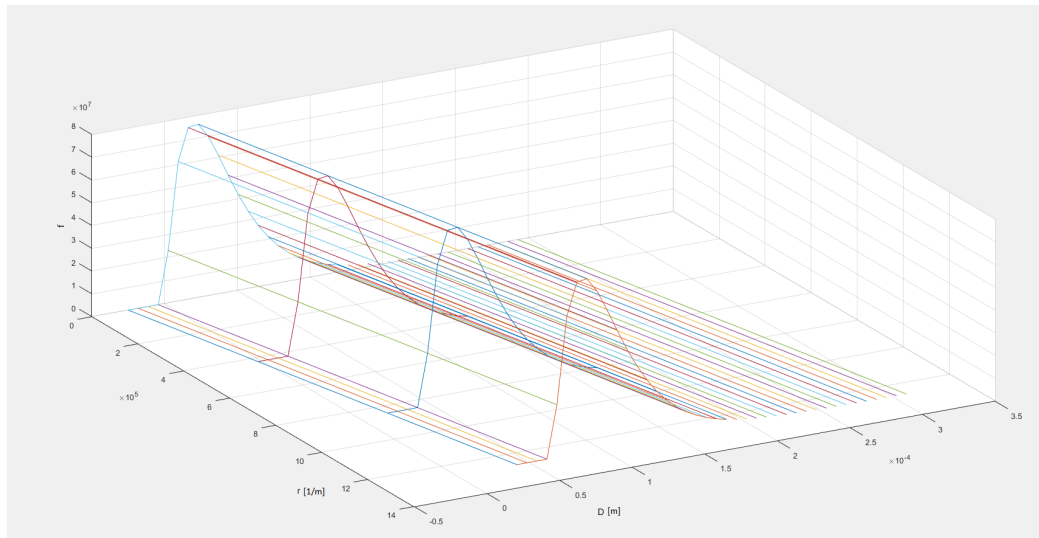


Figure 5.15: A part of the distribution function, $a_p = 1.03154 \times 10^{+6}$.

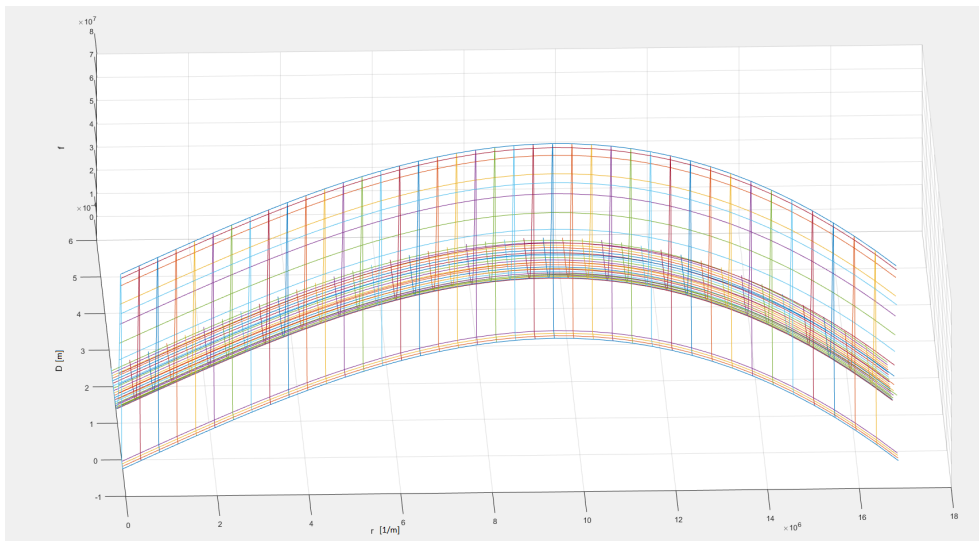


Figure 5.16: Full distribution function, $a_p = 1.03154 \times 10^{+6}$.

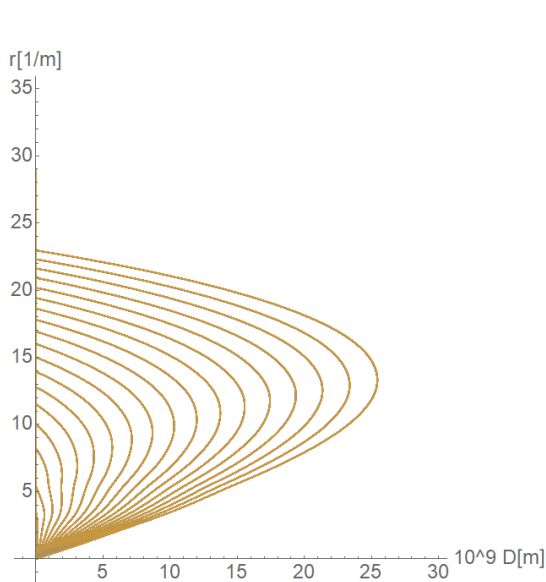


Figure 5.17: The “life cycle” of grains.

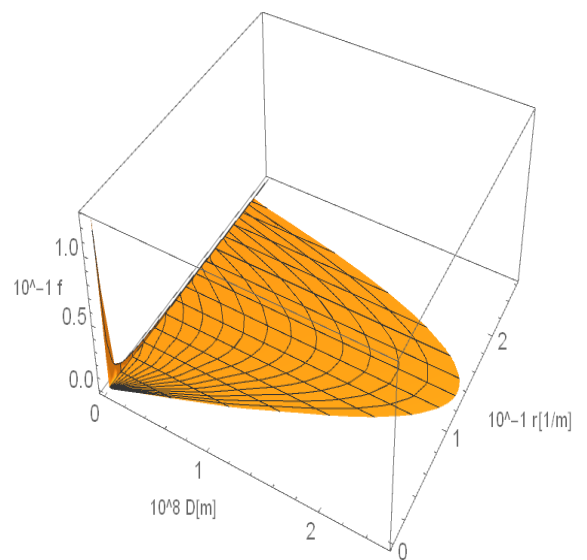


Figure 5.18: Full distribution function.

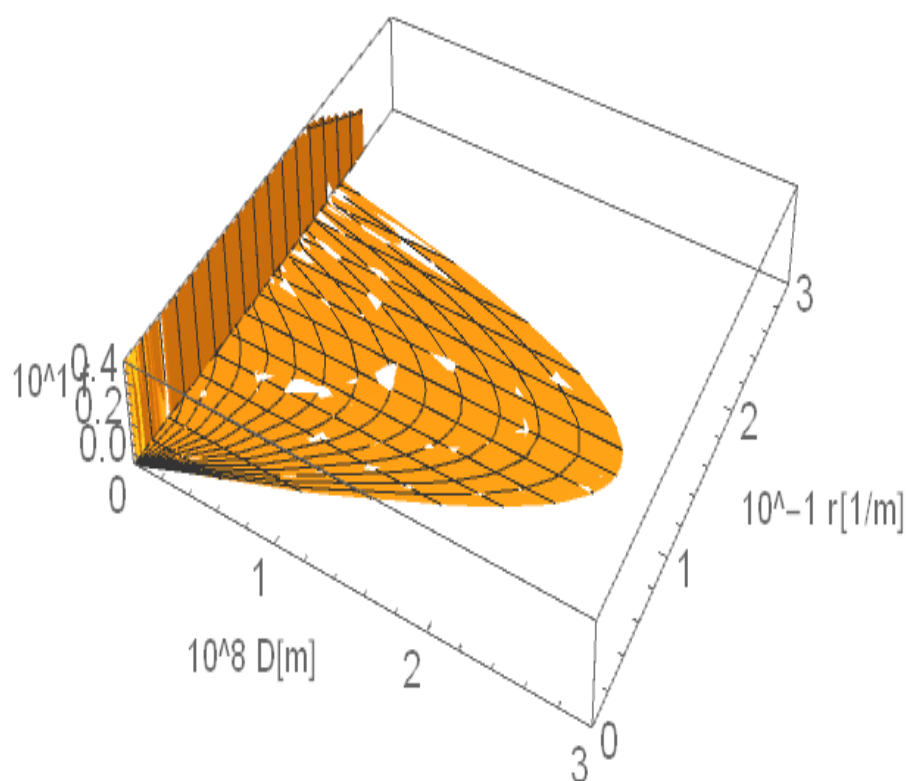


Figure 5.19: A part of the distribution function, $a_p = 1.03154 \times 10^{+6}$.

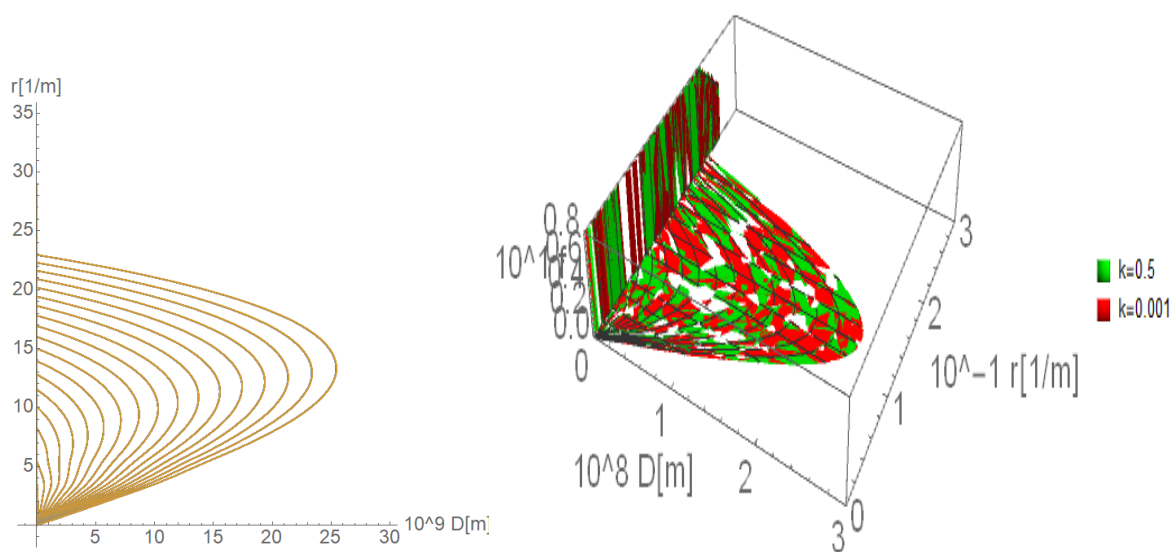


Figure 5.20: "Life cycle" of grains, the distribution function, $k = 0.5$ and $k = 0.001$.

5.2.3 Results for the distribution function, $f(p, D, r)$

Due to the limitation of the previous results concerning the distribution function, $\bar{f}(D, r)$ and $\tilde{f}(s, r)$, the updated version of distribution function is proposed to prevent this limitation. To implement the problem at the microscale, the set of parameters (in Table 5.2) will be used. As can be see in Figure 5.17, this limitation disappears. Let us talk again about the “life cycle” again. Grains with large value of dislocation densities and with small dislocation densities are old grains and young grains, respectively. The young grains are formed via an assembling of old grains. The young grains will grow further by accumulating the high energy grains to gain the maximum grain size. Because of the highest energy, the old grain will be vanished by consuming of the young ones. The result is shown in the contour line as in Figure 5.17, each grain will nucleate with different grain size. Opposing to the previous versions of distribution function, the result still has the disagreement with phenomenological ones. The new model provides the more reasonable agreement. Only young grains (with small dislocation densities) are “born” by accumulating old grains. However, we only developed this model, the next work to apply this model to the next level will be in the future investigated. As same as in the model with the distribution function, $\tilde{f}(s, r)$, the modification of material parameters will be applied to study more about the influence of material parameters on the distribution function. Firstly, the initial value of k will be altered. However, it is easy to see from Figure 5.20, this value plays no important role in obtaining the value of distribution function.

Parameter	Value	Unit	Physical interpretation
v	1.13812×10^{12}	-	Material parameter
μ	$1. \times 10^{+9}$	Pa	Shear modulus
k	0	m^{-1}	Material parameter in Eq. 3.87
b	0.0001	m	Burger’s vector
γ	0.0001	Jm^{-2}	Interfacial energy
g_0	5.78845×10^{-12}	-	Material parameter for nucleation function
D_0	0.000001	m	Material parameter for nucleation function
$\ \dot{\epsilon}_p\ $	0.1407780×10^{-5}	1/s	Norm of the rate of plastic strain

Table 5.2: Material parameters for the model, $f(p, D, r)$.

As plotted in Figure 5.21, the modification in γ will make a big change in the nucleation process. The maximum grain size’s value is bigger than these values in the case of $\gamma = 0.00001 \text{ Jm}^{-2}$. The grains also disappear with higher dislocation density in $\gamma = 0.0001 \text{ Jm}^{-2}$ than in $\gamma = 0.00001 \text{ Jm}^{-2}$. While the size of small grains D_0 reduces from $D_0 = 0.0001$ to $D_0 = 0.000001$, the maximum value of grain size during nucleation process will increase slightly. Lastly, the change of the distribution function and the “life cycle” are shown in Figure 5.23 and in Figure 5.24 when v and μ are changed.

5.3 Relaxation test and creep test

As discussed above, to characterize the creep test and relaxation test, the flow law, the relationship between the rate of plastic strain and stress, will be essential. Now let us discuss this law for diffusion creep, respectively. However, in this thesis, we consider that

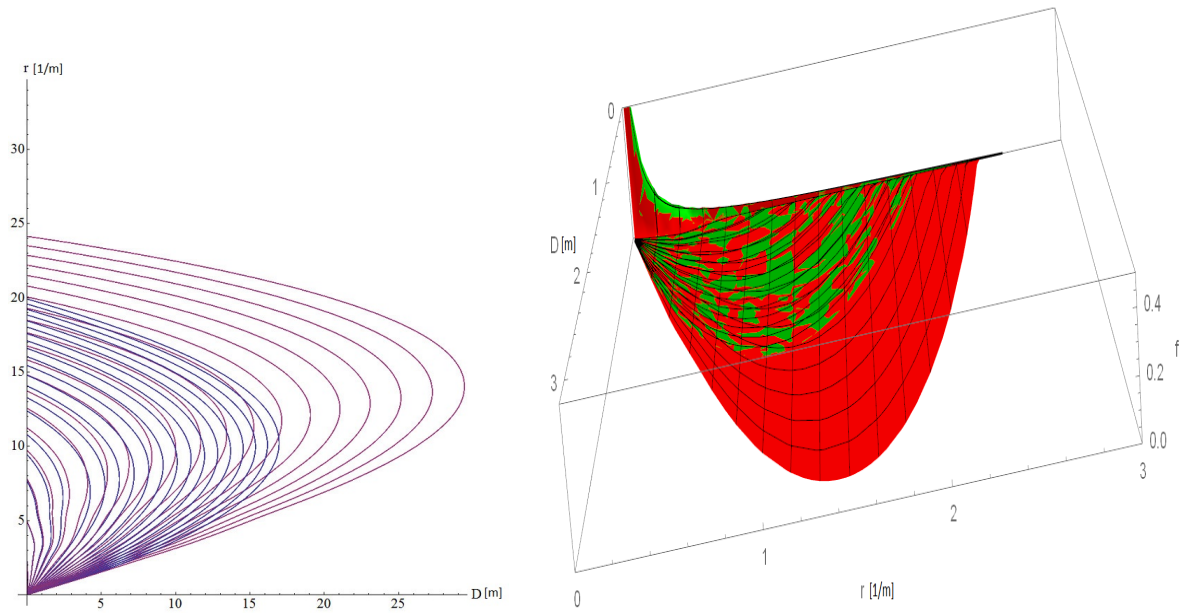


Figure 5.21: “Life cycle” of grains, the distribution function, $\gamma = 0.0001$ and $\gamma = 0.00001$.

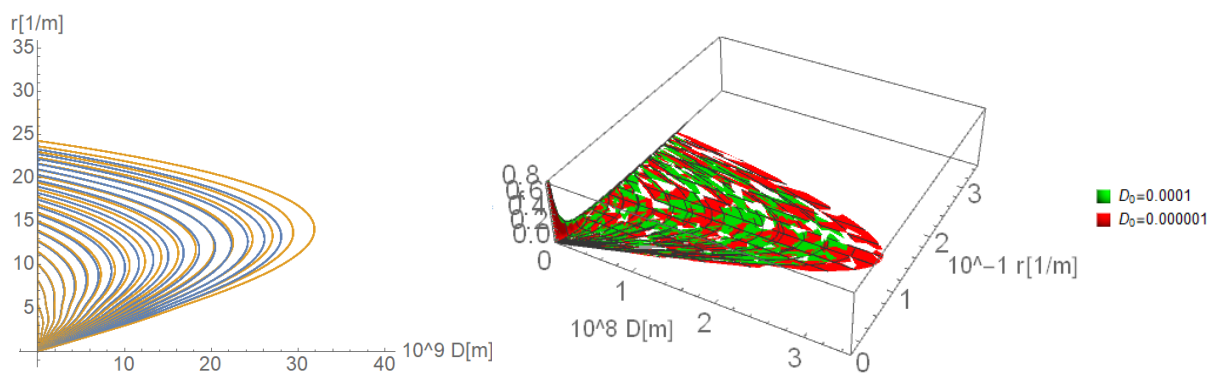


Figure 5.22: “Life cycle” of grains, the distribution function, $D_0 = 0.0001$ and $D_0 = 0.000001$.

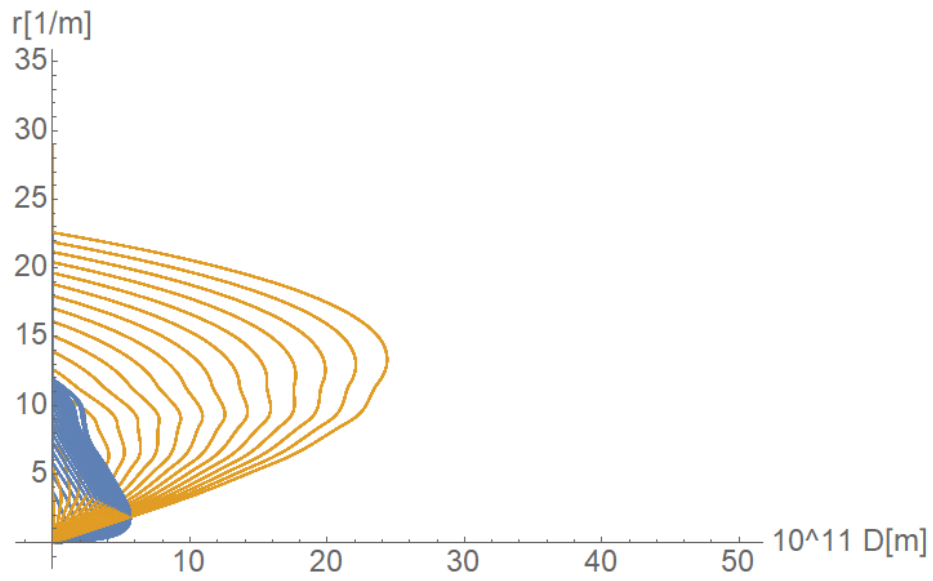


Figure 5.23: Distribution function, $v = 1.13812 \times 10^{13}$.

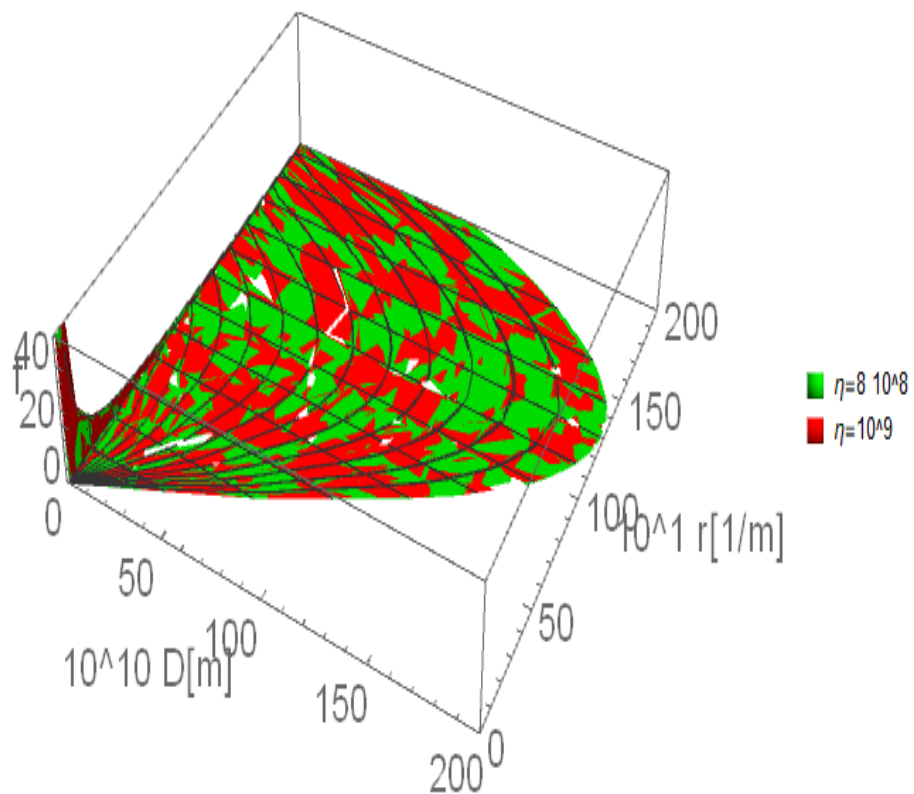


Figure 5.24: Distribution function, $\mu = 8 \cdot 10^{+8}$ and $\mu = 1 \cdot 10^{+9}$.

dislocation creep is the most influential mechanism, or $\epsilon_d \ll \ll \epsilon_p$, then only the plastic strain rate is analyzed here. Its flow rule is rewritten as

$$\dot{\epsilon}_p = A_p \|\sigma^d\|^{(1-m)/m} \sigma^d. \quad (5.1)$$

Consequently, its norm is calculated by the following equation

$$\|\dot{\epsilon}_p\| = A_p \|\sigma^d\|^{\frac{1}{m}}. \quad (5.2)$$

By defining the effective value of the plastic strain as well as of the plastic's train rate by

$$\dot{\epsilon}_p = \sqrt{2/3} \|\dot{\epsilon}_p\| = (\sqrt{2/3}) A_p \|\sigma^d\|^{\frac{1}{m}}. \quad (5.3)$$

When m is equal to 0.5, as a result, we obtain

$$\sqrt{2/3} \|\dot{\epsilon}_p\| = \left(\frac{2}{3}\right)^{3/2} A_p \sigma_{vm}^2, \quad (5.4)$$

where Von-Mises stress is computed as $\sigma_{vm} = \sqrt{3/2} \|\sigma^d\|$. Eq.(5.4) is rewritten as

$$\dot{\epsilon}_p = \left(\frac{2}{3}\right)^{3/2} A_p \sigma_{vm}^2. \quad (5.5)$$

In the material library of Abaqus, with creep materials, we need the relationship between the effective value of the plastic strain rate in the form of $\dot{\epsilon}_p = A \sigma_{vm}^k$. Therefore, k and A will be inputs in Abaqus. Since in Abaqus, there are existing models relating to rate-dependent plastic deformation, for example, creep test. There will be reasonable to compare our result and the Abaqus' s result. The comparison will be shown in two distinct tests: creep test and relaxation test. SDVS (State-dependent variables) are variables to store the material's behavior at the integration points at each step. Depending on each type of different distribution functions as well as the theory of nucleation, we will have different amount of SDVs. SDVS are the variables showing the connection of the problem at the microscale and one at the macroscale. These values of these variables are stored in an array, namely, statev in UMAT. In Abaqus, a plain strain element (CPE4) and linear shape functions are used.

Relaxation test

The geometry and boundary conditions of a specimen loaded by tension are shown in Figure. 5.25. Let us consider a typical rectangular cube. A rectangular cube has the length h and the width a as can be seen in this Figure. The thickness of this cube is small enough compared to two other sides, then it is considered to be neglected. Consequently, all the components of strain in z direction, which is perpendicular to the plane created by x and y directions, are neglectable. Figure 5.25(a) describes the geometry and boundary conditions for this test. The below side AB can not move in x -direction and y -direction, except the point A. Moreover, the point A is restricted only in y -direction. This cube should be considerable as a bar. Furthermore, this bar is subject to the constraint concerning the given displacement, u , as depicted in Figure 5.25.

Creep test

The geometry and boundary conditions of a tensile specimen are shown in Figure. 5.26. As in the relaxation test, the same restriction to the point A and the base AB are applied.

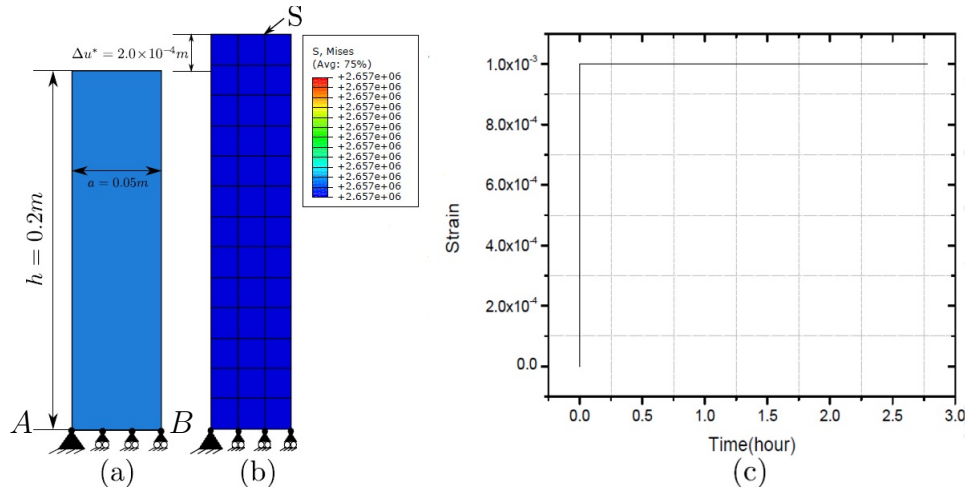


Figure 5.25: Relaxation test; a) Geometry and boundary conditions; b) Applied deformation ; c) Applied strain, (from V. E.Isfahani, 2014). Images reprinted by permission.

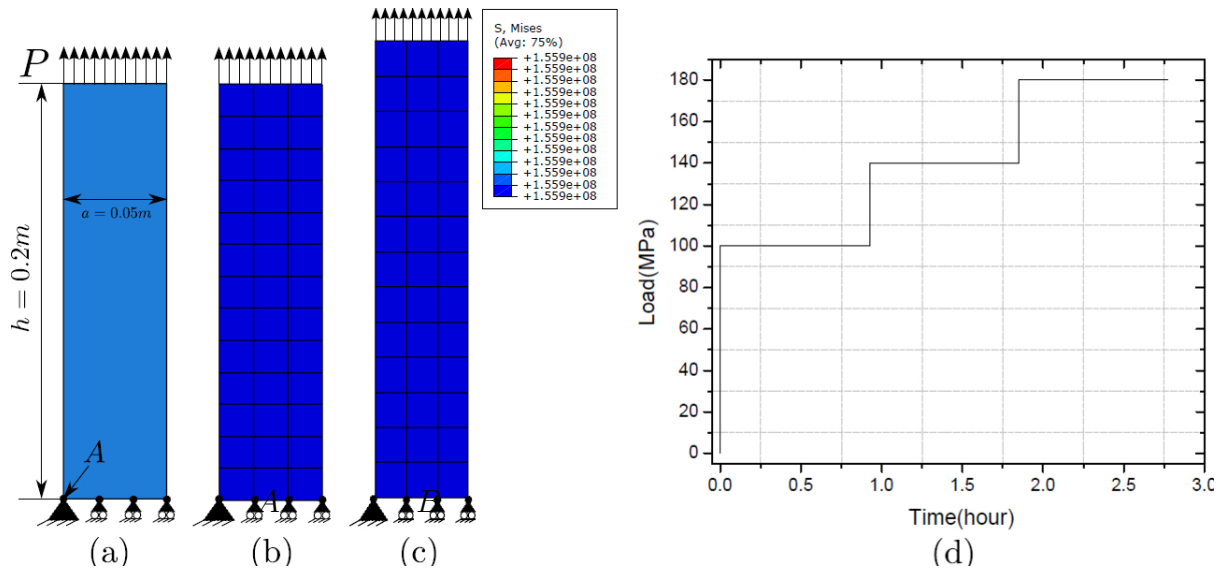


Figure 5.26: Creep test; a) geometry and boundary conditions; b) Undeformed meshed body at $t_0 = 0s$, c) Deformed shape. Stress is constant in the spatial space, d) Applied pressure, (from V. E.Isfahani, 2014). Images reprinted by permission.

Moreover, the bar is subject to a time-dependent load. The creep test is analysed in three implicit steps. The firstly explicit step is implemented since the first time when m is equal to 0. The increment of time varies from small to large value during on step. An increment of time step is set up automatically by ABAQUS from $\Delta t_0 = 1. \times 10^{-4}s$ to $\Delta t_{max} = 300s$. The total time is 1000 seconds for simulation of this test .

5.4 Numerical results in the macroscale

5.4.1 The first model results

In the first model, we use the distribution function in the form of $\tilde{f}(s, r)$ as well as the first theory of nucleation. Consequently, we will SDVS with 17 components which are shown in Table 5.4. Moreover, by fitting parameters with Abaqus existing models, we obtained the value set of material parameters as in Table 5.3

Creep test

This model was implemented by Mr. Vahid Ebrahimzade. Then the short result is here discussed. We know that the main mechanism is dislocation creep. Then only this regime is conducted in order to compare with the existing models in Abaqus. As can be seen in Figure 5.27, the total effective creep strain is nearly equal to the plastic strain.

Parameter	Value	Unit	Physical interpretation
b	5.34×10^{-10}	m	Burger's vector
a_p	$1.03154 \times 10^{+4}$	-	Material parameter
M_{\perp}	2.2×10^{-16}	$\text{m}^3 \text{s kg}^{-1}$	Diffusion mobility
λ	-	Jm^{-3}	Lagrange multiplier
λ	$90. \times 10^{+9}$	Pa	Lamé parameter
k_p	4.8×10^{-29}	$\text{m}^{2+m/2} \text{N}^{-1/m} \text{s}^{-1}$	Dislocation velocity in Eq. (3.46)
m	0.5	-	Dislocation velocity in Eq. (3.46)
μ	$60.0 \times 10^{+9}$	Pa	Shear modulus
δ	1.0×10^{-9}	m	Grain boundary thickness
γ	$5.0 \times 10^{-3} - 2.0$	Jm^{-2}	Interfacial energy
g_0	5.78845×10^{-12}	-	Material parameter for nucleation function
D_0	1.0×10^{-4}	m	Material parameter for nucleation function

Table 5.3: Material parameters for the first model.

Definition	Description
ϵ_d	Creep strain due to diffusion
ϵ_p	Plastic strain
$\dot{\epsilon}_d = \sqrt{2/3} \ \dot{\epsilon}_d\ $	Effective value of ϵ_d
$\dot{\epsilon}_p = \sqrt{2/3} \ \dot{\epsilon}_p\ $	Effective ϵ_p
$\epsilon_d = \sqrt{2/3} \ \epsilon_d\ $	Effective ϵ_d
$\epsilon_p = \sqrt{2/3} \ \epsilon_p\ $	Effective plastic strain
$\dot{\epsilon} = \dot{\epsilon}_d + \dot{\epsilon}_p$	Total creep strain rate
$\epsilon = \epsilon_d + \epsilon_p$	Total creep strain
λ	Lagrange multiplier
A_d	Flow law multiplier for diffusion creep
A_p	Flow law multiplier for dislocation creep

Table 5.4: State-dependent variables for the first model.

When the load is raised with an ascending rate, the creep strain increases. Based on Eq. (3.46) and Eq. (3.36), it is obviously to see when stress raises, the evolution of creep strain goes up as well. This model was carried out numerically with two different interfacial energy. The full results were discussed in [Isfahani, 2014]. Readers who are interested in this part, can have a look at it. The comparison of the flow law multiplier for dislocation creep and distribution function corresponding to different strain rates, the readers can refer to [Isfahani, 2014].

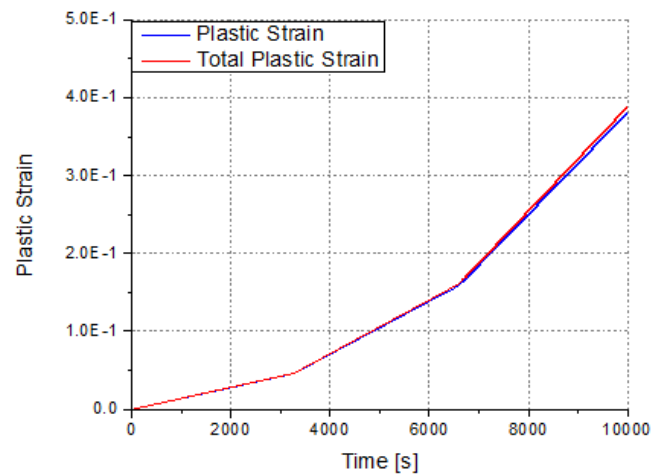


Figure 5.27: Total effective creep strain v.s plastic strain.

Relaxation test

The relaxation test was conducted with the same set of the material parameters as in the creep test. Now let us first discuss the change of the mean rescaled dislocation density as well as the change of the mean grain size.

Figure 5.28 sketches the average of dislocation density, after a heavy decrease, this value reaches slightly to a stable value. In contrary to the evolution of mean dislocation density, the mean of grain size starts with a big increase, and then with a slighter increase. This can be illustrated in Figure 5.28. As can be seen in Figure 5.28 and Figure 5.29, the average of dislocation density decreases according to time while the average of grain size increases. Moreover, the value of λ reduces regularly according to the time as in Figure ??.

The result also shows the good match of the total effective creep between Hackl- Renner (H-R) model and the existed model in Abaqus. The evolution of other material informations such as Von Mises stress, plastic strain, plastic strain rate, diffusion strain rate, the flow multiplier for dislocation creep and the flow multiplier for diffusion creep, the readers can refer to [Isfahani, 2014].

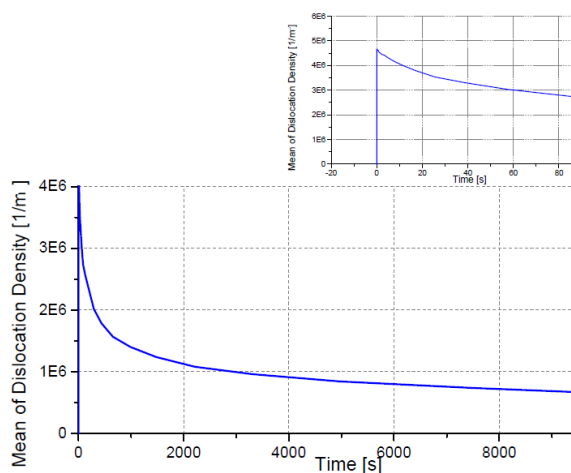


Figure 5.28: Evolution of mean rescaled dislocation density.

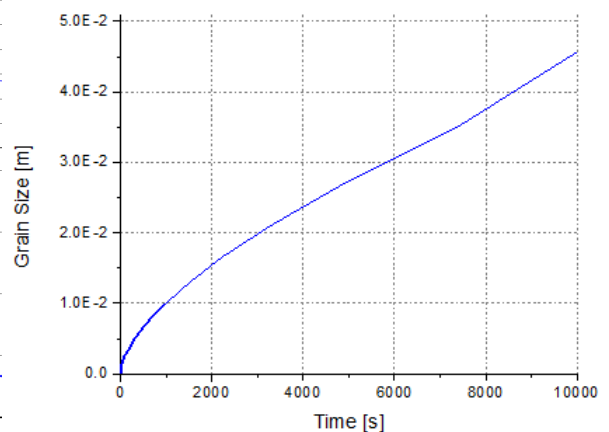
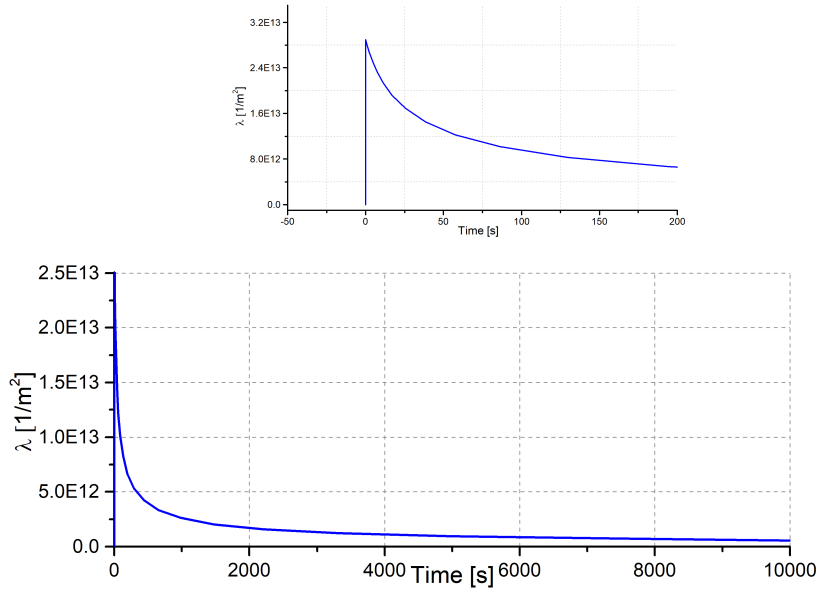


Figure 5.29: Evolution of mean grain size.

Figure 5.30: Evolution of λ .

5.4.2 The second model results

In this model, we implemented numerically for the two-scale model. For the problem at the microscale, the distribution function differentiating each grain by grain size and rescaled dislocation density has the form of $\tilde{f}(s, r)$. Furthermore, the second nucleation theory is applied in this model. Again, the information of material parameters are given. As same as in the first model, we still have parameters: Burger's vector, diffusion mobility, nucleation mobility, shear modulus, grain boundary thickness, interfacial energy.

Parameter	Value	Unit	Physical interpretation
b	5.34×10^{-10}	m	Burger's vector
a_p	$1.03154 \times 10^{+4}$	-	Material parameter
M_{\perp}	2.2×10^{-16}	$\text{m}^3 \text{s kg}^{-1}$	Diffusion mobility
C	-	-	Lagrange multiplier
λ	-	Jm^{-3}	Lagrange multiplier
k_p	4.8×10^{-29}	$\text{m}^{2+m/2} \text{N}^{-1/m} \text{s}^{-1}$	Dislocation velocity in Eq. (3.46)
m	0.5	-	Dislocation velocity in Eq. (3.46)
μ	$6 \times 10^{+10}$	Pa	Shear modulus
δ	1.0×10^{-9}	m	Grain boundary thickness
γ	5.0×10^{-3}	Jm^{-2}	Interfacial energy
g_0	5.78845×10^{-12}	-	Material parameter for nucleation function
k	$6.9389 \times 10^{+13}$	-	Material parameter in Eq. (3.150)

Table 5.5: Material parameters for the second model.

Creep test

Firstly, this creep test is carried out with the interfacial energy γ . In this test, we can see the

relationship of plastic strain rate and plastic strain. As can be obtained from the flow rules, the trend of the plastic strain rate increase when the stress gets larger. In addition, Figure 5.32 shows that the stress is constant in the spatial space.

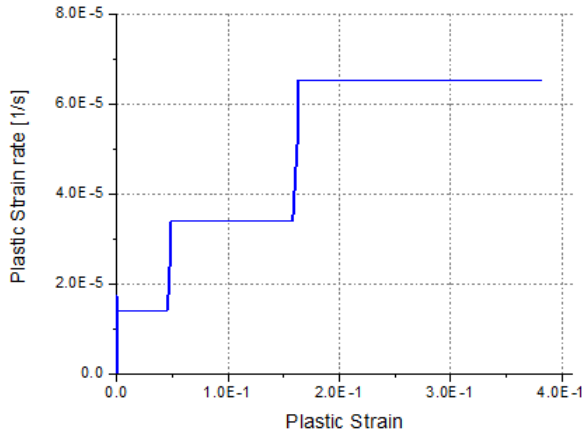


Figure 5.31: Diffusion strain rate v.s diffusion strain.

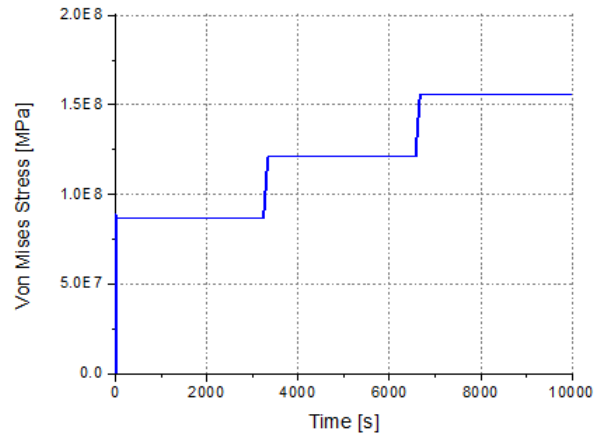


Figure 5.32: Evolution of Von Mises stress.

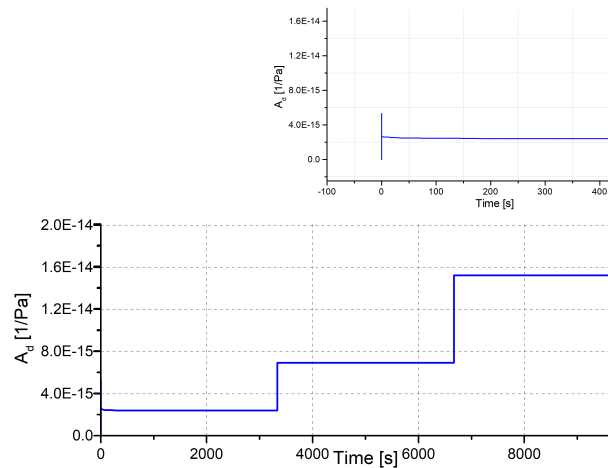


Figure 5.33: Flow law multiplier of dislocation creep.

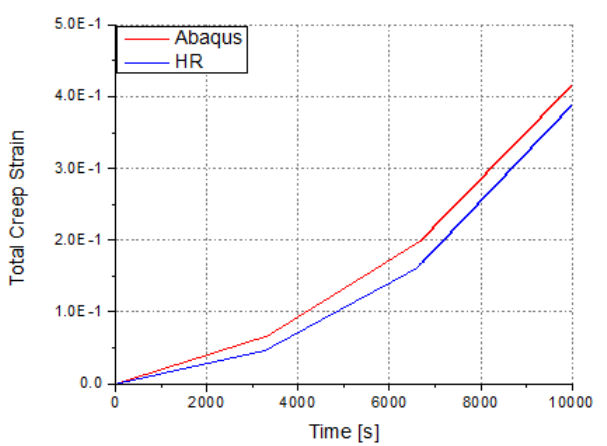


Figure 5.34: Total effective creep strain in H-R model and in Abaqus.

In this test, we implemented the simulation with two different values of Burger's vector, $b = 5.34 \times 10^{-10}$ and $b = 5.34 \times 10^{-9}$. Let us discuss more about it. Figure 5.35 plotted that the flow law multiplier of diffusion creep in the case $b = 5.34 \times 10^{-10}$ is heavily larger than in the case $b = 5.34 \times 10^{-9}$. Thus, in Figure 5.35, this value is nearly constant when $b = 5.34 \times 10^{-9}$. However, actually, when this value is zoomed out, it increases due to an increased load. As same as the flow law multiplier of diffusion creep, the flow law multiplier of dislocation creep has the bigger value if $b = 5.34 \times 10^{-10}$ than it if $b = 5.34 \times 10^{-9}$.

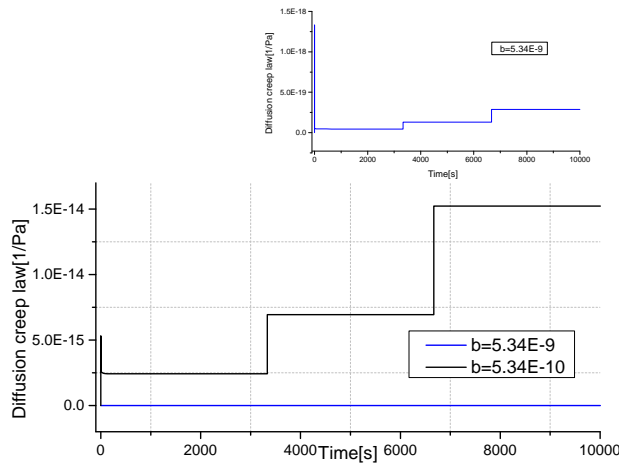


Figure 5.35: Flow law multiplier of diffusion creep, $b = 5.34 \times 10^{-9}$.

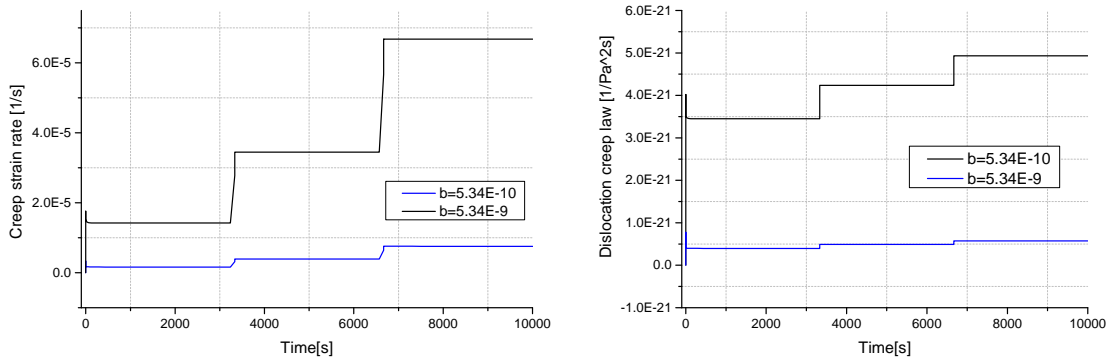


Figure 5.36: Evolution of creep strain rate, Figure 5.37: Flow law multiplier of dislocation creep, $b = 5.34 \times 10^{-9}$.

As can be seen in Figure 5.36, the creep strain rate when $b = 5.34 \times 10^{-9}$ is larger than in the case $b = 5.34 \times 10^{-10}$. On the contrary, the diffusion creep strain rate is much smaller when b is changed from $b = 5.34 \times 10^{-10}$ to $b = 5.34 \times 10^{-9}$ as in Figure 5.38. Now let us change the shear modulus.

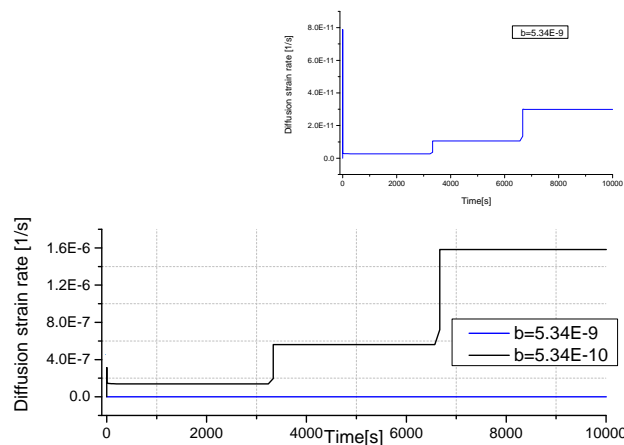


Figure 5.38: Evolution of diffusion creep rate, $b = 5.34 \times 10^{-9}$.

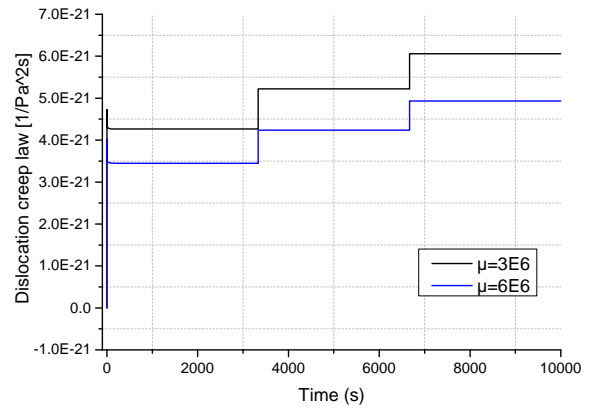
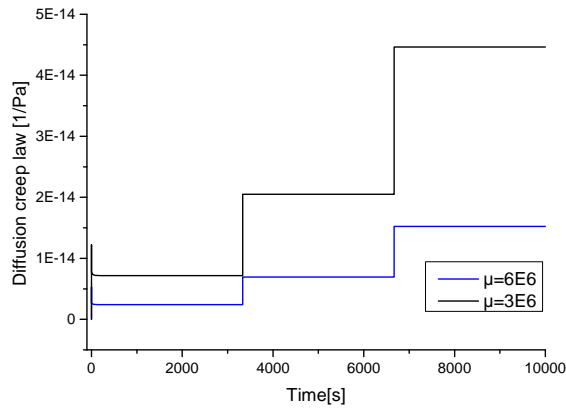


Figure 5.39: Evolution of creep strain rate, $\mu = 3 \times 10^{+10}$, Figure 5.40: Evolution of diffusion creep rate, $\mu = 3 \times 10^{+10}$.

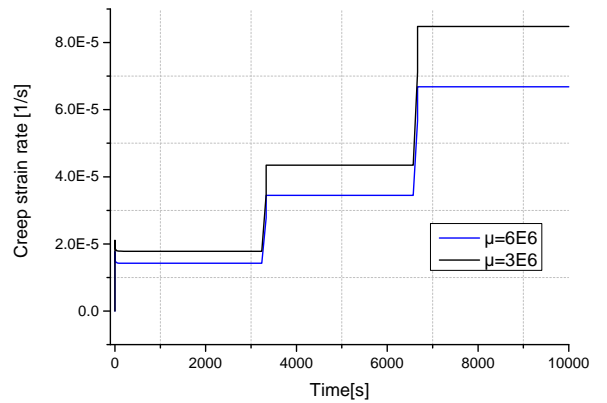
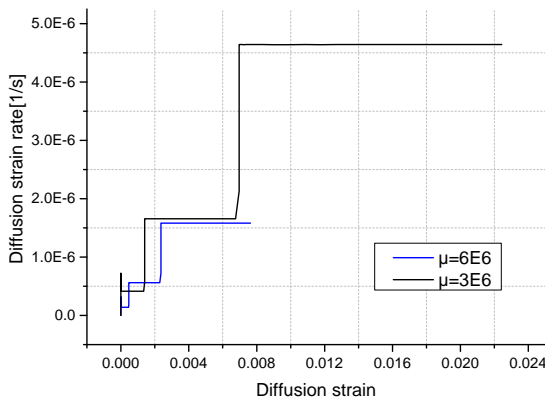


Figure 5.41: Evolution of creep strain rate, $\mu = 3 \times 10^{+10}$, Figure 5.42: Evolution of diffusion creep rate, $\mu = 3 \times 10^{+10}$.

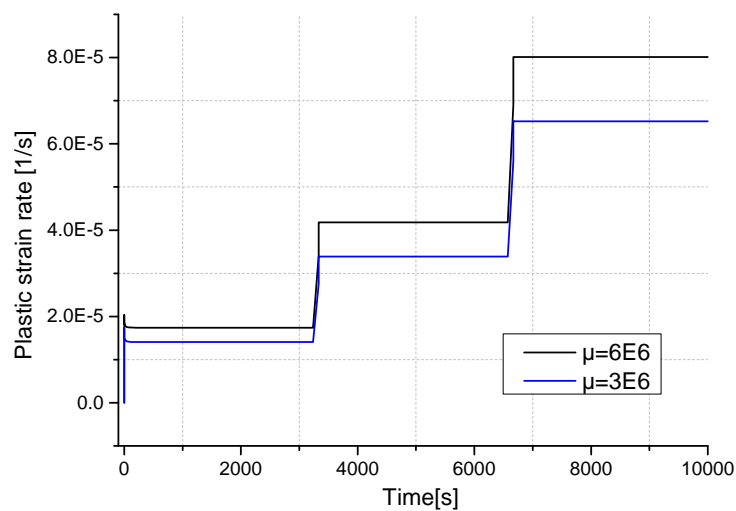


Figure 5.43: Evolution of creep strain rate, $\mu = 3 \times 10^{+10}$.

Relaxation test

Totally different from the creep test, in relaxation test, the trend of Von Mises stress reduces with the high rate and then after 0.5 hour, the rate is much smaller (Figure 5.44). One more time, Figure is an evidence to show that the dislocation creep is the dominant process. The dislocation creep is caused by the plastic strain. In Figure 5.45, the total effective creep strain ϵ is approximated to the plastic strain, ϵ_p . Although the diffusion strain is small comparing to the plastic strain, its trend is still shown in Figure 5.46. This quantity also reaches a stable value after a big jump. The evolution of $\bar{\lambda}$ in this model is similar to in the first model. To end this model, as usual, to compare two models, the model proposed by Hackl-Renner and the existing model in Abaqus, the a reasonable agreement in the total effective creep strain is sketched in Figure 5.49. The evolution of the flow multiplier of dislocation creep is drawn in Figure 5.50. Figure 5.48 shows the influence of plastic strain rate on the plastic strain.

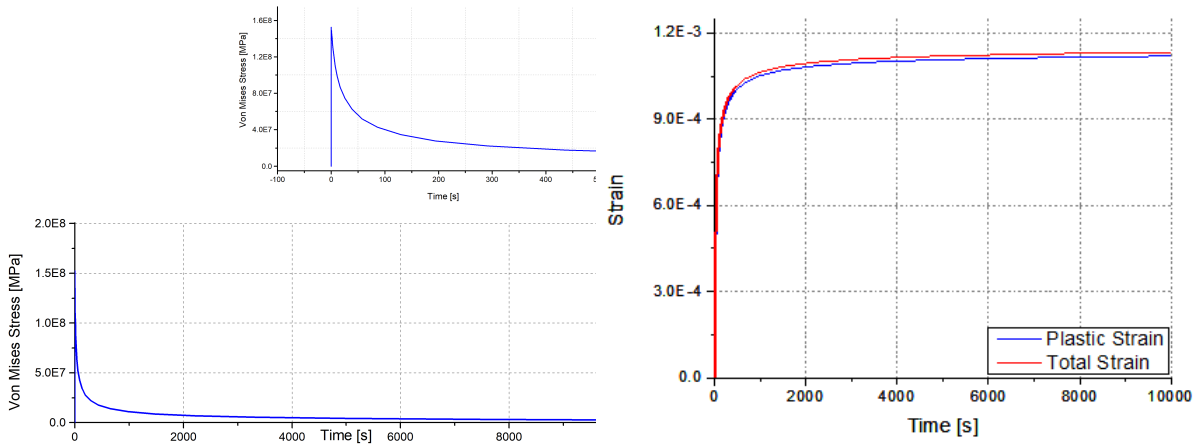


Figure 5.44: Evolution of Von Mises stress. Figure 5.45: Plastic strain and total creep strain.

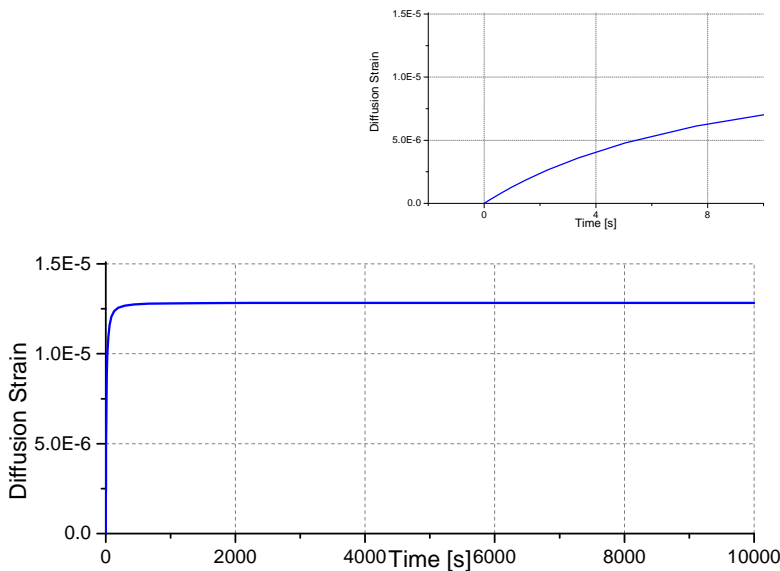


Figure 5.46: Evolution of diffusion strain.

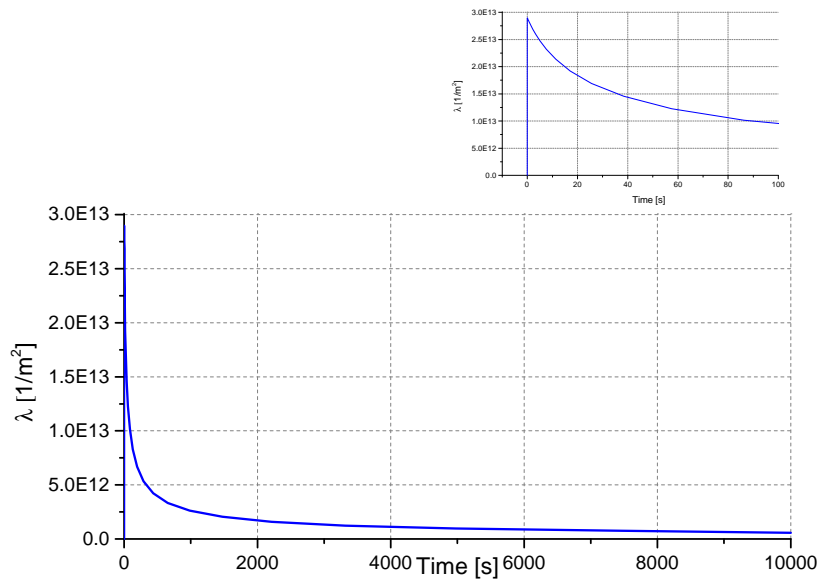


Figure 5.47: Evolution of $\bar{\lambda}$.

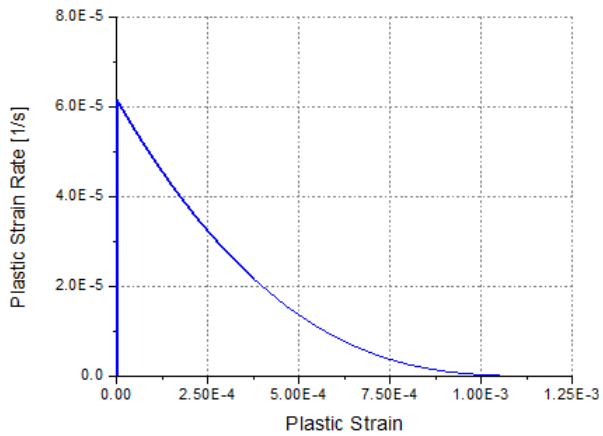


Figure 5.48: Plastic strain rate and plastic strain.

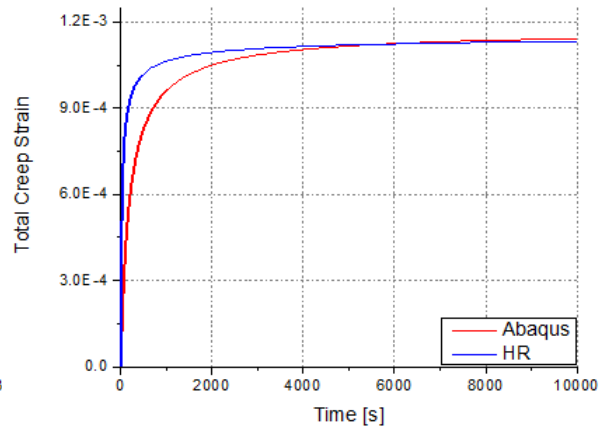


Figure 5.49: Total creep strain in Abaqus and in HR.

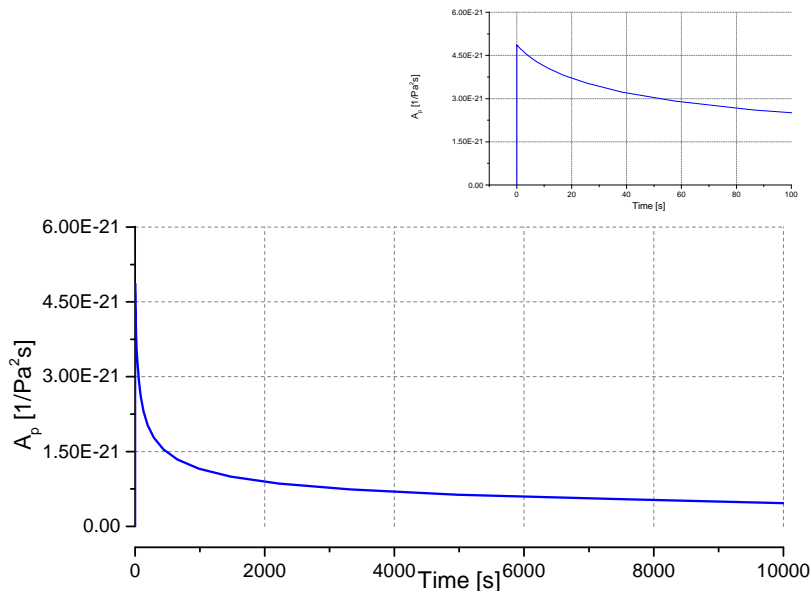


Figure 5.50: Flow multiplier of dislocation creep.

Now let us discuss briefly about disadvantages of two models. During the process to implement two models, the parameters implementation was conducted. In both models, m , has different values in the problem at the microscale and in the problem at the macroscale.

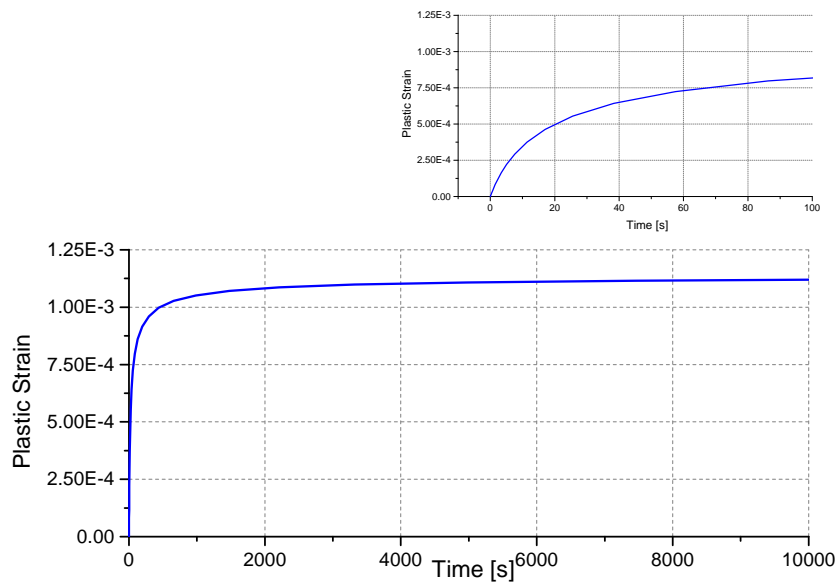


Figure 5.51: Evolution of plastic strain.

5.4.3 The third model results

Within the third model, the standard distribution function $\bar{f}(D, r)$ and the third theory of nucleation are deployed. In this model, only creep test is implemented to fit material parameters.

Creep test

Parameter	Value	Unit	Physical interpretation
b	1.34×10^{-8}	m	Burger's vector
a_p	$1.03154 \times 10^{+4}$	-	Material parameter
M_{\perp}	1.0×10^{-15}	$\text{m}^3 \text{s kg}^{-1}$	Diffusion mobility
M_{nuc}	3.86853×10^{10}	$\text{m}^3 \text{s kg}^{-1}$	Nucleation mobility
λ	-	Jm^{-3}	Lagrange multiplier
k_p	4.8×10^{-29}	$\text{m}^{2+m/2} \text{N}^{-1/m} \text{s}^{-1}$	Dislocation velocity in Eq. (3.46)
m	0.5	-	Dislocation velocity in Eq. (3.46)
μ	$9.9 \times 10^{+14}$	Pa	Shear modulus
δ	1.0×10^{-8}	m	Grain boundary thickness
γ	$5.0 \times 10^{-3} - 2.0$	Jm^{-2}	Interfacial energy
D_0	1.0×10^{-4}	m	Material parameter for nucleation function

Table 5.6: Material parameters for the third model

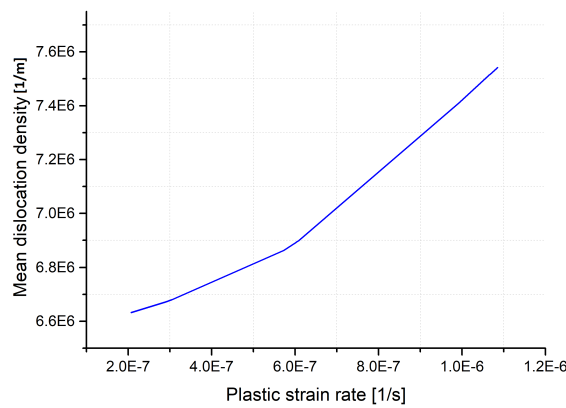


Figure 5.52: Evolution of mean rescaled dislocation density.

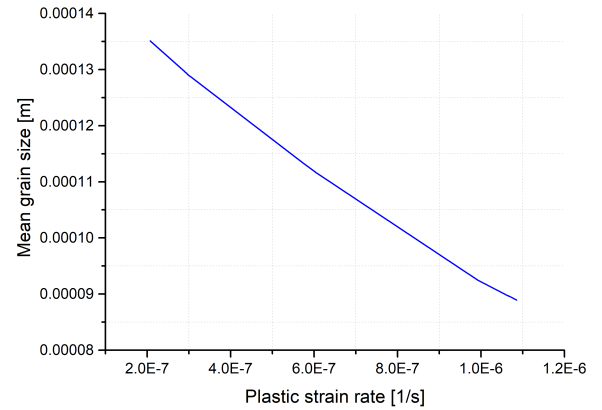


Figure 5.53: Evolution of mean grain size.

In this model, we implemented numerically for the two-scale model. Furthermore, the second nucleation theory is applied in this model. Again, the information of material parameters are given. As in the first model and in the second model, we still have parameters: Burger's vector, diffusion mobility, nucleation mobility, shear modulus, grain boundary thickness, interfacial energy. Moreover, we have one new parameter concerning nucleation process, this is nucleation mobility. The results of the model proposed by Hackl and Renner are presented. We executed the creep test for two specific values of the interfacial energy, γ . Firstly, the result of the first implementation with $\gamma = 0.810^{-4}$ is talked about. The dominant regime is the dislocation creep. Then the total effective strain is nearly identical to the plastic strain, this can be illustrated in Figure 5.57. Furthermore, in Figure 5.61, the total creep strain, summation of plastic strain and dislocation strain increases step by step when the applied force raises over time. This fact can be obviously observed in Eq. (3.117) and

Eq. (3.118). Secondly, in Figure, we can see the reasonable agreement between the total effective creep strain of our model and of Abaqus model. We plotted the change of flow law multiplier of dislocation, flow law multiplier of diffusion on creep test, plastic strain as from Figure 5.54 to Figure 5.57. An interesting result is that when the plastic strain rate increases, the flow law multipliers for diffusion creep and dislocation creep, A_d and A_p increase. The flow multipliers A_p and A_d depend on the mean values, $\langle D^3/\rho \rangle$ and $\langle D^5/M_{\text{eff}} \rangle$, obtained from the result of micro-level. Figure 5.52 and Figure 5.53 show the change of the mean dislocation density and the mean grain size. When plastic strain rate gets bigger, the average of grain size is reduced. Differing from the mean grain size, the average of dislocation raise regularly. From these evolutions, the tendency of $\langle D^3/\rho \rangle$ and of $\langle D^5/M_{\text{eff}} \rangle$ is to go down. This leads to the increase in the flow law multipliers. As stress grows, the mean rescaled dislocation density becomes larger (see Figure 5.52). The mean grain size decreases due to DRX (see Figure 5.53). Hence $\langle D^3/\rho \rangle$ and $\langle D^5/M_{\text{eff}} \rangle$ are expected to decrease, which means the increase in A_p and A_d . We know that the grain boundary plays an important part in controlling the dynamic recrystallization. Therefore, we also need to investigate the effect of interfacial energy. Then we used two different values of interfacial energy. We implemented our model numerically with two different interfacial energy. Comparing with the smaller interfacial energy, the average of grain size at the larger one is bigger. The average of grain size for the larger interfacial energy is larger than the average of grain size for the smaller interfacial energy. During the grain growth process, grains with high dislocation density are predominantly consumed. Moreover, Eq. (3.134) indicates that the nucleation function, g doesn't depend on the interfacial energy. The number of nucleated grains for two cases of the interfacial energy are nearly the same. Plastic strains in two cases have no difference as in Figure 5.60. As a result, the total effective creep strain have a slight dissimilarity (Figure 5.61).

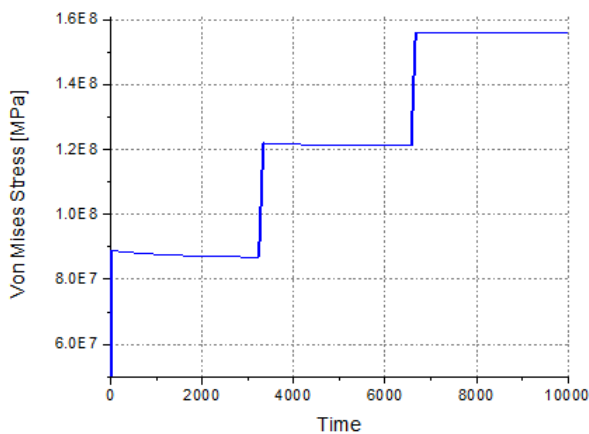


Figure 5.54: Evolution of Von Mises stress.

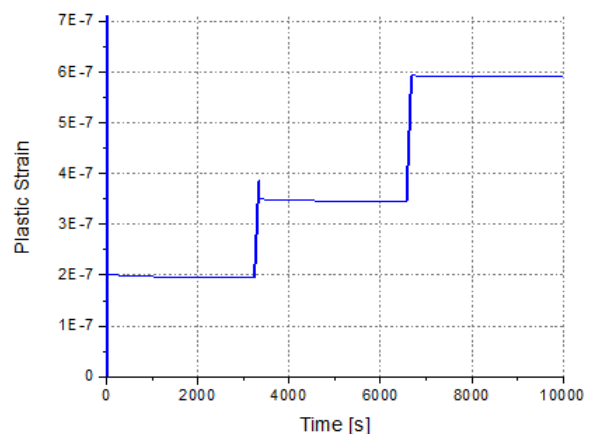


Figure 5.55: Evolution of plastic strain rate.

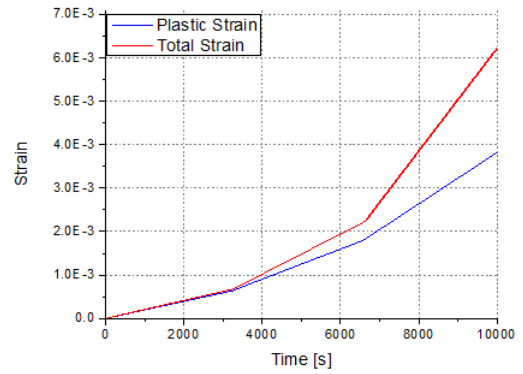
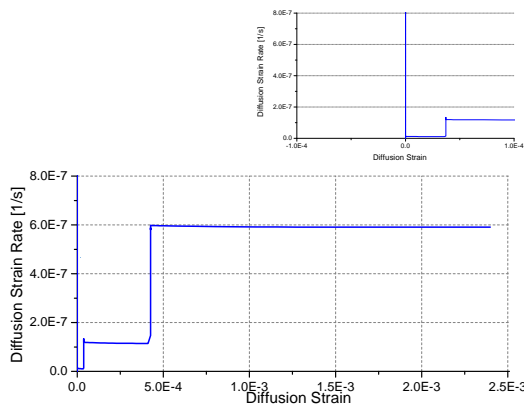


Figure 5.56: Diffusion strain rate v.s diffusion strain. Figure 5.57: Plastic strain v.s total creep strain.

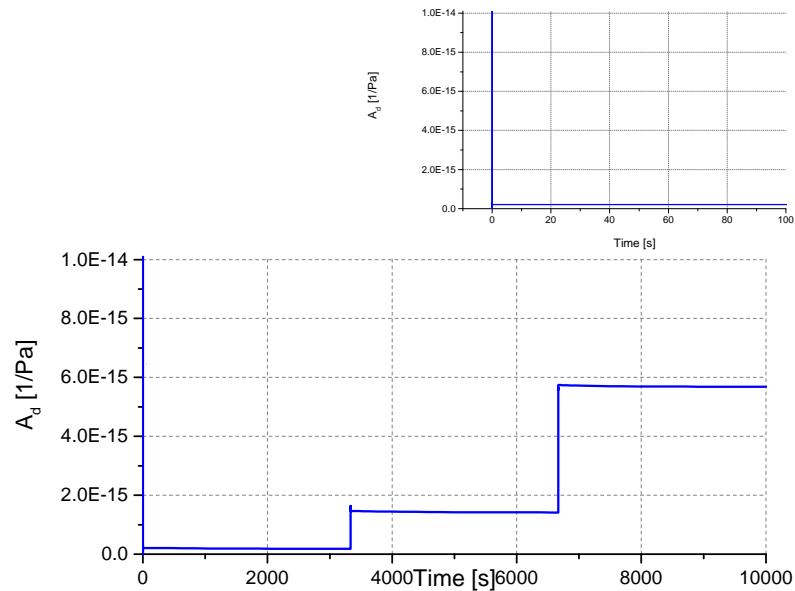


Figure 5.58: The flow multiplier for diffusion creep.

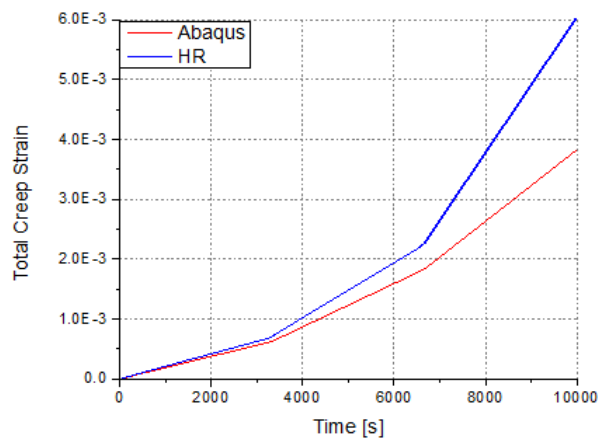


Figure 5.59: Total effective creep strain in H-R model and in Abaqus.

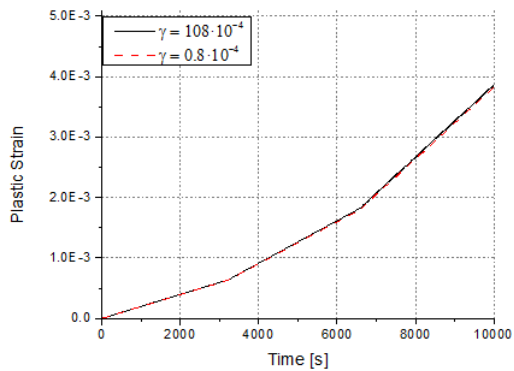


Figure 5.60: Plastic strain.

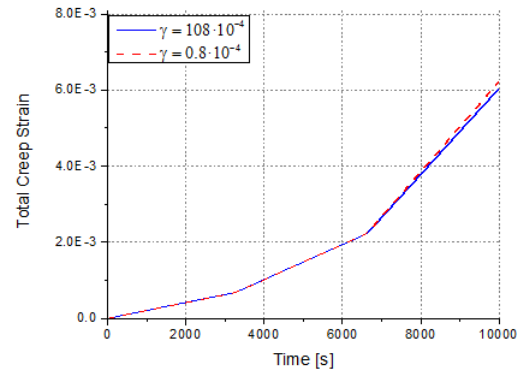


Figure 5.61: Total effective creep strain.

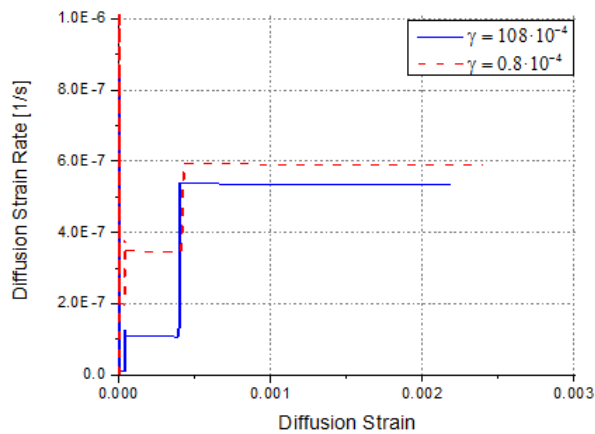


Figure 5.62: Diffusion strain rate v.s diffusion strain.

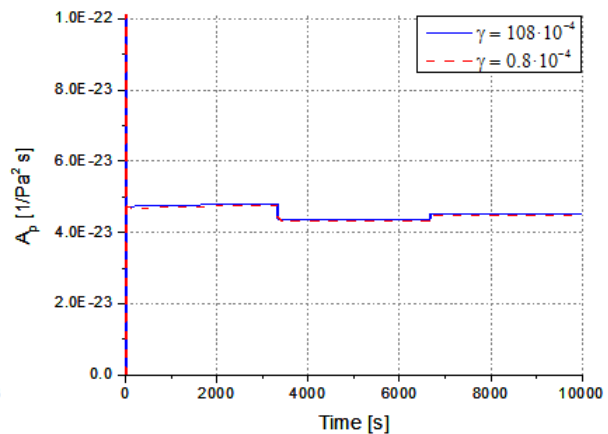


Figure 5.63: Flow law multiplier for dislocation creep.

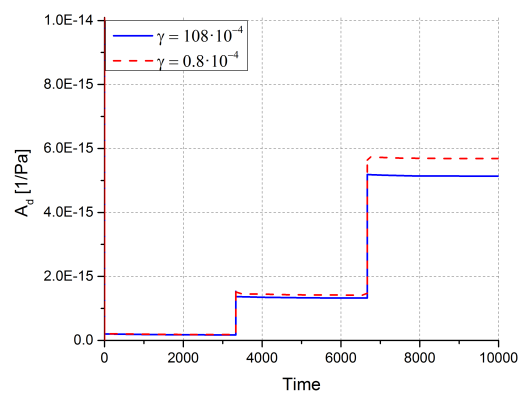


Figure 5.64: Flow law multiplier for diffusion creep.

Moreover, the simulation result shows the comparison of the total creep strain between Hackl-Renner (H-R) model and Abaqus model (in the library of Abaqus). The good agreement between two models is shown in Figure. 5.59. After the numerical implementation, a comparison of the present model with existing phenomenological ones is conducted. In Figure 5.65, we found that there is an exact match between the homogenized result and the real phenomena. This match can be explained as follows. The rescaled dislocation density increases with time due to the accumulation of dislocations during deformation the r-axis represents time, too. Thus grains with small rescaled dislocation density are young, those with high rescaled dislocation density are old. It can be seen in Figure 5.65 that newly formed grains, having low energy, grow by consuming old ones which have high energy. At a certain age, the grains have accumulated so many dislocations that they start to be consumed and finally disappear completely. This match is concerning the life cycle of grains. In contrast to reality, the result of the numerical simulation shows that grains will nucleate at the same size. Moreover, as can be seen in Figure 5.65, there are still some nucleated grains with the high rescaled dislocation density.

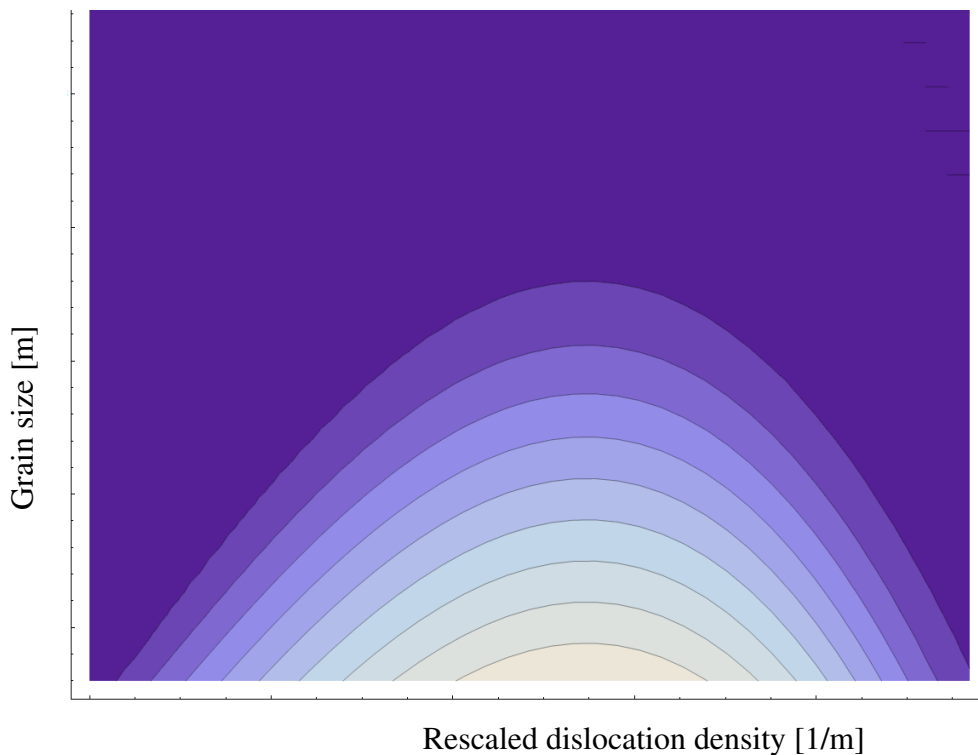


Figure 5.65: Probability distribution function.

6 Conclusions and Outlook

The main aim of this thesis was to construct not only a mathematical model to simulate the dynamic recrystallization phenomena in polycrystalline materials but also develop a numerical treatment for this model. It is obvious to see that many equations of the mathematical model were derived from the principle of the minimum for the dissipation. Therefore, a review of this principle was conducted first. Moreover, the mathematical model was derived from the variational analysis of evolution equations for deformation at high temperature. Hence, a brief introduction and derivation of this variational approach was presented. The evolution equations for grain size, dislocation density, which would be used in the problem at the microscale were obtained. The plastic strain rate and the dislocation strain rate concerning the flow rule at the problem at the macroscale were derived as well.

After this review, the original mathematical problem at the microscale was established. "Original" means that the distribution function which characterizes individual grains is a function of grain size and dislocation density. However, after inserting the evolution equations of grain size and dislocation density into the mass conservation or the continuity equation, singularity problem was encountered. Thus, a demand to modify the originally mathematical problem by transforming from ρ to r see (3.63) via the following relationship

$$r = \sqrt{\rho}. \quad (6.1)$$

This version of the model was called the standard. Nevertheless, we suspected that the distribution function has the larger value around the characteristic curve, $D = s + \frac{1}{v} (\bar{\lambda}r - \frac{1}{3}r^3)$, then one more time, the alteration of variable was made from D to s . The distribution function would depend on "grain size", s and dislocation density r .

Then up to this point, we have three versions of the mathematical model. After establishing the model, to solve these versions numerically by utilizing numerical tools such as Euler-Backward method, finite element method, Newton-Raphson method and Simpson rule. We require the initial value of distribution function which relates to the nucleation process. As a consequence, three ansatzes were proposed in this thesis. At the beginning, guess for this term was given. Afterwards, stemming from the physical phenomena, two upcoming theories were proposed.

To complete the mathematical model for dynamic recrystallization, a connection between the problem at the microscale and the counterpart at the macroscale was given. The problem at the macroscale was discussed in this thesis. After deriving the full problem, we presented the numerical implementation. It was a two-scale scheme. The link between two problems at two different scales via the average expression as

$$\langle g \rangle = \int_{\Omega} g f \, d\Omega. \quad (6.2)$$

To solve our model, the numerical algorithm for both problems at two scales were established. Distinct distribution functions and different nucleation theories, we implemented

three combinations: the distribution function $f(s, r)$ with the first and the second nucleation theory, the distribution function $f(D, r)$ with the third theory of nucleation. While for the problem at the microscale, the marching algorithm was developed, to deal with the problem at the macroscale, a return mapping was conducted.

To demonstrate the relevance of our model, we used the creep model which exists in the library of Abaqus to compare with our model and to fit the material parameters via the creep test. Lastly we judge the numerical result by a comparison of the present model with phenomenological phenomena. Since we observed the disagreement between the newest model and existing phenomenological ones, we also investigated the new direction to resolve the problem. With the new direction, the distribution function would be a function of three variables: the neighboring dislocation density, grain size, dislocation density. At the same time, we also derived a fixpoint algorithm to solve the problem at the microscale. In this algorithm, we did not consider the volume constraint. As the result, we could see the contour line of the distribution function or the relationship between the grain size and dislocation density.

In the further, how to apply the new direction should be investigated. In order to see the behavior of the materials, a comparison with laboratory experiments is also planned to be executed. Then we will extend our model by adding the recovery term in the evolution equation of dislocation density.

References

- Barnhoorn, A. (2003). *Rheological and microstructural evolution of carbonate rocks*. Ph. D. thesis, ETH Zürich.
- Bernacki, M., H. Resk, T. Coupez, and R. Logé (2009). Finite element model of primary recrystallization in polycrystalline aggregates using a level set framework. *Modelling and Simulation in Materials Science and Engineering* 17(6), 064006.
- Callister, W. D. (2007). *Materials Science and Engineering: An Introduction*. John Wiley Sons, Inc.
- Chadwick, P. (1999). *Continuum Mechanics: Concise Theory and Problems*. Courier Corporation.
- Chen, F., Z. Cui, J. Liu, X. Zhang, and W. Chen (2009). Modeling and simulation on dynamic recrystallization of 30Cr2Ni4MoV rotor steel using the cellular automaton method. *Modelling Simul. Mater. Sci. Eng.* 17, 01–19.
- Chou, P. C. and N. J. Pagano (1992). *Elasticity: Tensor, Dyadic, and Engineering Approaches*. Dover Publications, Inc., New York.
- Ding, R. and Z. Guo (2001). Coupled quantitative simulation of microstructural evolution. *Acta. Mater.* 49, 3163–3175.
- Dmitrieva, O., P. W. Dondl, S. Müller, and D. Raabe (2009). Lamination microstructure in shear deformed copper single crystals. *Acta. Mater.* 57(12), 3439 – 3449.
- Doherty, R., D. Hughes, F. Humphreys, J. Jonas, D. Jensen, M. Kassner, W. King, T. McNelley, H. McQueen, and A. Rollett (1997). Current issues in recrystallization: a review. *Mater. Sci. Eng. A* 238, 219–274.
- E. A. de Souza Neto, D. P. and D. R. J. Owen (2008). *Computational methods for plasticity: theory and application*. A John Wiley and Sons, Ltd, Publication.
- Gourdet, S. and F. Montheillet (2003). A model of continuous dynamic recrystallization,. *Acta. Materialia* 51, 2685–2699.
- Guillope, M. and J. Poirier (1979). Dynamic recrystallization during creep of singlecrystalline. *J. Geophys. Res. (B)* 84, 5557–5567.
- Hackl, K. and F. D. Fischer (2008). On the relation between the principle of maximum dissipation and inelastic evolution given by dissipation potentials. *Proceedings of The Royal Society A* 464, 117–132.
- Hackl, K. and J. Renner (2013). High-temperature deformation and recrystallization: A variational analysis and its application to olivine aggregates. *Geophys. Res. Solid Earth* 118, 943–967.

- Hirth, J. P. (1972). The influence of grain boundaries on mechanical properties. *Metall. Trans.* 3, 3047–3067.
- Holzappel, G. A. (2000). *Nonlinear Solid Mechanics: A Continuum Approach for Engineering*, Volume 6. John Wiley Sons Ltd., Baffins Lane, Chichester, West Sussex PO19 1UD, England.
- Huber, D., C. Stotter, C. Sommitsch, S. Mitsche, P. Poelt, B. Buchmayr, and M. Stockinger (2008). Microstructure modeling of the dynamic recrystallization kinetics during turbine disc forging of the nickel based superalloy Allvac 718Plus. *TMS*, 01–07.
- Humphreys, F. J. and M. Hatherly (2004). *Recrystallization and related annealing phenomena*. Elsevier.
- Isfahani, V. E. (2014). A finite element approach for simulating dynamic recrystallization in polycrystalline materials. Master's thesis, Ruhr Univeristy, Bochum.
- Junker, P. (2011). *Simulation of Shape Memory Alloys: Material Modeling using the Principle of Maximum Dissipation*. Ph. D. thesis, Ruhr University, Bochum.
- Khai, P. Q. (2014). A marching algorithm with non-uniform mesh for the calculation of distribution functions. Master's thesis, Ruhr University, Bochum.
- Kim, S., C. Jin, S. Chun, and Y. Yoo (2001). Recrystallization and grain growth. *1st Joint Int. Conf. Aachen (Germany): Springer Verlag*, 917–922.
- Liu, J., Z. Cui, and C. Li (2008). Modelling of flow stress characterizing dynamic recrystallization for magnesium alloy AZ31B. *Comput. Mater. Sci* 41, 375–382.
- Luton, M. and C. Sellars (1969). Dynamic recrystallization in nickel and nickel-iron alloys during high temperature deformation. *Acta. Metall.* 17, 1033–1043.
- Nguyen, H. V., V. Ebrahimzade, K. Hackl, J. Renner, and B. T. Trinh (2015). Modeling dynamic recrystallization in polycrystalline materials via probability distribution function. *PAMM* 15, 339–340.
- Nguyen, H. V., K. Hackl, and J. Renner (2013). A variational approach to dynamic recrystallization using probability distributions. *PAMM* 13, 275–276.
- Peczak, P. (1995). A monte carlo study of influence of deformation temperature on dynamic recrystallization. *Acta. Metall. Mater.* 43, 1279–1291.
- Peczak, P. and M. Luton (1993a). The effect of nucleation models on dynamic recrystallization i. homogeneous stored energy distribution. *Philos. Mag. B* 68, 115–144.
- Peczak, P. and M. Luton (1993b). A monte carlo study of the influence of dynamic recovery on dynamic recrystallization. *Acta. Metall. Mater.* 41, 59–71.
- Peczak, P. and M. Luton (1994). The effect of nucleation models on dynamic recrystallization ii. heterogeneous stored-energy distribution. *Philos. Mag. B* 70, 817–849.
- Poirier, J. and A. Nicolas (1975). Deformation-induced recrystallization due to progressive misorientation of subgrains, with special reference to mantle peridotites. *J. Geol* 83, 707–720.

- Qian, M. and Z. Guo (2004). Cellular automata simulation of microstructural evolution during dynamic recrystallization of an hy-100 steel. *Mater. Sci. Eng. A* 365, 180–185.
- R. B. Hetnarski, J. I. (2010). *The mathematical theory of elasticity*. CRC Press.
- Roberts, W. and B. Ahlblom (1978). A nucleation criterion for dynamic recrystallization during hot working. *Acta. Metall.* 26, 801–813.
- Rollett, A., M. Luton, and D. Srolovitz (1992). Microstructural simulation of dynamic recrystallization. *Acta. Metall. Mater.* 40, 43–55.
- Sandström, R. and R. Lagneborg (1975). A model for hot working occurring by recrystallization. *Acta. Metall.* 23, 387–398.
- Sitdikov, O. and R. Kaibyshev (2002). Dislocation glide and dynamic recrystallization in lif single crystals,. *Mater. Sci. Eng. A* 328, 147–155.
- Urai, J., W. Means, and G. Lister (1986). Dynamic recrystallization of minerals. *Am. Geophys. Un. Geophys. Monogr* 36, 161–199.
- Zienkiewicz, O. C. and R. L. Taylor (2005). *The Finite Element Method*. Butterwoth - Heinemann.

Curriculum Vitae

Personal Informtion

Name: Nguyen Hai Van
Date of Birth: 02 January 1986
Place of Birth: Ha Noi, Viet Nam
Marital Status: Married
Nationality: Vietnamese

Education

1997-2004 Foreign Languages Specializing High School,
Hanoi, Vietnam
2004-2009 Hanoi University of Science and Technology
(HUST), Vietnam
2009-2011 Ruhr-University, Bochum, Germany

Professional Occupation

2011 Student Assistant, Chair of Computing in Engineering, Ruhr-
University, Bochum, Germany
2011-2012 Panasonic RD Center Vietnam Co., Ltd
2012-2013 Research and Teaching Assistant, Vietnamese-German University,
Binh Duong, Vietnam
2014-2016 Teaching Assistant, Faculty for Mathematics, Ruhr-University,
Bochum, Germany

**Mitteilungen aus dem Institut für Mechanik
RUHR-UNIVERSITÄT BOCHUM
Nr. 177**

ISBN 978-3-935892-55-1